Development of Photoelectrochemically-active Tin-Tungsten Oxide Electrodes for Organic Wastewater Treatment and Water Disinfection

by

Saloumeh Ghasemian

Department of Chemical Engineering
McGill University
Montreal, Quebec, Canada

May 2017

A thesis submitted to McGill University in partial fulfillment of the requirements of the degree of

Doctor of Philosophy

“Everyone is gifted, but some people never open their package.”

Wolfgang Riebe

Acknowledgments

I would like to sincerely thank my advisor, Prof. Sasha Omanovic, for his invaluable guidance and support during my Ph.D. study. I am also greatly thankful to Prof. Nathalie Tufenkji and Prof. Viviane Yargeau for their support and collaboration in my Ph.D. research and making it more enjoyable for me.

I would like to thank Mr. Marco Aurelio Pineda Castro and Mrs. Marie-line Peyot for their great work in the analysis of my experimental samples. A big “thank you” to Jean-Sébastien Renault-Crispo for translating the abstract of my thesis to French.

I thank my friends, Dr. Zeinab Hosseinidoust, who helped me all the times from the very first day of my Ph.D. study, and Dr. Bahareh Asadishad, for always being there for me.

Many thanks to Dr. Deniz Nasuhoglu, my colleagues Sarah Jaynob, Deepak Sridhar, Aqeel Alrebh and others who have helped me along the way.

I thank Mr. Frank Caporuscio, Andrew Golsztajn and other technical and administrative staff at Chemical Engineering Department. I would also like to acknowledge McGill Engineering Doctoral Award Program (MEDA) for financial support.

Last but not least, I would like to express my deepest gratitude to my family for their patience, unconditional love, and support throughout this long journey.

Abstract

Deterioration of water quality, increased risk of water-related diseases, inadequate fresh water supply, lack of access to clean water and basic sanitation due to human population growth, expansion of industrialized activities, and climate change have become global issues of concern. In addition to waterborne pathogen contamination, water quality issues arise from the continuous input of recalcitrant organic pollutants such as pharmaceuticals, which are resistant to biodegradation and cannot be removed by conventional water treatment methods. The emerging concerns over the negative impacts of these compounds on the ecosystem and human health have led to an increase in scientific research on new treatment technologies for water purification, such as advanced oxidation processes (AOPs). Among AOPs, the semiconductor-based (photo)electrochemical oxidation methods based on the anodic oxidation, have demonstrated to be promising techniques for the degradation of bio-refractory organic contaminants from wastewaters. Therefore, the main objective of this work was to develop mixed metal oxide (MMO) electrodes (anodes) with good photo- and electrocatalytic activity for the oxidative decomposition of complex organic molecules and bacteria from aqueous solutions using UV light, electrical current or both combined.

First, thin metal oxide anode coatings with different compositions of tin and tungsten (Sn_x-$W_{(100-x)mol\%}$-oxide; x = 0, 20, 40, 60, 80 and 100) doped with a small amount of antimony (~ 3 mol%) were fabricated on Ti substrates *via* a thermal deposition method. The coatings were then characterized by various electrochemical and surface-characterization techniques, such as cyclic voltammetry (CV), X-ray photoelectron spectroscopy (XPS), X-ray diffraction (XRD), scanning electron microscopy (SEM) coupled with energy-dispersive X-ray spectroscopy (EDX). As-prepared electrodes of different compositions were screened and tested for the photochemical

(PC), electrochemical (EC) and photoelectrochemical (PEC) degradation of phenol red (PR) dye, which was employed as a model organic molecule. The coating composition of $Sn_{80\%}$-$W_{20\%}$-oxide was selected as the most intrinsically photoelectrochemically-active material for further experiments.

In the second part of the project, a potential use of the Sb-doped $Sn_{80\%}$-$W_{20\%}$-oxide electrodes for the EC inactivation of bacteria in chloride-containing solutions was studied. The influence of various experimental factors such as current density, initial population of bacteria, initial chloride concentration, pH, type of bacterial strain, the presence of natural organic matter (NOM) and radical scavengers on the disinfection efficacy of the EC system was investigated. The results demonstrated the strong bactericidal activity of the Sb-doped $Sn_{80\%}$-$W_{20\%}$-oxide anodes, proportional to the applied current density and chloride concentration.

In the third part of the project, the Sb-doped $Sn_{80\%}$-$W_{20\%}$-oxide electrode was used for the PEC degradation of pharmaceutical carbamazepine (CBZ), at different current densities. For comparison purposes, photolytic and photocatalytic degradation experiments were also performed. The kinetic rate constants for degradation reactions were determined. The formation of the transformations products of carbamazepine during degradation processes was investigated to assess the toxicity of the treated solution. Moreover, the energy consumption under different operating conditions was estimated.

Abrégé

La détérioration de la qualité de l'eau, un risque accru de maladies liées à l'eau, l'approvisionnement insuffisant en eau douce, le manque d'accès à l'eau potable et à l'assainissement de base en raison de la population humain croissante, l'expansion des activités industrielles, et les changements climatiques sont devenus des problématiques d'intérêt mondial. Outre la contamination par les agents pathogènes d'origine hydrique, les problèmes de qualité de l'eau découlent de l'apport continu de polluants organiques récalcitrants tels que les produits pharmaceutiques qui sont résistants à la biodégradation et ne peuvent être éliminés par des méthodes classiques de traitement des eaux. Les nouvelles préoccupations concernant les effets négatifs de ces composés sur l'écosystème et la santé humaine ont conduit à une augmentation de la recherche scientifique sur les nouvelles technologies de traitement de l'eau, telles que les procédés d'oxydation avancée (POA). Parmi les POAs, les méthodes d'oxydation (photo)électrochimique à base de semi-conducteurs, basées sur l'oxydation anodique, se sont avérées être des techniques prometteuses pour la dégradation des contaminants organiques bio-réfractaires des eaux usées. Par conséquent, l'objectif principal de ce travail était de développer des électrodes d'oxydes métalliques mixtes (OMM) avec une bonne activité photo et électrocatalytique pour la décomposition oxydante de molécules organiques complexes et de bactéries à partir de solutions aqueuses utilisant la lumière UV, le courant électrique ou les deux combinés.

Tout d'abord, des couches minces métalliques d'oxyde d'anode avec différentes compositions d'étain et de tungstène (Sn_x-$W_{(100-x)mol\%}$-oxyde; x = 0, 20, 40, 60, 80 and 100) dopés avec une petite quantité d'antimoine (~ 3 mol%) ont été fabriquées sur des substrats de titane via un procédé de dépôt thermique. Les couches ont ensuite été caractérisées par diverses techniques

électrochimiques et de caractérisation de surface, telles que la voltampérométrie cyclique (CV), la spectroscopie photoélectronique X (XPS), la diffusion des rayons X (XRD) et la microscopie électronique à balayage (SEM) couplée avec une analyse dispersive en énergie (EDX). Des électrodes préparées à l'aide de compositions différentes ont été criblées et testées pour la dégradation photochimique (PC), électrochimique (CE) et photoélectrochimique (PEC) du colorant rouge phénol (PR), qui a été utilisé comme molécule organique modèle. La composition de la couche de l'oxyde $Sn_{80\%}$-$W_{20\%}$ a été choisie comme matériau le plus photoélectrochimiquement actif pour des expériences additionnelles.

Dans la deuxième partie du projet, l'utilisation potentielle d'électrodes d'oxyde $Sn_{80\%}$-$W_{20\%}$ dopées au Sb a été étudiée pour l'inactivation électrochimique de bactéries dans des solutions contenant des chlorures. L'investigation consistait à étudier l'influence de divers facteurs expérimentaux comme la densité de courant, la population initiale de bactéries, la concentration initiale en chlorure, le pH, le type de souche bactérienne, la présence de matière organique naturelle (MON) et de piégeurs de radicaux sur l'efficacité de désinfection de ce système électrochimique. Les résultats ont démontré la forte activité anti-bactéricide des anodes $Sn_{80\%}$-$W_{20\%}$ dopées au Sb, proportionnelles à la densité de courant appliquée et à la concentration en chlorure.

Dans la troisième partie du projet, l'électrode d'oxyde $Sn_{80\%}$-$W_{20\%}$ dopée au Sb a été utilisées pour la dégradation PEC de la carbamazépine pharmaceutique (CBZ), à différentes densités de courant. À des fins de comparaison, des expériences de dégradation photolytique et photocatalytique ont également été effectuées. La formation de produits de transformation de la carbamazépine durant le procédé de dégradation a été investigué pour évaluer la toxicité de la solution traitée. De plus, la consommation d'énergie dans différentes conditions de fonctionnement a été estimée.

Table of Contents

List of Figures

List of Tables

Abbreviations

WWTP	Waste Water Treatment Plant
SCE	Saturated Calomel Electrode
NHE	Normal Hydrogen Electrode
SHE	Standard Hydrogen Electrode
AOP	Advanced Oxidation Process
DSA	Dimensionally Stable Anode
NOM	Natural Organic Matter
MMO	Mixed Metal Oxide
SEM	Scanning Electron Microscopy
EDX	Energy Dispersive X-Ray
XPS	X-Ray Photoelectron Spectroscopy
XRD	X-Ray Powder Diffraction
CBZ	Carbamazepine
ROS	Reactive Oxygen Species
RCS	Reactive Chlorine Species
OER	Oxygen evolution Reaction
THM	Trihalomethane
HAA	Haloacetic Acid
DBP	Disinfection By-Product
PEC	Photoelectrochemical
EC	Electrochemical
PC	Photochemical
TP	Transformation Product

CHAPTER 1

1. General Introduction

Declining water quality and inadequate access to clean water and sanitation are of the most pervasive environmental concerns, which are expected to become worse in the next decades due to the global water scarcity. Water pollutants, including toxic organic compounds and pathogenic microorganisms, enter natural water bodies through direct or indirect discharge of industrial effluents, domestic swage, urban run-off, and farm wastes, affecting the quality of fresh water systems. These pollutants are known to be persistent in the environment and resistant to biodegradation and, thus, they cannot be effectively removed by conventional wastewater treatment methods such as chemical, physical or biological [1]. Addressing the adverse effects of these contaminants on the ecosystem and human health calls out for a great deal of research to be conducted to develop new technologies for purifying water with higher effectiveness, lower energy demand, minimal use of chemicals and minimal negative impacts on the environment.

Advanced oxidation processes (AOPs) are a promising technology for the treatment of different types of wastewater, having ability to oxidize a wide variety of organic pollutants [2]. AOPs are chemical oxidation processes that utilize electricity, ultraviolet (UV) light, ozone, and/or hydrogen peroxide to generate highly reactive and powerful oxidizing species such as hydroxyl radicals ($^{\bullet}OH$) or sulfate radicals ($SO_4^{\bullet-}$) to oxidize organic compounds efficiently [3]. AOPs were first proposed in 1980s for the treatment of drinking water [4]. **Figure 1-1** shows different applications of AOPs for wastewater treatment. AOPs offer several advantages including environmental compatibility, rapid reaction rate, modularity, ability to eliminate organic pollutants in aqueous phase rather than collecting or transferring them from one phase to another, small

footprint, effectiveness in degradation of (bio)refractory and highly concentrated organic compounds (that are not treatable by means of biological processes) and do not produce excessive amounts of solid waste as with physical, chemical, or biological processes [5]. Generally, the efficiency of an AOP is enhanced to the greatest extent by employing a suitable catalyst and/or UV light [6]. Among AOPs, electrochemical technologies have gained much interest due to simplicity, versatility, ease of control, modularity, portability, environmental compatibility and the possibility to treat very (bio)refractory wastes [7].

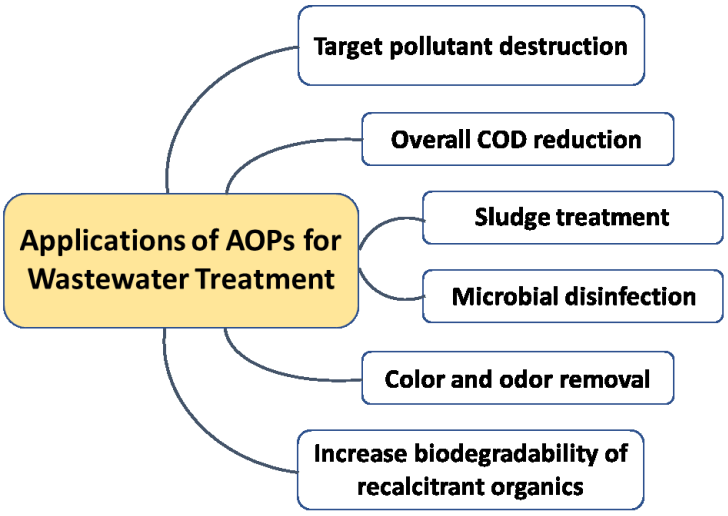

Figure 1-1: Applications of AOPs for wastewater treatment (Adopted from Bergendahl and O'Shaughnessy (2004) [8]).

The electrochemical technology has been demonstrated to be effective for the treatment of wastes containing organics such as phenols, dyes, and benzoic compounds [9] as well as for the water disinfection [10]. Other advantages of this technology include applicability on a wide variety of contaminants, safe operating conditions, no need to add auxiliary chemicals, no need to separate the catalysts (electrodes) from the reaction mixture since it is a heterogeneous (electro)catalytic system [11]. Furthermore, the electrochemical systems can be easily paired with other operations

such as biological, chemical and physical processes to increase the efficiency of the treatment [12]. The efficiency of the electrochemical technology for wastewater treatment can further be improved by utilizing UV light, in which the electrochemical oxidation of the pollutant is also supported by the photocatalytic oxidation [13]. It has been shown that photoelectrochemical processes are potential methods for oxidation of a wide spectrum of substances [14] and disease-causing microorganisms [15].

The key part of a photoelectrochemical reactor is the photoelectrocatalyst (usually an anode), which dictates the efficiency, stability, cost, catalytic activity, and selectivity of the system. Hence, the electrode material plays a crucial role in the photoelectrochemical treatment of wastewater containing organic pollutants [16].

Among various materials for electrode construction, Dimensionally Stable Anodes (DSA®) (active mixed metal oxide coatings on titanium substrates), are seen as promising materials for treatment of bio-refractory wastewaters [17]. DSA® electrodes have large specific surface area and desired mechanical and chemical properties such as excellent resistance to corrosion at high currents and in a strong acidic environment [13]. These electrodes were first developed in the 1960's and intensely used by the chlor-alkali industry [18]. It has been demonstrated that using DSA® electrodes improves the efficiency of the photoelectrochemical oxidation of a wide range of organic contaminants and wastes with strong colors [19]. The high degradation efficiency of photoelectrochemical processes using DSA® electrodes is attributed to the combination of two mechanisms [20]: (i) the electrochemical mechanism, which involves the production of hydroxyl radicals from water at an electrode surface and, (ii) the photo-electrochemical mechanism, which pertains to the heterogeneous photocatalysis at the electrode surface (it should be noted that DSA®s are non-stoichiometric mixed metal oxides that possess semiconducting properties, and are usually

photoactive). To bring this technology closer to large-scale commercialization, it is necessary to develop new photoelectrochemically-active DSA®s that would offer higher photoelectrochemical activity, higher energy efficiency, better stability (and thus longevity) and potentially lower cost than currently used photo-active DSA®s.

1.1. Research Objectives

The main objective of this project was to synthesize new mixed metal oxide photoelectrochemically-active dimensionally stable anodes composed of tungsten (W) and tin (Sn) for effective and energy-efficient photoelectrochemical degradation of organic pollutants in wastewaters and electrochemical water disinfection. Specific objectives are listed as follows:

1. Development of a Sn-W-oxide coating-formation procedure in order to achieve satisfactory *photo*- and *electro*-catalytic activity, selectivity, and durability,
2. Electrochemical, optical and surface characterization of as-prepared Sn-W-oxide electrode coatings to obtain information on the bulk and surface distribution of elements, crystallinity, surface morphology, true surface area (considering surface roughness), band gap energy, and photocurrent production,
3. Screening of the Sn-W-oxide coatings of various Sn/W ratio with respect to their photoelectrocatalytic activity towards the degradation of a model wastewater organic molecule, phenol red dye,
4. Electrochemical disinfection of water contaminated with bacteria employing the best-performing oxide coating selected based on the results obtained in the previous step,

5. Removal of pharmaceutical carbamazepine from wastewater by photoelectrochemical oxidation employing the best-performing coating selected based on the results obtained in step (3),
6. Evaluation of the overall performance of the developed anode material for environmental applications from the energy consumption point of view.

1.2. Thesis Organization

As just seen, **Chapter 1** provides a general introduction to the subjects studied in this project. Furthermore, the objectives of this research are outlined, followed by the thesis organization showing the flow of contents and, then, contribution of authors of the manuscripts coming out of the results of the research presented in this thesis.

Chapter 2 provides an overview of literature, explaining several types of advanced oxidation processes (AOPs) and related reactions, possible mechanisms of electrochemical oxidation in general, and detailed mechanisms of photoelectrocatalytic oxidation of organics. A review of some common semiconductor oxide materials for photo-, electro-, and photoelectrocatalytic oxidation of organics is presented. Furthermore, the common approaches for tuning the band structure and possibly enhancing the photo- and electrocatalytic activity of semiconductors (e. g. doping and coupling) are discussed. Moreover, common techniques for disinfection of water and wastewaters are described in general, and the electrochemical disinfection process and the possible mechanisms of actions in the presence and absence of chloride in the solution are discussed.

In **Chapter 3**, the mixed metal oxide electrode coatings with six different compositions of tin-tungsten oxide (Sn_x-$W_{(100-x)mol\%}$-oxide; x = 0, 20, 40, 60, 80 and 100) doped with a small amount of antimony (~ 3 mol% Sb) were formed on Ti substrates. Then, the as-prepared coatings were

characterized using various state-of-the-art techniques to determine their electrochemically-active surface area, surface roughness, surface microstructure and elemental composition, crystalline structure, band gap energy, and photocurrent production. Then, the electrode coatings were tested for their photoelectrocatalytic activity in a series of photochemical, electrochemical, and photoelectrochemical screening experiments for the degradation of phenol red dye as a test (model) wastewater organic molecule. Based on the results obtained, the Sb-doped $Sn_{80\%}$-$W_{20\%}$-oxide coating composition was selected as the most intrinsically photoelectrochemically-active coating material for degradation of organic compounds in aqueous solutions.

Chapter 4 presents results on the electrochemical inactivation of bacteria in an electrolyte employing Sb-doped $Sn_{80\%}$-$W_{20\%}$-oxide anodes in a three-electrode batch electrochemical reactor. The influence of current density, initial population of bacteria, initial chloride concentration, pH, the type of bacterial strain (*E. coli* D21, *E. coli* O157:H7, and *E. faecalis*), the presence of natural organic matter (NOM) and radical scavengers (e. g. methanol) on the bacterial inactivation rate and thus the disinfection efficacy of the electrochemical system, was investigated. The anti-bactericidal ability of the developed Sb-doped $Sn_{80\%}$-$W_{20\%}$-oxide anodes was demonstrated by the inactivation results. Moreover, the calculations of the energy requirement for the experiments carried out at different current densities were performed and the optimal experimental conditions in terms of the energy efficiency were determined.

Chapter 5 presents results on the photoelectrocatalytic degradation of pharmaceutical carbamazepine using Sb-doped $Sn_{80\%}$-$W_{20\%}$-oxide anodes. For comparison purposes, photolysis (in the present of UV light, but in the absence of electrodes and applied current) and photocatalysis (in the present of UV light and electrodes in the cell, but in the absence of applied current) experiments were also performed. The effect of current density on the kinetics of

photoelectrocatalytic degradation of carbamazepine was investigated. The identification of intermediates and carbamazepine transformation products in the samples of photolysis, photocatalysis, and photoelectrocatalysis experiments were carried out, allowing the assessment of the toxicity of the final treated solution. Lastly, the energy consumption during photoelectrocatalytic degradation experiments performed at different current densities was estimated and the experimental conditions pertaining to the highest energy efficiency were identified.

Chapter 6 includes a summary and the main conclusions of the project, original contributions to knowledge, and recommendations for future works.

1.3. Contribution of Authors

This thesis is presented in the manuscript-based format in accordance with the McGill's "Guidelines for Thesis Preparation". Chapter 3 presents a manuscript that has been published in the journal of Applied Surface Science. Chapters 4 and 5 present manuscripts that have been submitted to scientific journals for consideration for publication. All the manuscripts were written by the author of this thesis. Co-authorship of the manuscripts presented in chapters 3–5 is detailed as follows:

- **S. Ghasemian, S. Omanovic.** "Fabrication and characterization of photoelectrochemically-active Sb-doped Sn_x-$W_{(100-x)\%}$-oxide anodes: Towards the removal of organic pollutants from wastewater". Applied Surface Science, 416 (2017) 318-328.

  Authors' contributions:

- S. Ghasemian: Developed experimental procedures, conducted experiments, performed analysis of the results, and wrote the manuscript.

- S. Omanovic: Supervised the research, helped in the design of experiments and revision of the manuscript.

- **S. Ghasemian, B. Asadishad, S. Omanovic. N. Tufenkji.** "Electrochemical disinfection of bacteria-laden water using antimony-doped tin-tungsten oxide electrodes", submitted.

Authors' contributions:

- S. Ghasemian: Conducted experiments, performed analysis of the results, and wrote the manuscript.
- B. Asadishad: Helped in the design of experiments, and in teaching and training of the handling of bacteria and analysis of microbial samples, and revised the manuscript.
- S. Omanovic and N. Tufenkji: Supervised the research and revised the manuscript.

- **S. Ghasemian, D. Nasuhoglu, S. Omanovic, V. Yargeau.** "Photoelectrochemical degradation of pharmaceutical carbamazepine using Sb-doped $Sn_{80\%}$-$W_{20\%}$-oxide/Ti Anodes", submitted.

Authors' contributions:

- S. Ghasemian: Designed and conducted experiments, performed analysis of the results, and wrote the manuscript.
- D. Nasuhoglu: Helped in the design of experiments and revised the manuscript.
- S. Omanovic and V. Yargeau: Supervised the research and revised the manuscript.

1.4. References

[1] M. Panizza, G. Cerisola, Direct And Mediated Anodic Oxidation of Organic Pollutants, Chemical Reviews, 109 (2009) 6541-6569.

[2] J.O. Tijani, O.O. Fatoba, G. Madzivire, L.F. Petrik, A Review of Combined Advanced Oxidation Technologies for the Removal of Organic Pollutants from Water, Water, Air, & Soil Pollution, 225 (2014) 2102.

[3] C.B. Chidambara Raj, H. Li Quen, Advanced oxidation processes for wastewater treatment: Optimization of UV/H2O2 process through a statistical technique, Chemical Engineering Science, 60 (2005) 5305-5311.

[4] W.H. Glaze, Drinking-water treatment with ozone, Environmental Science & Technology, 21 (1987) 224-230.

[5] I. Abbas, S. Zaheer, ADVANCED OXIDATION PROCESS FOR WASTEWATER

TREATMENT: A REVIEW, American International Journal of Research in Science, Technology, Engineering & Mathematics, 7 (2014) 189-191.

[6] A. Matilainen, M. Sillanpää, Removal of natural organic matter from drinking water by advanced oxidation processes, Chemosphere, 80 (2010) 351-365.

[7] C.A. Martínez-Huitle, L.S. Andrade, Electrocatalysis in wastewater treatment: recent mechanism advances, Química Nova, 34 (2011) 850-858.

[8] J. Bergendahl, J. O'Shaughnessy, Advanced oxidation processes for wastewater treatment, Journal of New England Water Environment Association, 38 (2004) 179-189.

[9] G. Chen, Electrochemical technologies in wastewater treatment, Separation and Purification Technology, 38 (2004) 11-41.

[10] G. Patermarakis, E. Fountoukidis, Disinfection of water by electrochemical treatment, Water Research, 24 (1990) 1491-1496.

[11] K. Jüttner, U. Galla, H. Schmieder, Electrochemical approaches to environmental problems in the process industry, Electrochimica Acta, 45 (2000) 2575-2594.

[12] O. Ganzenko, D. Huguenot, E.D. van Hullebusch, G. Esposito, M.A. Oturan, Electrochemical advanced oxidation and biological processes for wastewater treatment: a review of the combined approaches, Environmental Science and Pollution Research, 21 (2014) 8493-8524.

[13] C.A. Martínez-Huitle, E. Brillas, Decontamination of wastewaters containing synthetic organic dyes by electrochemical methods: A general review, Applied Catalysis B: Environmental, 87 (2009) 105-145.
[14] H. Zhang, G. Chen, D.W. Bahnemann, Photoelectrocatalytic materials for environmental applications, Journal of Materials Chemistry, 19 (2009) 5089-5121.
[15] N. Philippidis, E. Nikolakaki, S. Sotiropoulos, I. Poulios, Photoelectrocatalytic inactivation of E. coli XL-1 blue colonies in water, Journal of Chemical Technology & Biotechnology, 85 (2010) 1054-1060.
[16] C. Comninellis, G. Chen, Electrochemistry for the Environment, Springer New York, 2009.
[17] P.S. Patel, N. Bandre, A. Saraf, J.P. Ruparelia, Electro-catalytic Materials (Electrode Materials) in Electrochemical Wastewater Treatment, Procedia Engineering, 51 (2013) 430-435.
[18] S. Trasatti, Electrocatalysis: understanding the success of DSA®, Electrochimica Acta, 45 (2000) 2377-2385.
[19] R.T. Pelegrini, R.S. Freire, N. Duran, R. Bertazzoli, Photoassisted Electrochemical Degradation of Organic Pollutants on a DSA Type Oxide Electrode: Process Test for a Phenol Synthetic Solution and Its Application for the E1 Bleach Kraft Mill Effluent, Environmental Science & Technology, 35 (2001) 2849-2853.
[20] P. Peralta-Zamora, Photoelectrochemical or electrophotochemical processes?, Journal of the Brazilian Chemical Society, 21 (2010) 1621-1625.

CHAPTER 2

2. Background and Literature Review

2.1. Conventional Wastewater Treatment Methods

Most-commonly employed conventional wastewater treatment techniques include physical, chemical, and biological processes that are designed to remove two types of wastes [1]:

- Inorganic wastes (physical-chemical treatment)
- Aqueous/organic wastes (chemical-biological treatment)

Each of these types of treatment processes is briefly described below.

Physical treatment processes are generally the first step in wastewater treatment designed to remove small and large amounts of dissolved and suspended materials without altering their chemical structure. These processes mainly employ naturally-occurring forces (*e. g.* gravity and electrostatic forces) or physical barriers (*e. g.* filters) to separate and concentrate substances. Physical treatment processes include screening, sedimentation, flotation, filtration, and adsorption. Chemical treatment processes refer to processes that use auxiliary chemicals to promote chemical reactions and change the chemical structure of the components with the goal of removal or reduction of the toxicity of specific components. Oxidation and precipitation are two examples of chemical treatment processes. In biological treatment, microorganisms such as algae, fungi, or bacteria are used under aerobic or anaerobic conditions to decompose and/or transform the dissolved organic compounds into a dense biomass that can be easily separated from the treated effluent by sedimentation. Application of pre-treatment processes such as chemical precipitation of heavy metals can increase the efficiency of biological degradation. The virtue of biological

treatment is its relatively low cost, but the main drawback is the lack of effectiveness in removal of recalcitrant and bio-refractory organic compounds. In addition, systems based on biological treatment are mostly large foot-print systems.

2.2. Advanced Oxidation Processes (AOPs)

Advanced oxidation processes (AOPs) have been defined by Glaze et al. (1987) [2, 3] as the chemical oxidation processes that involve *in situ* generation of highly reactive oxidizing species such as hydroxyl radicals ($^{\bullet}OH$) at ambient temperature and pressure in a sufficient quantity to effectively purify water. The yield of $^{\bullet}OH$ in processes involving ozone (O_3), hydrogen peroxide (H_2O_2), catalysts, and UV systems has also been reviewed in the concept of AOP [3, 4]. Later, the scope of AOPs has been extended to the processes based on the oxidative action of sulfate radicals ($SO_4^{\bullet-}$) [5, 6]. The oxidizing ability of an oxidant depends on its redox potential, E^O. The E^O value for several well-known oxidizing agents is listed in **Table 2-1**. All oxidants listed in **Table 2-1** are stronger than O_2, nevertheless, the oxidation reactions are often governed by the kinetic factors rather than the thermodynamic properties [4]. AOPs provide promising solutions for the treatment of wastewaters containing recalcitrant organics such as dyes, pharmaceuticals, and phenolic compounds that are difficult to degrade by means of existing conventional treatment methods due to their high chemical stability and/or toxicity towards microorganism. By application of AOPs, the powerful oxidants that are generated *in situ* attack complex pollutants and break them apart to simpler and less or even non-toxic compounds [4]. Moreover, AOPs are environmentally-friendly processes applicable on a wide variety of organic and inorganic contaminants, and usually require a significantly lower foot-print than the above-mentioned conventional processes.

Table 2-1

Standard oxidation-reduction potentials of oxidizing agents at 25°C and 1 atm. (pH 0).

Half redox reaction	E^O vs. SHE (Volts)	Reference
$F_2 + 2H^+ + 2e^- = 2HF$	3.05	[7]
$F_2 + 2e^- = 2F^-$	2.87	[7]
$HO^\bullet + H^+ + e^- = H_2O$	2.73	[8]
$SO_4^{\bullet-} + e^- = SO_4^{2-}$	2.60	[9]
$S_2O_8^{2-} + 2H^+ + 2e^- = 2HSO_4^-$	2.12	[7]
$O_3 + 2H^+ + 2e^- = O_2 + H_2O$	2.07	[7]
$HO^\bullet + e^- = OH^-$	2.02	[7]
$S_2O_8^{2-} + 2e^- = 2SO_4^{2-}$	2.01	[7]
$H_2O_2 + 2H^+ + 2e^- = 2H_2O$	1.77	[7]
$HClO_2 + 2H^+ + 2e^- = HClO + H_2O$	1.64	[7]
$HOCl + H^+ + 2e^- = Cl^- + H_2O$	1.48	[7]
$Cl_2 + 2e^- = 2Cl^-$	1.36	[7]
$O_3 + H_2O + 2e^- = O_2 + 2OH^-$	1.24	[7]
$O_2 + 4H^+ + 4e^- = 2H_2O$	1.23	[7]

$ClO_{2\,(aq)} + e^- = ClO_2^-$	0.95	[7]
$ClO^- + H_2O + 2e^- = Cl^- + 2OH^-$	0.84	[7]
$ClO^{2-} + 2H_2O + 4e^- = Cl^- + 4OH^-$	0.76	[7]

2.2.1. AOPs Based on Hydroxyl Radicals

Hydroxyl radicals are the second strongest inorganic oxidant after fluorine (F_2) (**Table 2-1**). Having a half-life of approximately 10^{-9} s [10], •OH can only be produced *in situ* during the application of different methods. Hydroxyl radicals are stable over a wide range of pH up to pH 10 and exhibit higher oxidizing activity under acidic conditions [4]. Hydroxyl radicals possess high and non-selective reactivity and thus can react with most types of organics and inorganics. Their reaction with organic compounds can occur through four different pathways: hydroxy addition, hydrogen abstraction, electron transfer, and radical combination [4]. The reaction of hydroxyl radicals with organic compounds with carbon-carbon multiple bonds produces carbon-centered radicals, *e. g.*:

$$HO^{\bullet} + C_6H_6 \rightarrow {}^{\bullet}C_6H_6OH \qquad (2\text{-}1)$$

Hydrogen abstraction usually takes place in reaction of •OH with unsaturated organics, *e. g.*:

$$HO^{\bullet} + CH_3COH_3 \rightarrow CH_2COH_3 + H_2O \qquad (2\text{-}2)$$

Electron transfer usually occurs when •OH react with inorganic ions, *e. g.*:

$$HO^{\bullet} + Fe^{2+} \rightarrow OH^- + Fe^{3+} \qquad (2\text{-}3)$$

Reactions involving both hydroxy addition and hydrogen abstraction can result in mineralization of the organic compound. For example, mineralization of benzene through a serial reaction [4]:

$$HO^{\bullet} + HOOC - C_4H_4 - COOH \rightarrow products + CO_2 + H_2O \quad (2\text{-}4)$$

The mechanisms of $^{\bullet}$OH generation in most common AOPs applied in wastewater treatment are briefly described below.

2.2.2. AOPs Based on Ozone

Ozone (O_3), with an oxidation potential of 2.07 V vs. SHE, is known as a strong oxidant. However, due to its selective oxidation action, O_3 discriminately reacts with ionized or dissociated form of organic compounds, rather than the original form [11]. Under certain conditions, non-selective $^{\bullet}$OH can be produced from O_3 according to the following reaction [11]:

$$3O_3 + H_2O \rightarrow 2HO^{\bullet} + 4O_2 \quad (2\text{-}5)$$

The production of $^{\bullet}$OH can be greatly enhanced in the presence of other oxidizing species such as H_2O_2, as expressed by a two-step reaction:

$$H_2O_2 \rightarrow HO_2^- + H^+ \quad (2\text{-}6)$$

$$HO_2^- + O_3 \rightarrow HO^{\bullet} + O_2^- + O_2 \quad (2\text{-}7)$$

Under UV irradiation, H_2O_2 is first generated from the photolysis of O_3, leading to a subsequent production of $^{\bullet}$OH:

$$O_3 + H_2O + hv \rightarrow H_2O_2 + O_2 \quad (2\text{-}8)$$

$$H_2O_2 + hv \rightarrow 2HO^{\bullet} \quad (2\text{-}9)$$

2.2.3. AOPs Based on Hydrogen Peroxide (Fenton-Related Processes)

Iron is the most widely used metal to react with H_2O_2 in water and produce hydroxyl radicals in the so-called Fenton process. Although $^{\bullet}OH$ is recognized as the primary reactive product in Fenton processes, some other reactive species are also produced. Fenton-related processes typically involve the following reactions [11]:

$$Fe^{2+} + H_2O_2 \rightarrow Fe^{3+} + HO^{\bullet} + OH^{-} \quad (2\text{-}10)$$

$$Fe^{3+} + H_2O_2 \rightarrow Fe^{2+} + HO_2^{\bullet} + H^{+} \quad (2\text{-}11)$$

$$HO^{\bullet} + H_2O_2 \rightarrow HO_2^{\bullet} + H_2O \quad (2\text{-}12)$$

$$HO^{\bullet} + Fe^{2+} \rightarrow Fe^{3+} + HO^{-} \quad (2\text{-}13)$$

$$2HO_2^{\bullet} \rightarrow H_2O_2 + O_2 \quad (2\text{-}14)$$

Hydroxyl radicals are produced from the reaction of Fe^{2+} with H_2O_2 through electron transfer (Eq. (2-10)). However, the $^{\bullet}OH$ yield can be diminished by the scavenging effect of Fenton reagents, as shown in Eqs. (2-11) and (2-12). Therefore, the molar ratio of Fe^{2+} to H_2O_2 should be optimized for minimization of the undesired scavenging reactions.

2.2.4. AOPs Based on Sulfate Radical

Persulfate ion ($S_2O_8^{2-}$) is one of the strongest oxidants in aqueous solution with a standard oxidation potential (E^O) of 2.01 V. However, the oxidation reactions involving this ion are kinetically slow at room temperature [12]. Persulfate ions can be activated by application of sufficient heat [13, 14], UV irradiation [15], or transition metal ions (*e. g.* Fe^{2+} and Fe^{3+}) [16, 17]

to produce sulfate radicals ($SO_4^{\bullet-}$, E^O = 2.6 V) which are more powerful oxidants, through following reactions [18]:

$$S_2O_8^{2-} + \Delta/hv\,(heat/UV) \rightarrow 2SO_4^{\bullet-} \quad (2\text{-}15)$$

$$S_2O_8^{2-} + M^{n+} \rightarrow SO_4^{\bullet-} + SO_4^{2-} + M^{(n+1)+} \quad (2\text{-}16)$$

Highly reactive sulfate radicals ($SO_4^{\bullet-}$) can further start a series of radical chain reactions to degrade organic compounds (R), as expressed below [19]:

$$S_2O_8^{2-} + R\,(organic\ compounds) \rightarrow 2SO_4^{\bullet-} + R^{\bullet} \quad (2\text{-}17)$$

$$SO_4^{-} + H_2O \rightarrow HO^{\bullet} + HSO_4^{-} \quad (2\text{-}18)$$

$$SO_4^{-} + R \rightarrow R^{\bullet} + SO_4^{2-} \quad (2\text{-}19)$$

$$HO^{\bullet} + R \rightarrow R^{\bullet} + OH^{-} \quad (2\text{-}20)$$

$$R^{\bullet} + S_2O_8^{2-} \rightarrow SO_4^{\bullet-} + products \quad (2\text{-}21)$$

2.2.5. AOPs Based on UV Irradiation (Photolysis and Photocatalysis)

Hydroxyl radicals can be produced by the action of photons in the presence of proper photocatalysts (photocatalysis) or oxidants (photolysis). Photocatalysis has shown to be a promising technique for the treatment of wastewaters containing organic contaminants [20, 21]. Briefly, when a photosensitive substrate (*i. e.* semiconductor photocatalyst) is irradiated with a suitable energy (equal to or greater than its band gap), electrons from the valence band (VB) move to the conduction band (CB), resulting in the creation of electron-hole pairs (e^-/h^+). **Figure 2-1** shows a schematic of the photocatalysis through a semiconductor photocatalyst.

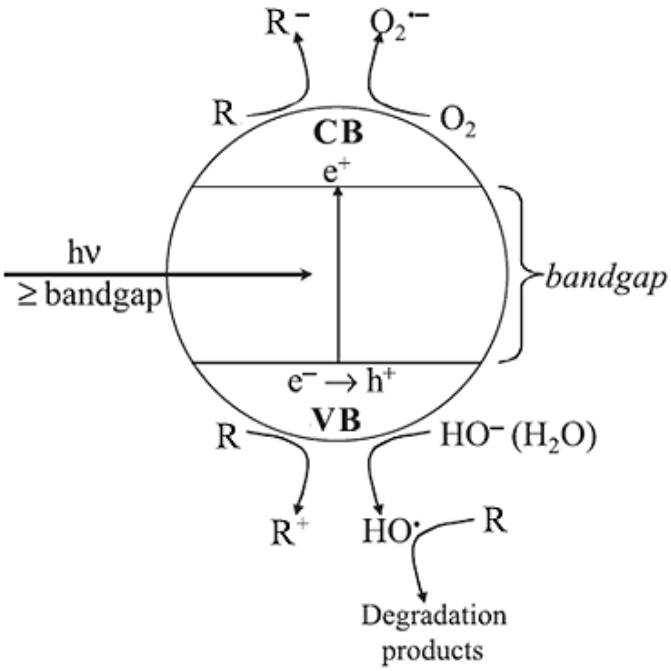

Figure 2-1: Schematic of a semiconductor-mediated photocatalysis [22].

The performance of a photocatalytic process depends on the reactivity of electron-hole pairs, which are photo-generated on the semiconductor surface (photocatalyst) (S) under irradiation (hν):

$$S\ (semiconductor) + hv\ \leftrightarrow\ h_{VB}^{+} + e_{CB}^{-} \qquad (2\text{-}22)$$

Ideally, the generated holes (h^+) are neutralized by accepting electron from water (i.e. hydroxyl ions) to form surface-adsorbed hydroxyl radicals ($^{\bullet}OH)_{ads}$ species, which then efficiently oxidize organic pollutants (R):

$$h_{VB}^{+} + OH^{-} \rightarrow HO_{ads}^{\bullet} \qquad (2\text{-}23)$$

$$HO_{ads}^{\bullet} + R \rightarrow S + OH^{-} + products \qquad (2\text{-}24)$$

However, direct oxidation and direct reduction of the organic substance on the semiconductor surface can also take place through the photo-generated holes and electrons in the valence band

and conduction band, respectively (**Figure 2-1**). In order to minimize the recombination of the photo-generated charge carriers (e^-/h^+), the photocatalytic processes are generally assisted by introducing an electron-capture agent, e.g. molecular oxygen, into the solution, which is then reduced by electrons:

$$e_{CB}^- + O_2 \rightarrow O_2^{\bullet -} \quad (2\text{-}25)$$

Thus, the scavenging effect of oxygen increases the lifetime of photo-generated holes, which favorably contributes to the production of hydroxyl radicals and, consequently, improves the efficiency of the treatment process.

In addition, UV utilization may lead to $^{\bullet}$OH production in the presence of some oxidants such as H_2O_2 or O_3 [11]:

$$H_2O_2 + hv \rightarrow 2HO^{\bullet} \quad (2\text{-}26)$$

$^{\bullet}$OH can also be yielded through photolysis of water under radiation with a wavelength less than 254 nm, according to the following reaction [11]:

$$H_2O + hv \rightarrow HO^{\bullet} + H^{\bullet} \quad (2\text{-}27)$$

Catalysts can be used either in the form of suspension of particles or immobilized on solid supports. The use of catalysts as fine particles provides high surface area to volume ratio and minimizes the mass transfer limitations, however, the use of powder photocatalysts is associated with some problems [22, 23]: (i) difficulty in separating the catalysts from the purified medium that needs long sedimentation time or fine filters, (ii) low quantum efficiency for the process due to the poor penetration of light into the bulk solution, and (iii) need for electron scavengers such

as oxygen. On the other hand, a drawback of the immobilized phtocatalysis is that the reaction zone is reduced to the area proportional to the catalyst support.

2.2.6. Electrochemical Advanced Oxidation Processes

The utilization of electricity for water treatment was first proposed in England in 1889 [24]. Among AOPs, electrochemical technology has gained great attention in recent years for the treatment of wastes containing organic compounds [25, 26]. In some cases, electrochemical methods may be indispensable solution to remove refractory pollutants from wastewaters. The major advantage of electrochemical technology is its environmental compatibility owing to its ability to produce *in situ* oxidizing species by the action of "clean" electrons [27] without adding auxiliary chemicals or large amounts of catalyst into the medium, allowing the direct discharge of the treated effluents into the receiving water bodies where applicable [28, 29]. The other advantages of this technology include versatility, modularity, easy automation, high energy-efficiency, and mild operating conditions [27, 30]. The electrochemical technology offers two options for the degradation of organic contaminants in wastewaters [31]:

i) **Direct anodic oxidation:** in which the organic contaminant (R) is first adsorbed on the anode surface and then oxidized by the direct electron transfer to the anode (direct electrolysis) (**Figure 2-2**a), as expressed below:

$$R_{ads} \rightarrow products + ne^{-} \qquad (2\text{-}28)$$

This type of oxidation mainly occurs at the surface of anodes with high electrocatalytic activity, and generally exhibits low degradation efficiency. In this mechanism, the rate of anodic oxidation depends on the electrode activity, the diffusion rate of organic molecule to the active sites of anode, and current density [32].

ii) **Indirect anodic oxidation:** oxidation via intermediation of active species generated from water discharge such as:

(a) physically-adsorbed hydroxyl radicals $(\bullet OH)_{ads}$ at so-called "non-active" electrodes (**Figure 2-2**b), leading to total mineralization:

$$M + H_2O \rightarrow M - HO^{\bullet}_{ads} + H^+ + e^- \quad (2\text{-}29)$$

$$M - HO^{\bullet}_{ads} + R \rightarrow M + RO + H^+ + e^- \quad (2\text{-}30)$$

(b) chemically adsorbed oxygen in the structure of a metal oxide anode (MO) at so-called "active" electrodes where higher oxidation states are available on the electrode surface (**Figure 2-2**c), resulting in a partial mineralization:

$$M - HO^{\bullet}_{ads} \rightarrow MO + H^+ + e^- \quad (2\text{-}31)$$

$$MO + R \rightarrow M + RO \quad (2\text{-}32)$$

There is another anodic reaction that occurs competitively in aqueous electrolytes in most anodic processes, known as the oxygen evolution reaction (OER) (Eq. (2-33)). OER is an inevitable but undesirable side reaction since it consumes produced hydroxyl radicals and, therefore, reduces the efficiency of the treatment process.

$$HO^{\bullet}_{ads} + H_2O \rightarrow O_2 + 3H^+ + 3e^- \quad (2\text{-}33)$$

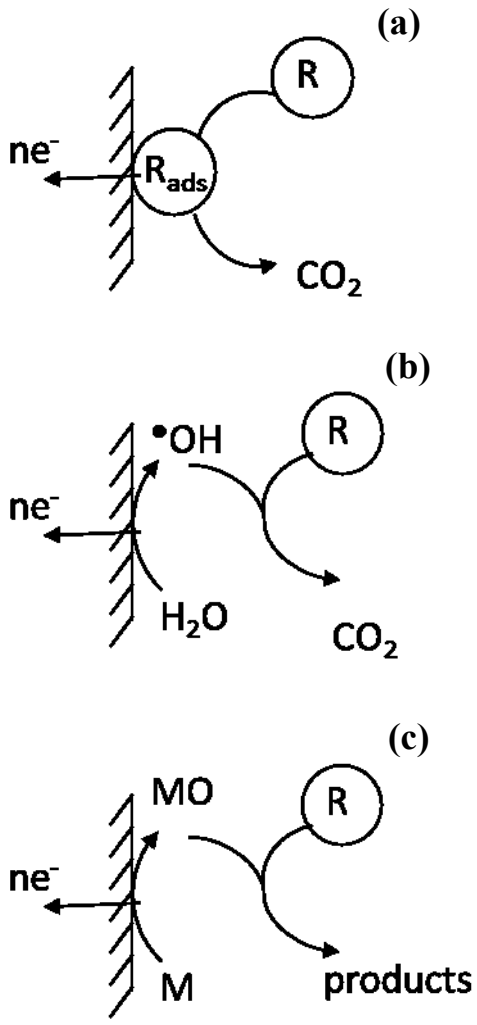

Figure 2-2: Schematics of the electrochemical processes for the degradation of organic compounds (R); (a) direct electrolysis , (b) hydroxyl radical-mediated oxidation, and (c) inorganic compound-mediated oxidation (Adopted from Comninellis and Chen (2010) [33]).

2.2.7. Photoelectrocatalysis

In recent decades, the emerging technology of photoelectrocatalysis has received great attention for the wastewater remediation. Photoelectocatalysis is the enhanced form of photocatalysis process, where an external anodic voltage is applied to draw electrons away from the catalyst, thus, minimizing the recombination of photo-generated electron-hole pairs and, consequently, increasing the degradation capacity of the system [34, 35]. Literature review has

revealed that combined treatment methods often provide greater pollutant removal efficiency and cost-effectiveness at the same time. A schematic of a photoelectrocatalytic cell is depicted in **Figure 2-3**. This figure shows that upon light absorption by photoactive semiconductors, electrons transit from VB to CB creating holes in VB. These holes react with water and produce powerful hydroxyl radicals which can effectively oxidize organic contaminants. Applying a potential bias can take the electrons away from the holes reducing the probability of electron-hole recombination, thus, enhancing the efficiency of the organic degradation. Photoelectrocatalytic processes offer several advantages over classical photocatalytic processes including no need for photo-generated electrons to be scavenged by O_2 (as they are drawn by the positive bias), no need for constant oxygen content in the solution (as the applied potential usually causes water reduction at the cathode), and, thus, no need for continuous air purging [23].

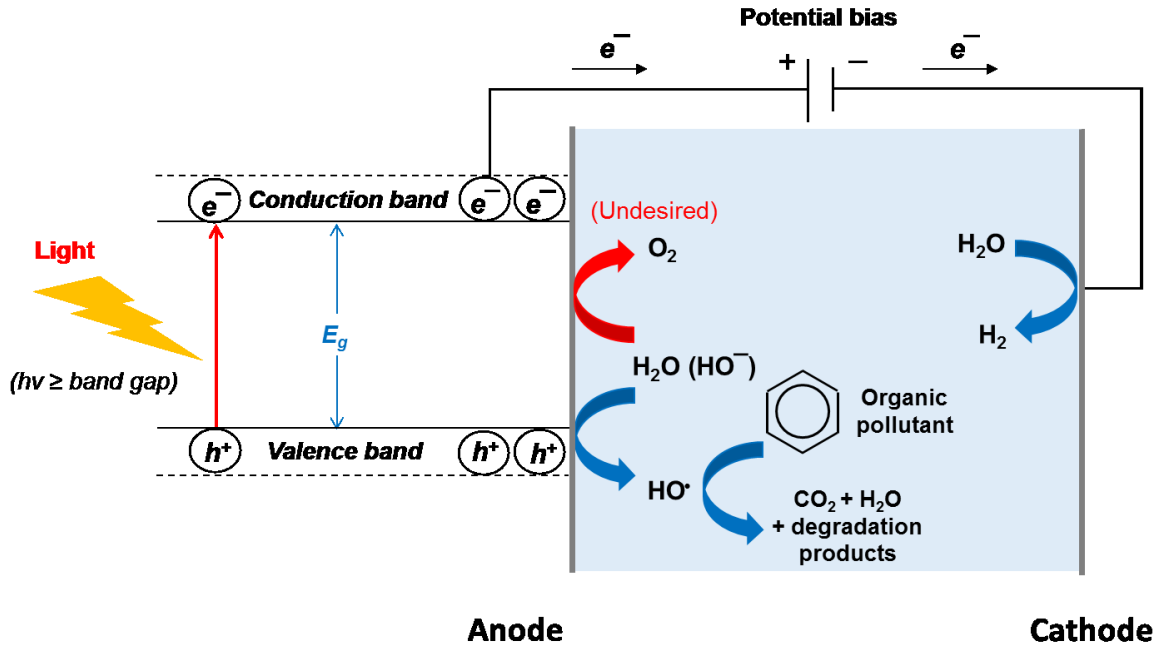

Figure 2-3: Schematic representation of a photoelectrocatalytic cell for the treatment of wastewaters containing organic contaminants.

2.3. Overview of Semiconductor Electrode Materials

Comninellis et al. [31, 36] found that the electrode material plays a very important role in governing both selectivity and efficiency of the processes. In other words, some anodes favor OER leading to a partial and selective oxidation of contaminants, while others favor the complete mineralization to CO_2. A large number of semiconductor oxide electrodes such as doped (mixed with impurity) or undoped PbO_2, WO_3, mixed metal oxides of Ti, Ru, Ir, Sn and Sb, and boron-doped diamond (BDD) have been tested for the treatment of organic-containing wastewaters [37-43]. Some common semiconductor oxide electrode materials and the advantages and drawbacks associated with their use in advanced treatment of wastewaters are listed in **Table 2-2**. The positions of VB and CB of several semiconductors in contact with aqueous electrolyte at pH 1 are illustrated in **Figure 2-4**. Theoretically, the semiconductors that have CB position more negative than hydrogen evolution potential (0 V vs. NHE at pH 0) can reduce H^+, and semiconductors having VB position more positive than oxygen evolution potential (1.23 V vs. NHE at pH 0) can oxidize water and, thus, can be used as catalysts for organic degradation.

Table 2-2

List of some common semiconductor oxide electrodes for wastewater treatment.

Semiconductor electrode	Advantages	Drawbacks
Boron-Doped Diamond (BDD)	- extremely wide potential window - inert surface with low adsorption / fouling properties - corrosion stability - very low double-layer capacitance - low sensitivity to dissolved oxygen	- high cost
PbO_2	- inexpensive - easy to prepare - good conductivity - chemical stability - high overpotential for oxygen evolution	- release of toxic lead ions
SnO_2	if doped with Sb: - good conductivity - high oxygen evolution overpotential	- low electrical conductivity at room temperature
TiO_2	- environmental compatibility - chemically and photo-chemically resistant - high stability - low cost	- wide band gap ($E_g \sim 3.2$ eV), as a result, low photoactivity under visible light - fast charge carrier recombination
WO_3	- narrow band gap ($E_g \sim 2.6$ eV), and, thus, high photocatalytic activity - high photostability in acidic aqueous solutions	- Instability toward anodic photocorrosion

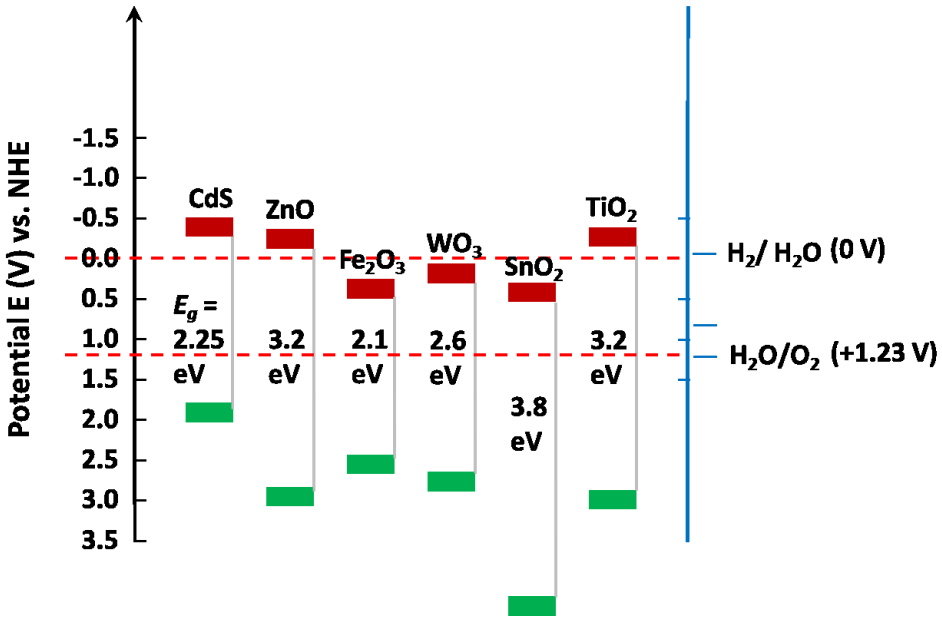

Figure 2-4: Energy diagram representing VB and CB energy levels of common semiconductors in contact with aqueous electrolyte at pH 1 (Adopted from Gratzel (2001) [44]).

2.3.1. Dimensionally Stable Anode (DSA®)-Type Electrodes

Dimensionally Stable Anodes (DSA®) are metal-oxide electrodes composed of a base metal (i.e. substrate, most frequently titanium) coated with pure or mixed electrochemically-active metal oxides of Ti, Ir, Ru, Sn, Sb, etc. DSA® electrodes have significantly improved many industrial processes such as water electrolysis, metal electrowinning, and electrochemical degradation of organic pollutants since their discovery by Beer in 1960's [45]. DSA®s possess large surface area and high mechanical and chemical resistance even at elevated current density and strongly acidic conditions [38]. The principles and success of DSA® electrodes have been discussed well by Trasatti in the literature [46, 47]. A DSA® should offer high oxygen evolution reaction (OER) overpotential and low surface fouling susceptibility in order to be a good candidate for the treatment of aqueous organic wastes [48].

2.3.2. Tin Oxide (SnO_2)

SnO_2 is an *n*-type semiconductor with band gap energy of 3.5 ~ 3.8 eV and have light absorption capacity only at wavelengths below 330 nm [40]. SnO_2 cannot be used alone to make electrodes, due to its low electrical conductivity at room temperature. However, doping with Ar, B, Bi, F, Cl, P, and particularly Sb increases its conductivity and makes it a promising electrode material for electro-oxidation of organics [49]. Especially, Sb-doped SnO_2 electrodes with oxygen evolution reaction (OER) potential of 1.9 V vs NHE have been widely used in electrochemical applications [50, 51]. A study of oxygen evolution at different anodes using *N,N*-dimethyl-*p*-nitrosoaniline (RNO) as a spin trap has shown that there is production and accumulation of $^{\bullet}OH$ radicals at the SnO_2 surface (during water discharge) leading to complete combustion of organics, whereas the selective oxidation of organics occurs at IrO_2 and Pt anodes [33]. The use of Sb-doped SnO_2 electrodes with titanium base (Ti/SnO_2-Sb_2O_5) for electrochemical treatment of wastewater was first proposed by Stucki et al. (1991) [52]. Their results showed complete TOC removal of organics, which was not influenced by pH change in the media. These electrodes demonstrated a much higher current efficiency in comparison with Pt electrodes. Further, Li et al. (2005) [53] found that the use of Ti/SnO_2-Sb resulted in a relatively fast mineralization of phenol and subsequent rapid oxidation of intermediate products such as benzoquinone and organic acids, whereas Ti/RuO_2 and Pt anodes exhibited low catalytic activity and the production of intermediates more refractory than the original compound.

2.3.3. Tungsten Oxide (WO_3)

WO_3 has a relatively narrow band gap (E_g ~ 2.6 eV) which makes it photoactive under visible light, even more than TiO_2 (E_g ~ 3.2 eV). Since the valence band energy level of WO_3 is more positive than the H_2O/O_2 oxidation potential (1.23 V vs. NHE at pH 0) (**Figure 2-4**), photo-generated holes in WO_3 have the capacity to oxidize a wide variety of compounds [40]. Another advantage of WO_3 is its relative photostability in acidic aqueous solutions, that allows its use as an effective photocatalyst for the removal of organic acids from wastewaters [54]. One of the major applications of WO_3 is hydrogen gas production through photocatalytic or photoelectrochemical water splitting under solar light, owing to its narrow band gap [55, 56]. The disadvantages of WO_3 is its thermodynamic instability toward anodic photocorrosion, and relatively high onset potential (*ca.* 0.4 V) for water oxidation in water splitting application [57]. Literature survey shows that many studies have been done on the application of WO_3 as an electron collector in conjunction with other semiconductors that have a more negative CB energy level (*e.g.* TiO_2, CdS) [58, 59], but there are relatively few reports on WO_3-based junctions where WO_3 is the main photoactive component.

2.3.4. Doping Semiconductor Oxide Electrodes

To extend the photocatalytic activity of semiconductors to visible light region and minimize the recombination of photo-generated electron-hole pairs, while maintaining or enhancing the electrocatalytic activity, proper modifications of the material should be made [60]. One suitable modification can be performed by doping the semiconductor with non-metal dopants such as Br, C, N, F, S, and Cl [61, 62] or metal dopants such as Fe, Pt, V, Au, Ag, Cu, and Ru [61, 63]. Doping semiconductors with ionic species can change the optical properties by introducing additional

energy levels into the band gap, thus, reducing the energy barrier such that a secondary electron transfer can happen between the metal and electron acceptors/donators in the redox reactions [40], as depicted in **Figure 2-5**. For instance, Sb-doped SnO_2 is considered as one of the most promising electrode materials for degradation of organic pollutants [64], while SnO_2 cannot be used directly as an electrode material due to its low conductivity at room temperature [50]. This approach is one of the best ways to tune the electronic structure of a semiconductor oxide. Doped semiconductors are classified into two types: *n*-type semiconductors in which the majority of charge carriers are electrons (*i. e.* photoabsorbers), and *p*-type semiconductors in which the majority of charge carriers are holes. Generally, photoanode materials (*n*-type semiconductor) can participate in oxidation reactions if their VB level is more positive than the oxygen evolution potential (1.23 V vs. NHE at pH 0), while photocathode materials (*p*-type semiconductors), must have a CB level more negative than hydrogen evolution potential (0 V vs. NHE at pH 0) [57].

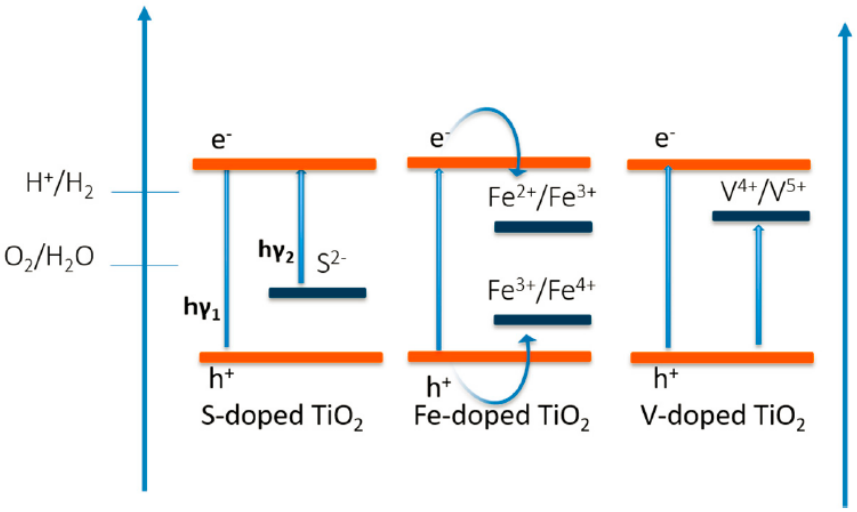

Figure 2-5: Schematic of band structure change in S-doped, Fe-doped, and V-doped TiO_2 [56].

2.3.5. Coupling Semiconductor Oxide Electrodes

Another approach to band alignment and minimization of the recombination rate of photo-generated electron-hole pairs is combining semiconductors that have different energy levels in terms of their valence and conduction band positions [65]. Coupling of semiconductors in proper alignment results in charge transfer from one component to another [57]. It is generally accepted that the coupled systems offer higher degradation rate and efficiency towards organic removal [64]. If one of the combined semiconductors has band gap energy equal or smaller than visible spectrum, these combinations can lead to solar light utilization. However, coupling of semiconductors does not always minimize the charge recombination, because the band structure of each component in junctions is controlled by several other factors such as surface area, defect density, crystal matrix, and quantum confinement effect [40].

TiO_2, the most popular photocatalyst (E_g ~ 3.2 eV), is widely used in combination with other semiconductors that have their valence and conduction band levels lower than those in TiO_2 [40, 66]. In that case, electrons transfer from TiO_2 to the other material and holes transfer in the opposite direction, resulting in the limited recombination in the same material [23]. **Figure 2-6** illustrates the energy diagram of two materials in contact (for the case of TiO_2-WO_3) as well as the hole and electron transfer directions. Energy diagrams illustrating valence and conduction band positions of potential semiconductors can be useful to find the suitable combinations.

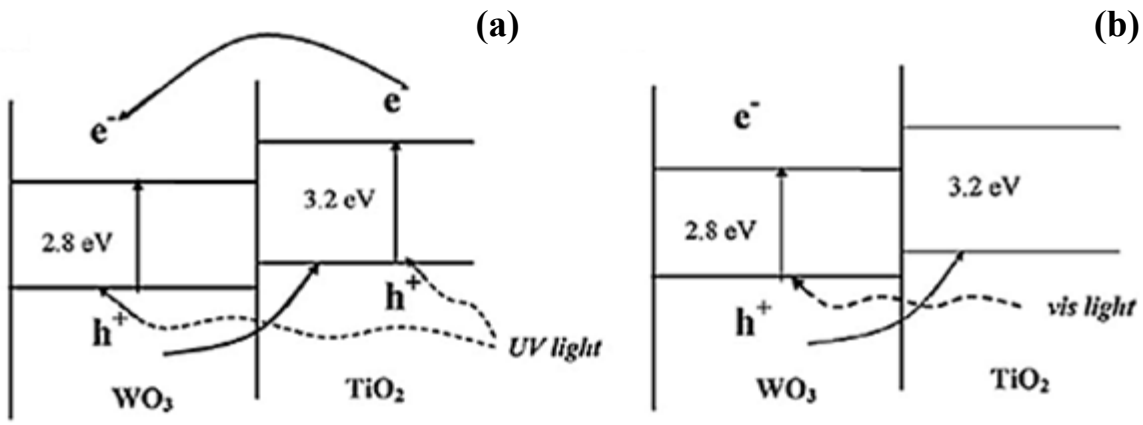

Figure 2-6: Energy diagrams of a TiO_2-WO_3 system for the case of (a) UV light and (b) visible light illumination [23].

2.4. Water Disinfection Methods

2.4.1. Conventional Water Disinfection Methods

Disinfection is almost always the final step of wastewater treatment to substantially reduce the number of pathogenic microorganisms in the water to be reused or discharged into the environment, in order to prevent the spread of waterborne diseases. The effectiveness of disinfection depends on a number of factors such as the characteristics of the water being treated (e. g. pH, turbidity, hardness, nitrogen content, etc.), type of disinfection and contact time, susceptibility of target microorganisms to the disinfectants, and other environmental variables. Conventional and advanced disinfection techniques include the use of chlorine, ozone, monochloramine, chlorine dioxide, hydrogen peroxide, UV light and the electrochemical treatment.

Chlorination is the most widely-used disinfection method due to its cost-effectiveness, long history of effectiveness, and residual disinfection effect that can prolong disinfection even after

the initial treatment [67]. However, the storage and transportation of dangerous chlorine is an issue and chlorination of water containing organic compounds can lead to the formation of potentially mutagenic and carcinogenic by-products such as trihalomethanes (THMs) and haloacetics acids (HAAs) [68]. Nieuwenhuijsen et al. (2000) [69] evaluated the toxicological and epidemiological data on chlorination disinfection by-products (DBPs) and their association with adverse reproductive outcomes. Utilization of chloramine, as a secondary disinfectant to chlorine, also resulted in the formation of some known DBPs associated with chlorination, but at lower concentrations [70]. A popular alternative to chlorine is ozone, that is a strong oxidant and can effectively oxidize many organic compounds and thereby destroy many kinds of microorganisms [71]. However, ozone is very unstable and needs to be generated onsite, which adds to the cost and complexity of the process [72]. This is also the case for chlorine dioxide [72]. Moreover, it has been shown that ozonation can lead to production of potentially harmful compounds including bromate and other brominated DBPs in the presence of concentrated bromide [73]. In terms of germicidal effectiveness, ozone is first in the order, followed by chlorine dioxide, then chlorine, and finally monochloramine [74]. UV irradiation is a physical, chemical-free, disinfection method that damages the genetic structure of pathogens, even parasites such as cryptosporidia or giardia, hindering their reproduction [75]. The disadvantages of UV disinfection are expensive lighting equipment, elevated energy consumption, and the lack of a residual effect.

2.4.2. Electrochemical Water Disinfection

Electrochemical water disinfection can be described as the removal or inactivation of microorganisms by passing an electric current through the solution by means of at least two electrodes (one anode and one cathode) and germicidal action of oxidants electrochemically generated onsite [76]. The mechanisms of action in electrochemical disinfection processes are: (1)

direct electron transfer and death of microorganisms at the electrode surface [77], and (2) indirect oxidation by means of disinfecting species generated *in situ* at the boundary between the electrode and the solution from water oxidation (*e. g.* hydroxyl radical, ozone, hydrogen peroxide) [78], or from the substances dissolved in the water (*e. g*. chloride) [76]. It has been shown that electric fields themselves damage cells mainly due to the irreversible permeabilization of the cell membrane [79].

2.4.2.1. Electrochemical Disinfection in the Absence of Chloride in the Solution

In a chloride-free solution, the generation of oxidants from water electrolysis, including hydroxyl radicals ($^{\bullet}OH$), atomic oxygen ($^{\bullet}O$), hydrogen peroxide (H_2O_2), and ozone (O_3) provides disinfection, as expressed in Eqs. (2-34) to (2-38) [80]:

$$H_2O \rightarrow HO^{\bullet} + H^+ + e^- \quad (2\text{-}34)$$

$$HO^{\bullet} \rightarrow O^{\bullet} + H^+ + e^- \quad (2\text{-}35)$$

$$2O^{\bullet} \rightarrow O_2 \quad (2\text{-}36)$$

$$2HO^{\bullet} \rightarrow H_2O_2 \quad (2\text{-}37)$$

$$O_2 + O^{\bullet} \rightarrow O_3 \quad (2\text{-}38)$$

Only anode materials with the characteristic of high overpotential for oxygen evolution (*e. g.* PbO_2, Sb-doped SnO_2, BDD, and glassy carbon) can produce ozone in water electrolysis [81], otherwise it is more favorable for water to be oxidized to oxygen (Eq. (2-39)) than ozone (Eq. (2-40)) [82]:

$$2H_2O \rightarrow O_2 + 4H^+ + 4e^- \quad (E^O = 1.23 \text{ V vs. NHE}) \quad (2\text{-}39)$$

$$3H_2O \rightarrow O_3 + 6H^+ + 6e^- \quad (E^O = 1.51 \text{ V vs. NHE}) \quad (2\text{-}40)$$

Reaction mechanisms vary with electrode materials. The primary cathodic reaction is the formation of hydrogen (Eq. (2-41)):

$$2H_2O + 2e^- \rightarrow H_2 + 2OH^- \quad (2\text{-}41)$$

2.4.2.2. Electrochemical Disinfection in the Presence of Chloride in the Solution

Under the conditions that chloride is present in the solution, the main anodic reaction is the formation of chlorine (Cl_2) [83], as shown in Eq. (2-42):

$$2Cl^- \rightarrow Cl_2 + 2e^- \quad (2\text{-}42)$$

The formation of hypochlorous acid (HClO) from hydrolysis of dissolved chlorine is the main side reaction, as shown in Eq. (2-43):

$$Cl_2(aq) + H_2O \rightarrow Cl^-(aq) + HClO + H^+(aq) \quad (2\text{-}43)$$

Then, hypochlorous acid can dissociate to hypochlorite ion (ClO^-), as per following equation:

$$HClO \rightarrow ClO^- + H^+ \quad (2\text{-}44)$$

The relative formation of each of these reactive chlorine species (RCS) (chlorine, hypochlorous acid, and hypochlorite ion) depends on pH, temperature, electrode material and electrode potential, and the summation of their concentrations is called the "active chlorine" content [83]. Electrochemical methods have been favorably used for disinfection of water that naturally contains chloride ions (10-250 mg/L), to produce active chlorine species as the main disinfectants responsible for killing microorganisms [84, 85]. Oxygen evolution is also an unfavorable side reaction in the anodic production of chlorine (Eq. (2-39)). The advantages of electrochemical disinfection include the possibility of *in situ* generation of disinfectants in a

desirable amount [77], relatively low energy requirement that allows utilization of green energy sources such as solar cells and fuel cells [86] and capacity of disinfecting water even in the absence of chloride ions and, thus, without formation of free chlorine and its potential toxic by-products (it should be noted that if chloride ions are not present, other ions should be in order to make the water ionically conductive) [77].

Li et al. (2011) [87] compared the *E. coli* cell surface damage after different disinfection treatments by means of scanning electron microscopy (SEM) (**Figure 2-7**). They observed more cell surface damage with the release of some intracellular materials after electrochemical treatment, compared with that after ozonation, chlorination, and chloramination. In a recent study, the subcellular mechanisms of *E. coli* inactivation by means of oxidants produced during electrochemical disinfection using BDD anode in solutions containing chloride, sulfate, or phosphate were investigated by Long et al. (2015) [88], as illustrated in **Figure 2-8**. They concluded that in the presence of chloride, *E. coli* inactivation could be the result of damage to the intracellular enzymatic systems. In sulfate solution, the cell inactivation was mainly induced by damage to the cell membrane and the loss of certain key proteins such as K+ ion transport systems. In phosphate-containing solution, mineralization of the organic components of the cell was mainly responsible for the cell inactivation.

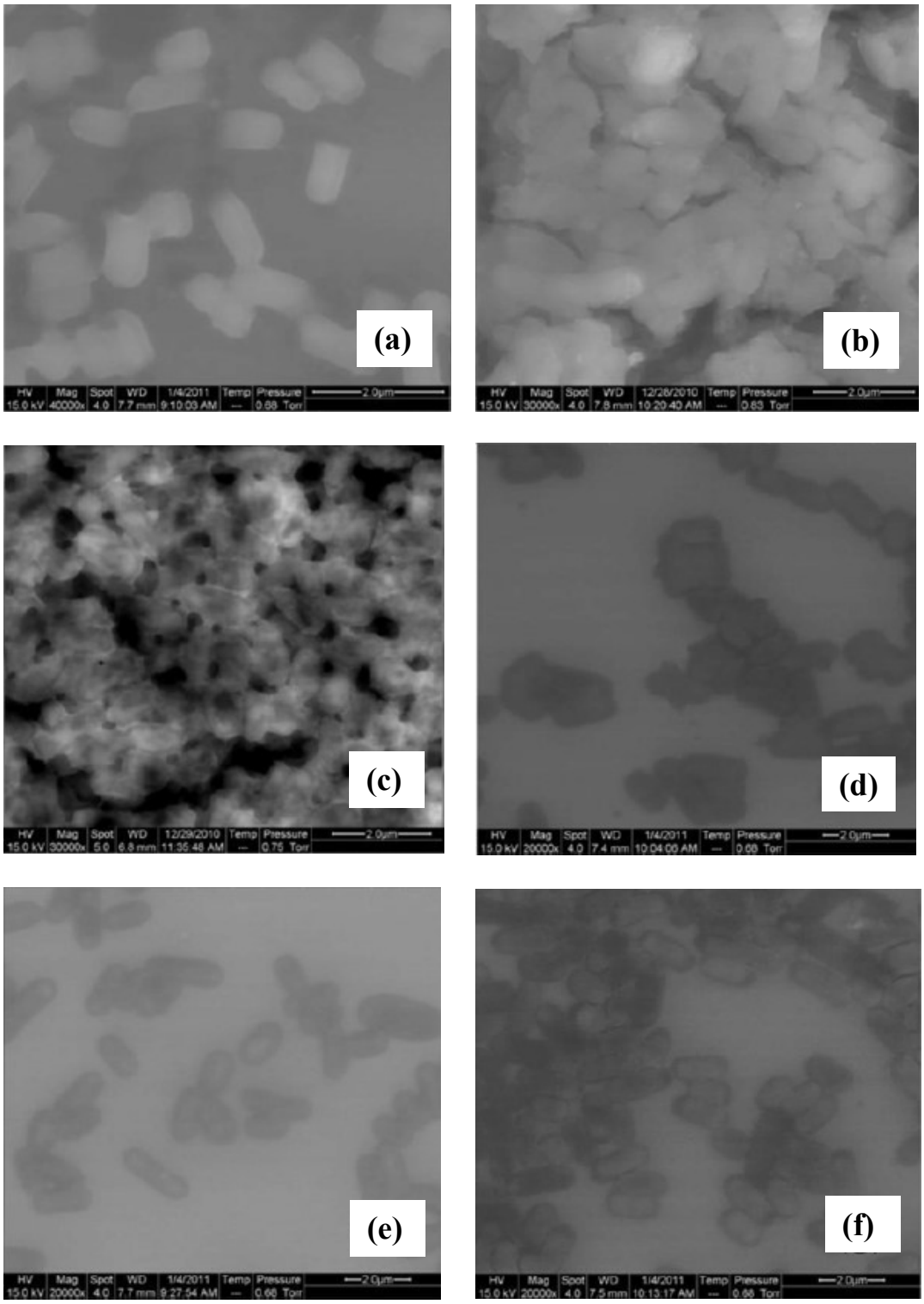

Figure 2-7: SEM images of *E. coli*. (a) Untreated cells; (b) cells after 30 min electrolysis; (c) cells after 60 min electrolysis; (d) cells after ozonation; (e) cells after chlorination; (f) cells after monochloramination [87].

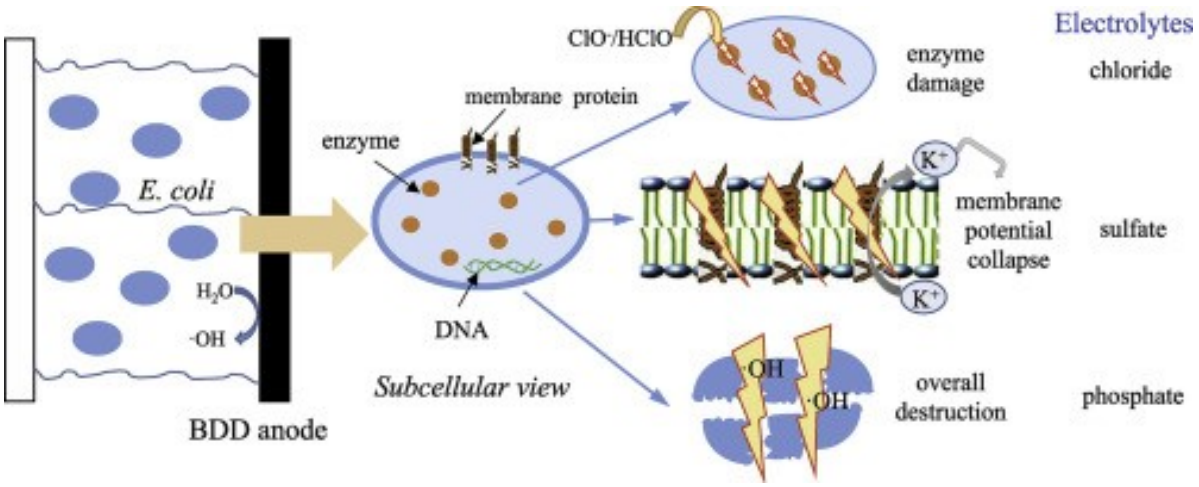

Figure 2-8: Schematic representing disinfecting actions of electrochemically generated oxidizing species against *E. coli* in electrolytes containing chloride, sulfate, and phosphate on BDD anode [88].

2.5. References

[1] National Guidelines on Physical-Chemical-Biological Tretament of Hazardous Waste, in, Canadian Council of the Ministers of the Environment, 1989.

[2] W.H. Glaze, Drinking-water treatment with ozone, Environmental Science & Technology, 21 (1987) 224-230.

[3] W.H. Glaze, J.-W. Kang, D.H. Chapin, The Chemistry of Water Treatment Processes Involving Ozone, Hydrogen Peroxide and Ultraviolet Radiation, Ozone: Science & Engineering, 9 (1987) 335-352.

[4] C.P. Huang, C. Dong, Z. Tang, Advanced chemical oxidation: Its present role and potential future in hazardous waste treatment, Waste Management, 13 (1993) 361-377.

[5] G.P. Anipsitakis, D.D. Dionysiou, Degradation of Organic Contaminants in Water with Sulfate Radicals Generated by the Conjunction of Peroxymonosulfate with Cobalt, Environmental Science & Technology, 37 (2003) 4790-4797.

[6] P. Manoj, K.P. Prasanthkumar, V.M. Manoj, U.K. Aravind, T.K. Manojkumar, C.T. Aravindakumar, Oxidation of substituted triazines by sulfate radical anion ($SO_4^{\bullet-}$) in aqueous medium: a laser flash photolysis and steady state radiolysis study, Journal of Physical Organic Chemistry, 20 (2007) 122-129.

[7] CRC Handbook of Chemistry and Physics, 84th Edition ed., CRC Press LLC, 2004.

[8] P. Wardman, Reduction Potentials of One‐Electron Couples Involving Free Radicals in Aqueous Solution, Journal of Physical and Chemical Reference Data, 18 (1989) 1637-1755.

[9] L. Eberson, Electron Transfer Reactions in Organic Chemistry, Springer-Verlag Berlin Heidelberg, Berlin, 1987.

[10] I.E. Dreosti, Trace elements, micronutrients, and free radicals, Humana Press, Clifton, N. J., 1991.

[11] Y. Deng, R. Zhao, Advanced Oxidation Processes (AOPs) in Wastewater Treatment, Current Pollution Reports, 1 (2015) 167-176.

[12] H. Marshall, LXXIV.-Contributions from the Chemical Laboratory of the University of Edinburgh. No. V. The persulphates, Journal of the Chemical Society, Transactions, 59 (1891) 771-786.

[13] K.-C. Huang, R.A. Couttenye, G.E. Hoag, Kinetics of heat-assisted persulfate oxidation of methyl tert-butyl ether (MTBE), Chemosphere, 49 (2002) 413-420.
[14] R.L. Johnson, P.G. Tratnyek, R.O.B. Johnson, Persulfate Persistence under Thermal Activation Conditions, Environmental Science & Technology, 42 (2008) 9350-9356.
[15] G.P. Anipsitakis, D.D. Dionysiou, Transition metal/UV-based advanced oxidation technologies for water decontamination, Applied Catalysis B: Environmental, 54 (2004) 155-163.
[16] C. Liang, C.J. Bruell, M.C. Marley, K.L. Sperry, Persulfate oxidation for in situ remediation of TCE. I. Activated by ferrous ion with and without a persulfate–thiosulfate redox couple, Chemosphere, 55 (2004) 1213-1223.
[17] C. Liang, C.J. Bruell, M.C. Marley, K.L. Sperry, Persulfate oxidation for in situ remediation of TCE. II. Activated by chelated ferrous ion, Chemosphere, 55 (2004) 1225-1233.
[18] D.A. House, Kinetics and Mechanism of Oxidations by Peroxydisulfate, Chemical Reviews, 62 (1962) 185-203.
[19] A.A. Berlin, Kinetics of radical-chain decomposition of persulfate in aqueous solutions of organic compounds, Kinet. Catal. (Engl. Transl.); (United States), (1986) Medium: X; Size: Pages: 34-39.
[20] M.R. Hoffmann, S.T. Martin, W. Choi, D.W. Bahnemann, Environmental Applications of Semiconductor Photocatalysis, Chemical Reviews, 95 (1995) 69-96.
[21] A. Mills, S. Le Hunte, An overview of semiconductor photocatalysis, Journal of Photochemistry and Photobiology A: Chemistry, 108 (1997) 1-35.
[22] P. Peralta-Zamora, Photoelectrochemical or electrophotochemical processes?, Journal of the Brazilian Chemical Society, 21 (2010) 1621-1625.
[23] J. Georgieva, E. Valova, S. Armyanov, N. Philippidis, I. Poulios, S. Sotiropoulos, Bi-component semiconductor oxide photoanodes for the photoelectrocatalytic oxidation of organic solutes and vapours: A short review with emphasis to TiO_2–WO_3 photoanodes, Journal of Hazardous Materials, 211–212 (2012) 30-46.
[24] P.P. Strokach, Mass Transfer Study of Three-Dimensional Electrodes Composed of Stacks of Nets, Electrochemistry in Industrial Processing and Biology, 55 (1975) 375.
[25] G. Chen, Electrochemical technologies in wastewater treatment, Separation and Purification Technology, 38 (2004) 11-41.

[26] Y. Feng, L. Yang, J. Liu, B.E. Logan, Electrochemical technologies for wastewater treatment and resource reclamation, Environmental Science: Water Research & Technology, 2 (2016) 800-831.
[27] K. Rajeshwar, J.G. Ibanez, Environmental Electrochemistry, Academic Press, San Diego, 1997.
[28] M.A. Oturan, An ecologically effective water treatment technique using electrochemically generated hydroxyl radicals for in situ destruction of organic pollutants: Application to herbicide 2,4-D, Journal of Applied Electrochemistry, 30 (2000) 475-482.
[29] I. Sirés, E. Brillas, Remediation of water pollution caused by pharmaceutical residues based on electrochemical separation and degradation technologies: A review, Environment International, 40 (2012) 212-229.
[30] C.A. Martinez-Huitle, S. Ferro, Electrochemical oxidation of organic pollutants for the wastewater treatment: direct and indirect processes, Chemical Society Reviews, 35 (2006) 1324-1340.
[31] C. Comninellis, Electrocatalysis in the electrochemical conversion/combustion of organic pollutants for waste water treatment, Electrochimica Acta, 39 (1994) 1857-1862.
[32] N. Mohan, N. Balasubramanian, C.A. Basha, Electrochemical oxidation of textile wastewater and its reuse, Journal of Hazardous Materials, 147 (2007) 644-651.
[33] C. Comninellis, G. Chen, Electrochemistry for the Environment, Springer-Verlag, New York, N. Y., 2010.
[34] Y. Zhang, X. Xiong, Y. Han, X. Zhang, F. Shen, S. Deng, H. Xiao, X. Yang, G. Yang, H. Peng, Photoelectrocatalytic degradation of recalcitrant organic pollutants using TiO_2 film electrodes: An overview, Chemosphere, 88 (2012) 145-154.
[35] S. Garcia-Segura, E. Brillas, Applied photoelectrocatalysis on the degradation of organic pollutants in wastewaters, Journal of Photochemistry and Photobiology C: Photochemistry Reviews, 31 (2017) 1-35.
[36] C. Comninellis, A. De Battisti, Electrocatalysis in anodic oxidation of organics with simultaneous oxygen evolution, Journal de Chimie Physique et de Physico-Chimie Biologique, 93 (1996) 673-679.

[37] Y. Samet, S.C. Elaoud, S. Ammar, R. Abdelhedi, Electrochemical degradation of 4-chloroguaiacol for wastewater treatment using PbO_2 anodes, Journal of Hazardous Materials, 138 (2006) 614-619.

[38] C.A. Martínez-Huitle, E. Brillas, Decontamination of wastewaters containing synthetic organic dyes by electrochemical methods: A general review, Applied Catalysis B: Environmental, 87 (2009) 105-145.

[39] X. Chen, G. Chen, F. Gao, P.L. Yue, High-Performance Ti/BDD Electrodes for Pollutant Oxidation, Environmental Science & Technology, 37 (2003) 5021-5026.

[40] H. Zhang, G. Chen, D.W. Bahnemann, Photoelectrocatalytic materials for environmental applications, Journal of Materials Chemistry, 19 (2009) 5089-5121.

[41] J. Luo, M. Hepel, Photoelectrochemical degradation of naphthol blue black diazo dye on WO_3 film electrode, Electrochimica Acta, 46 (2001) 2913-2922.

[42] K. Zhu, W. Zhang, H. Wang, Z. Xiao, Electro-Catalytic Degradation of Phenol Organics with SnO_2-Sb_2O_3/Ti Electrodes, CLEAN – Soil, Air, Water, 36 (2008) 97-102.

[43] J. Li, Z.-h. Yang, H.-y. Xu, P.-p. Song, J. Huang, R. Xu, Y.-j. Zhang, Y. Zhou, Electrochemical treatment of mature landfill leachate using Ti/RuO_2-IrO_2 and Al electrode: optimization and mechanism, RSC Advances, 6 (2016) 47509-47519.

[44] M. Gratzel, Photoelectrochemical cells, Nature, 414 (2001) 338-344.

[45] H.B. Beer, in: British Patents, England, 1965.

[46] S. Trasatti, Electrocatalysis: understanding the success of DSA®, Electrochimica Acta, 45 (2000) 2377-2385.

[47] S. Trasatti, Interfacial electrochemistry of conductive oxides for electrocatalysis, in: A. Wieckowski (Ed.) Interfacial Electrochemistry: Theory, Experiment, and Applications, Marcel Dekker, New York, N. Y., 1999, pp. 769.

[48] K.L. Meaney, S. Omanovic, $Sn_{0.86}$–$Sb_{0.03}$–$Mn_{0.10}$–$Pt_{0.01}$-oxide/Ti anode for the electro-oxidation of aqueous organic wastes, Materials Chemistry and Physics, 105 (2007) 143-147.

[49] M. Panizza, G. Cerisola, Direct And Mediated Anodic Oxidation of Organic Pollutants, Chemical Reviews, 109 (2009) 6541-6569.

[50] R. Kötz, S. Stucki, B. Carcer, Electrochemical waste water treatment using high overvoltage anodes. Part I: Physical and electrochemical properties of SnO_2 anodes, Journal of Applied Electrochemistry, 21 (1991) 14-20.

[51] Y.-H. Wang, G. Li, Q.-Y. Chen, X. Geng, W. Yan, Effect of drying periods on antimony-doped tin dioxide-coated titanium electrode, Journal of Solid State Electrochemistry, 17 (2013) 1985-1989.
[52] S. Stucki, R. Kötz, B. Carcer, W. Suter, Electrochemical waste water treatment using high overvoltage anodes Part II: Anode performance and applications, Journal of Applied Electrochemistry, 21 (1991) 99-104.
[53] X.-y. Li, Y.-h. Cui, Y.-j. Feng, Z.-m. Xie, J.-D. Gu, Reaction pathways and mechanisms of the electrochemical degradation of phenol on different electrodes, Water Research, 39 (2005) 1972-1981.
[54] D. Monllor‐Satoca, L. Borja, A. Rodes, R. Gómez, P. Salvador, Photoelectrochemical Behavior of Nanostructured WO_3 Thin‐Film Electrodes: The Oxidation of Formic Acid, ChemPhysChem, 7 (2006) 2540-2551.
[55] X. Liu, F. Wang, Q. Wang, Nanostructure-based WO_3 photoanodes for photoelectrochemical water splitting, Physical Chemistry Chemical Physics, 14 (2012) 7894-7911.
[56] T. Jafari, E. Moharreri, A. Amin, R. Miao, W. Song, S. Suib, Photocatalytic Water Splitting—The Untamed Dream: A Review of Recent Advances, Molecules, 21 (2016) 900.
[57] S.J.A. Moniz, S.A. Shevlin, D.J. Martin, Z.-X. Guo, J. Tang, Visible-light driven heterojunction photocatalysts for water splitting - a critical review, Energy & Environmental Science, 8 (2015) 731-759.
[58] L.J. Zhang, S. Li, B.K. Liu, D.J. Wang, T.F. Xie, Highly Efficient CdS/WO_3 Photocatalysts: Z-Scheme Photocatalytic Mechanism for Their Enhanced Photocatalytic H_2 Evolution under Visible Light, ACS Catalysis, 4 (2014) 3724-3729.
[59] Y. Li, P.-C. Hsu, S.-M. Chen, Multi-functionalized biosensor at WO_3–TiO_2 modified electrode for photoelectrocatalysis of norepinephrine and riboflavin, Sensors and Actuators B: Chemical, 174 (2012) 427-435.
[60] V.J. Babu, S. Vempati, T. Uyar, S. Ramakrishna, Review of one-dimensional and two-dimensional nanostructured materials for hydrogen generation, Physical Chemistry Chemical Physics, 17 (2015) 2960-2986.
[61] S. Piskunov, O. Lisovski, J. Begens, D. Bocharov, Y.F. Zhukovskii, M. Wessel, E. Spohr, C-, N-, S-, and Fe-Doped TiO_2 and $SrTiO_3$ Nanotubes for Visible-Light-Driven Photocatalytic Water

Splitting: Prediction from First Principles, The Journal of Physical Chemistry C, 119 (2015) 18686-18696.

[62] R. Asahi, T. Morikawa, T. Ohwaki, K. Aoki, Y. Taga, Visible-Light Photocatalysis in Nitrogen-Doped Titanium Oxides, Science, 293 (2001) 269-271.

[63] P. Maruthamuthu, M. Ashokkumar, K. Gurunathan, E. Subramanian, M.V.C. Sastri, Hydrogen evolution from water with visible radiation in presence of Cu(II)/WO_3 and electron relay, International Journal of Hydrogen Energy, 14 (1989) 525-528.

[64] C.-F. Lin, C.-H. Wu, Z.-N. Onn, Degradation of 4-chlorophenol in TiO_2, WO_3, SnO_2, TiO_2/WO_3 and TiO_2/SnO_2 systems, Journal of Hazardous Materials, 154 (2008) 1033-1039.

[65] K. Maeda, Z-Scheme Water Splitting Using Two Different Semiconductor Photocatalysts, ACS Catalysis, 3 (2013) 1486-1503.

[66] J. Resasco, H. Zhang, N. Kornienko, N. Becknell, H. Lee, J. Guo, A.L. Briseno, P. Yang, TiO_2/$BiVO_4$ Nanowire Heterostructure Photoanodes Based on Type II Band Alignment, ACS Central Science, 2 (2016) 80-88.

[67] G.C. White, Handbook of Chlorination and Alternative Disinfectants, Wiley, 1998.

[68] M.J. Pieterse, The Potential Health Risk of Trihalomethanes in Drinking Water: A Perspective, South African Journal of Science, 85 (1988) 166-170.

[69] M.J. Nieuwenhuijsen, M.B. Toledano, N.E. Eaton, J. Fawell, P. Elliott, Chlorination disinfection byproducts in water and their association with adverse reproductive outcomes: a review, Occupational and Environmental Medicine, 57 (2000) 73-85.

[70] A.C. Diehl, G.E.J. Speitel, J.M. Symons, S.W. Krasner, C.J. Hwang, S.E. Barrett, DBP Formation During Chloramination, American Water Works Association, 92 (2000) 76-90.

[71] A.M. Driedger, J.L. Rennecker, B.J. Mariñas, Sequential inactivation of Cryptosporidium parvum oocysts with ozone and free chlorine, Water Research, 34 (2000) 3591-3597.

[72] O.K. Dalrymple, E. Stefanakos, M.A. Trotz, D.Y. Goswami, A review of the mechanisms and modeling of photocatalytic disinfection, Applied Catalysis B: Environmental, 98 (2010) 27-38.

[73] S.D. Richardson, A.D. Thruston, T.V. Caughran, P.H. Chen, T.W. Collette, T.L. Floyd, K.M. Schenck, B.W. Lykins, G.-r. Sun, G. Majetich, Identification of New Ozone Disinfection Byproducts in Drinking Water, Environmental Science & Technology, 33 (1999) 3368-3377.

[74] F. Fiessinger, Y. Richard, A. Montiel, P. Musquere, Advantages and Disadvantages of Chemical Oxidation and Disinfection by Ozone and Chlorine Dioxide, in: H.v. Lelyveld, B.C.J. Zoeteman (Eds.) Studies in Environmental Science, Elsevier, 1981, pp. 245-261.
[75] J.R. Bolton, C.A. Colton, The Ultraviolet Disinfection Handbook, American Water Works Association, 2008.
[76] A. Kraft, Electrochemical Water Disinfection: A Short Review, Platinum Metals Review, 52 (2008) 177-185.
[77] J. Jeong, J.Y. Kim, M. Cho, W. Choi, J. Yoon, Inactivation of Escherichia coli in the electrochemical disinfection process using a Pt anode, Chemosphere, 67 (2007) 652-659.
[78] C.A. Martínez-Huitle, E. Brillas, Electrochemical Alternatives for Drinking Water Disinfection, Angewandte Chemie International Edition, 47 (2008) 1998-2005.
[79] J.C. Weaver, Y.A. Chizmadzhev, Theory of electroporation: A review, Bioelectrochemistry and Bioenergetics, 41 (1996) 135-160.
[80] W. Liang, J. Qu, L. Chen, H. Liu, P. Lei, Inactivation of Microcystis aeruginosa by Continuous Electrochemical Cycling Process in Tube Using Ti/RuO2 Electrodes, Environmental Science & Technology, 39 (2005) 4633-4639.
[81] P.C. Foller, C.W. Tobias, The anodic evolution of ozone, Journal of The Electrochemical Society, 129 (1982) 506-515.
[82] Y.-H. Wang, Q.-Y. Chen, Anodic Materials for Electrocatalytic Ozone Generation, International Journal of Electrochemistry, 2013 (2013) 7.
[83] M.V.B. Zanoni, J.J. Sene, H. Selcuk, M.A. Anderson, Photoelectrocatalytic Production of Active Chlorine on Nanocrystalline Titanium Dioxide Thin-Film Electrodes, Environmental Science & Technology, 38 (2004) 3203-3208.
[84] A. Kraft, M. Stadelmann, M. Blaschke, D. Kreysig, B. Sandt, F. Schröder, J. Rennau, Electrochemical water disinfection Part I: Hypochlorite production from very dilute chloride solutions, Journal of Applied Electrochemistry, 29 (1999) 859-866.
[85] G.E. Stoner, G.L. Cahen, M. Sachyani, E. Gileadi, The mechanism of low frequency a.c. electrochemical disinfection, Bioelectrochemistry and Bioenergetics, 9 (1982) 229-243.
[86] P. Drogui, S. Elmaleh, M. Rumeau, C. Bernard, A. Rambaud, Oxidising and disinfecting by hydrogen peroxide produced in a two-electrode cell, Water Research, 35 (2001) 3235-3241.

[87] H. Li, X. Zhu, J. Ni, Comparison of electrochemical method with ozonation, chlorination and monochloramination in drinking water disinfection, Electrochimica Acta, 56 (2011) 9789-9796.
[88] Y. Long, J. Ni, Z. Wang, Subcellular mechanism of Escherichia coli inactivation during electrochemical disinfection with boron-doped diamond anode: A comparative study of three electrolytes, Water Research, 84 (2015) 198-206.

CHAPTER 3

3. Fabrication and Characterization of Photoelectrochemically-active Sb-doped Sn_x-$W_{(100-x)\%}$-Oxide Anodes: Towards the Removal of Organic Pollutants from Wastewater

3.1. Preface

The ineffectiveness of conventional wastewater treatment methods in the removal of (bio)refractory or highly-concentrated organic compounds has manifested the urgent need for alternative treatment techniques. Electrochemical technology has proved to be effective in the removal of a wide variety organic compounds from wastewaters. The key part of the electrochemical systems is the electrode (in this case anode) which governs selectivity and efficiency of the process. The aim of this research was the development of photoelectrochemically-active yet inexpensive mixed metal oxide anode coating materials using tin and tungsten as the base elements for environmental applications: removal of organic compounds from wastewaters and water disinfection. This chapter is a reproduction of the manuscript published in the journal of Applied Surface Science, as:

S. Ghasemian, S. Omanovic. "Fabrication and characterization of photoelectrochemically-active Sb-doped Sn_x-$W_{(100-x)\%}$-oxide anodes: Towards the removal of organic pollutants from wastewater", Appl. Surf. Sci. 416 (2017) 318-328.

Abstract

Sn_x-$W_{(100-x)}$-oxide coatings (x = 0, 20, 40, 60, 80 and 100) doped with Sb (~ 3 at.%) were formed on a Ti substrate by a thermal deposition method in order to evaluate their potential use as electrodes for the photoelectrochemical oxidation of organic compounds. Surface microstructure/morphology and chemical composition of the coatings, as well as their photoelectrocatalytic activities were investigated using electrochemical and surface-characterization techniques. It was found that the surface roughness of the coatings depends on their composition, yielding an average value of $R_a = 1.1 \pm 0.5$ μm. The band gap energy was found to be independent on the coating composition up to the relative W/Sn at. ratio of 4/6, yielding an average value of 3.53 ± 0.05 eV (which corresponds to the band gap of doped SnO_2), but then it decreased for the three coatings with the highest W content, to an average value of 2.56 ± 0.10 eV (which corresponds to the value of pure WO_3). All the coatings were found to be photoactive under the anodic bias. Further, all the coatings were found to be photoelectrochemically active towards the degradation of phenol red dye solution under UV light irradiation. The intrinsic photoelectrocatalytic activity was found to be highest for the $Sn_{80\%}$-$W_{20\%}$-oxide electrode coating.

3.2. Introduction

One of the most serious environmental concerns of the 21st century is the increasing presence of synthetic and naturally occurring chemicals in the aquatic environment [1, 2]. These compounds include pharmaceuticals, hormones and phenolic organic contaminants which are prevalent in the wastewater of a number of industries such as oil refining, textiles, pharmaceuticals, pulp and paper, and plastics [3, 4], and have the potential to cause adverse ecological and/or human health effects. Conventional treatment methods such as physical, chemical or biological processes are in certain cases ineffective or insufficient in the removal or destruction of organics [5]. In recent decades, more and more efforts have been put in developing new technologies for the treatment of persistent organic contaminants [6, 7]. Ozonation and Advanced Oxidation Processes (AOPs) such as UV and visible light irradiation-based oxidation (e.g. photocatalysis) and electrochemical methods are among the most investigated techniques for the elimination of organic contaminants [8-10]. Electrochemical methods have proved to be effective for the treatment of organic-containing wastewaters, especially when it is combined with the photochemical oxidation process [11-14]. These processes involve the generation of strong oxidants such as hydroxyl radicals (•OH), because of the formation of electron-hole pairs in semiconductors upon photo-radiation, and consequent oxidative decomposition of organic molecules. In addition, direct electrochemical oxidation at the electrode surface (anode) is possible. The photo- and electrochemical technology offers many advantages such as low cost, simplicity, versatility, modularity, ease of control, environmental compatibility, and minimum waste production [15, 16].

Metal oxide materials are of great importance for environmental applications because of their photoactivity (capability to generate charge carriers when exposed to photo-radiation), electrochemical activity, and good stability [17]. Since the discovery of photoelectrochemical

water splitting using TiO_2 electrodes [18], this semiconductor photocatalyst has been of particular interest for wastewater purification as well as production of hydrogen as a renewable energy source [19, 20]. Until now, TiO_2 has been the most promising photocatalyst, because of its low cost, non-toxicity and good stability under irradiation [21, 22]. However, the lack of visible light activity due to its relatively wide band gap (3.2 eV) and low quantum efficiency, in addition to its low electrocatalytic activity for the anodic oxidation of organics, limits its practical applications. Therefore, more photo/electroactive metal oxide anode materials are needed. More closely, it is desirable to decrease the bandgap to facilitate the production of photogenerated charge carriers, while increasing (or at least maintaining) the electrochemical activity. In order to address the above-mentioned drawbacks, doping of TiO_2 and other metal-oxide photoactive electrode materials with a range of metals has been applied: anion-doping with N [23], C [24], S [25] and I [26], and cation-doping with some transition metals such as Pt [27], Au [28], Ag [29], Mg [30], Mn, Ru, Rh and Ir [31] to name but a few.

Sb-doped SnO_2 is considered as one of the most promising electrode materials for electrochemical degradation of organic pollutants [32-34], while undpoed SnO_2 (*n*-type semiconductor; $E_g \approx 3.5$ eV) cannot be used directly as an anode material due to its low conductivity at room temperature [35]. Another approach in the development of more (photo)electroactive anode materials is the use of coupled semiconductors such as SnO_2-TiO_2 [36, 37], WO_3-TiO_2 [38, 39], CeO_2-TiO_2 and ZrO_2-TiO_2 [37], which allows the desirable matching of their electronic band structure. It is generally accepted that the coupled systems offer higher degradation rate and efficiency in organic wastewater treatment [36]. In recent years, multi-component metal oxide semiconductors have also been extensively investigated for the effect of composition on their band gap and thus, the photocatalytic activity [40-46]. The ternary and

quaternary systems have shown enhanced solar-light response in addition to providing the possibility of band gap tuning, due to their various morphologies [47]. Zhang et al. [20] thoroughly reviewed the research and development of photoelectrocatalytic materials for environmental applications in their feature article.

Because of the interesting properties of doped SnO_2 as an electroactive material [48, 49] and WO_3 as a photoactive material [50, 51], these two materials were chosen as base electrode materials for their possible use as anodes for the wastewater treatment and disinfection. In this manuscript, we report results on the synthesis of antimony-doped tin-tungsten-oxide electrodes *via* a thermal deposition method and their characterization by electrochemical, optical, surface/structure techniques. Also, the effect of electrode composition on their photo- and electrochemical activity for degradation of phenol red dye was investigated. Their performance as anode materials for the oxidation of a pharmaceutical compound and for the water disinfection will be presented in separate manuscripts.

3.3. Materials and Methods

3.3.1. Electrode Preparation

Sb-doped Sn_x-$W_{(100-x)\%}$-oxide coatings (x = 0, 20, 40, 60, 80 and 100) were prepared on flat titanium substrates employing a thermal method. First, stock solutions of tin, tungsten and antimony salts were prepared by dissolving $SnCl_2.2H_2O$ (ACS reagent, ≥ 98.0%, Sigma Aldrich), $Na_2WO_4.2H_2O$ (Certified ACS, 100.0%, Fisher), and $SbCl_3$ (ACS reagent, ≥ 99.0%, Sigma Aldrich) salts in HCl (37wt.%, Fisher) and water. All solutions were prepared using ultra-pure deionized water (resistivity: 18.2 MΩ cm). For each coating composition, a precursor solution with a total metal content concentration of 0.3 M was prepared by mixing proper amounts of metal salt

stock solutions and adding deionized water to yield a final volume of 15 mL. The proper amount of each solution was calculated based on the desired composition of Sn and W in the coating material (Sb content of 3 mol% was kept constant in all coating compositions).

Titanium substrates, which were used as the support for metal-oxide films, were 15.9 mm diameter discs machined to a thickness of 2 mm for characterization experiments and 50 mm × 100 mm × 2 mm flat sheets for degradation experiments. Ti substrates were pretreated before the deposition of coatings: they were first mechanically polished using 600-grit SiC sandpaper, then washed ultrasonically in deionized water for 15 min, and then etched in a boiling solution of HCl (37wt.%) and water (1:1, v/v) for 30 min. Lastly, the substrates were rinsed sequentially with acetone, ethanol and deionized water and then dried with argon.

To form metal-oxide coatings, the precursor solution was applied onto the pretreated side of Ti substrate by brushing. The substrate was then dried in an oven at 110°C for 5 min to evaporate the solvent, and then placed into a preheated air furnace at atmospheric pressure and at 500°C for 15 min, followed by cooling in air at room temperature for 15 min. This process was repeated ten times (10 coats were formed). After the last application, the electrodes were annealed at 500°C for 2 hours in order to complete the formation of metal oxides in the coatings [52].

3.3.2. Coating Characterization

The active surface area of the as-prepared electrode coatings was determined by electrochemical measurements employing a ferricyanide/ferrocyanide redox reaction, in a three-electrode cell using a computer-controlled Potentiostat (Metrohm / Eco Chemie Autolab PGSTAT30). Graphite, separated from the working electrode compartment by a glass frit, served as counter electrode. All the potentials were measured versus a Saturated Calomel Electrode (SCE)

as reference. Electrochemical surface-area-determination experiments were carried out in 80 mL of 1 mM potassium hexacyanoferrate (III) ($K_3Fe(CN)_6$, also known as potassium ferricynide; ~ 99%, Sigma Aldrich) in 0.1 M KCl (≥ 99.0%, Fluka) at room temperature. The solution was deoxygenated by purging argon for 1 hr before the experiments, but the solution was not purged/stirred during the actual electrochemical experiment to ensure that the redox species were transported towards/form the electrode surface by pure diffusion.

The surface roughness of the coatings was measured by a confocal microscope (Leica DCM8 3D) using EPI-150X objective lens. To obtain information on the surface microstructure and elemental composition of the coatings, scanning electron microscopy (SEM) coupled with energy-dispersive X-ray spectroscopy (EDX) was performed on the samples at different parts of the surface using a Hitachi SU3500 scanning electron microscope. Transmission electron microscopy (TEM) images were obtained using FEI Tecnai G^2 F20 (200 kV) Cryo-STEM. X-ray photoelectron spectroscopy (XPS) measurements were carried out using a Thermo Scientific K-Alpha spectrometer equipped with an argon ion gun. The X-ray polychromatic source was AlKα (1486.6 eV). XPS survey scans of all samples were initially recorded to identify the elements present in the coating materials and their high-resolution spectra were acquired subsequently. The spectra were analysed using Avantage software (version 5.932) for data processing. Moreover, to examine the crystalline structure and lattice parameters of the electrode coatings, X-ray diffraction (XRD) analysis was performed employing a Bruker Discover D8-2D diffractometer with 0.5 mm dia. collimated Cu Kα (1.54 A) radiation at room temperature in a standard θ–2θ mode.

The optical band gap value for each coating composition was measured by photoluminescence (PL) spectroscopy employing a 266-nm excitation laser and by UV/Vis spectrometry (Thermo Scientific Evolution 300).

3.3.3. Degradation of Phenol Red Dye

The photoelectrocatalytic activity of as-prepared coatings was tested for the degradation of phenol red (PR) dye solution in a cylindrical batch reactor (Pyrex glass) under UV light irradiation using a 10W UV lamp (GPH212T5L, Atlantic Ultraviolet Corp.) with the maximum emission at 254 nm. A 550-mL solution of 0.1 mM PR in 0.1 M potassium phosphate buffer (pH 7) was used as the electrolyte. The temperature was set at 50°C at the beginning of experiments using a water bath. Filtered air was bubbled into the solution during the experiments to provide oxygen as an electron scavenger and for mixing. The working electrode was a 50 mm × 100 mm × 2 mm metal-oxide coated Ti electrode (only one side was coated by the oxide, while the other side was covered by an electrically insulating film). A 93 mm × 100 mm × 2 mm 316L stainless steel plate served as the counter electrode (cathode). The working electrode was sonicated in deionized water for 15 min before the experiments. Both electrodes were placed vertically in the cell at a separation distance of 5.5 cm, and the UV lamp was placed in between the two electrodes, in the middle of the cell. SCE was used as a reference electrode. During 2-hour PR degradation experiments, aliquots of 750 μL were taken from the solution at given intervals, diluted with 0.1 M potassium phosphate buffer, and subsequently analyzed by UV-Vis spectroscopy to determine PR concentration. Each experiment was performed at least 3 times. For comparison, photochemical and electrochemical experiments were also performed.

3.4. Results and Discussion

3.4.1. Surface Characterization

3.4.1.1. Scanning Electron Microscopy (SEM)

Figure 3-1 shows the SEM images displaying the microstructure of surfaces of as-prepared Sb-doped Sn-W-oxide coatings of different compositions. The morphology of the surfaces is typical of that for metal-oxide coatings [20], and it varies with changes in the coating composition. For the two pure compositions, Sn-oxide (**Figure 3-1**a) and W-oxide (**Figure 3-1**f), the surface displays a cauliflower-like morphology, while a cracked-mud morphology characterizes the mixed compositions in **Figure 3-1**c, d and e. The images indicate that the total surface area of the samples is larger than the corresponding geometric area, which will be discussed in more detail later in the manuscript. An elemental composition analysis of the coatings was performed at different locations on the surfaces using energy-dispersive X-ray spectroscopy (EDX). The results showed a good agreement between the actual average metal composition of the coatings and the nominal values (**Table 3-1**). An interesting finding was that Ti was also present in the coating, although it was not present in the precursor solution. The presence of Ti in the coating is due to its dissolution from the Ti substrate during the coating preparation method. Also, it has been proven that the affinity of titanium for oxygen is larger than that of tin and tungsten, and it is thus expected that Ti would diffuse towards the outer coating surface to form Ti-oxide [53].

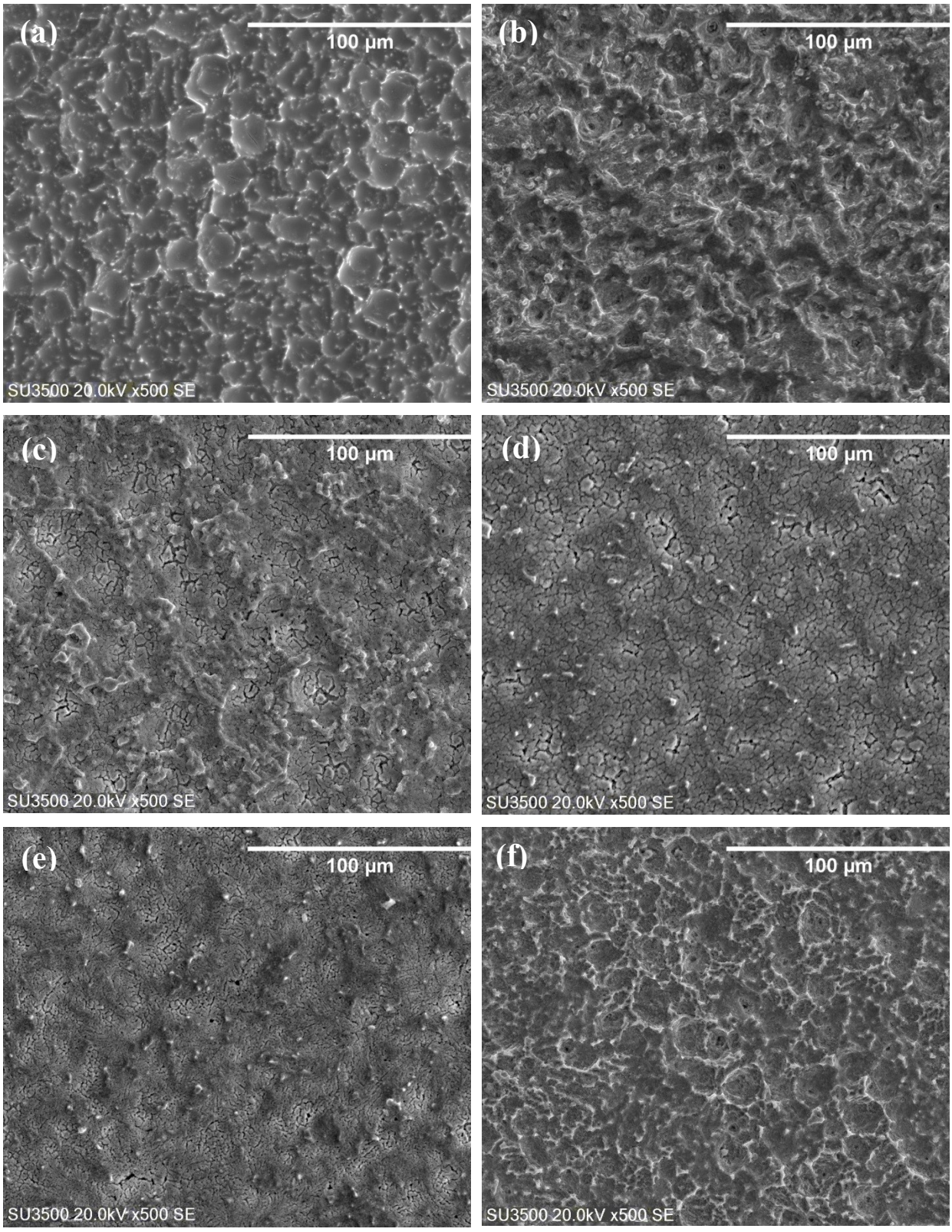

Figure 3-1: SEM images of Sn_x-W-$_{(100-x)\,\%}$-oxide coatings formed on a Ti substrate: (a) x = 100; (b) x = 80; (c) x = 60, (d) x = 40; (e) x = 20; (f) x = 0.

Table 3-1

Relative atomic percentage of Sn in Sn_x-$W_{(100-x)\%}$-oxide coatings (excluding the contribution of antimony, titanium and oxygen in the oxide film). Nominal values refer to the Sn content in the metal precursor solution. EDX and XPS values refer to the measured concentration of Sn in the surface of the coatings.

Sn content, at. %		
Nominal	EDX[a]	XPS[b]
0	2	0
20	22	36
40	36	42
60	51	54
80	76	95
100	99	100

[a]SD value: ± 2
[b]SD value: ± 5

3.4.1.2. Transmission Electron Microscopy (TEM)

Figure 3-2 represents TEM images of $Sn_{80\%}$-$W_{20\%}$-oxide. The ring electron diffraction pattern shown in **Figure 3-2**a is an indicator of a polycrystalline nature of the material. **Figure 3-2**b shows a TEM image taken in the bright field and demonstrates a nanostructured polycrystalline composite with an average crystallite size of 20-30 nm. Furthermore, distinct lattice planes with random orientations (**Figure 3-2**c) exhibit a high degree of crystallinity and isotropic behavior of the thin film.

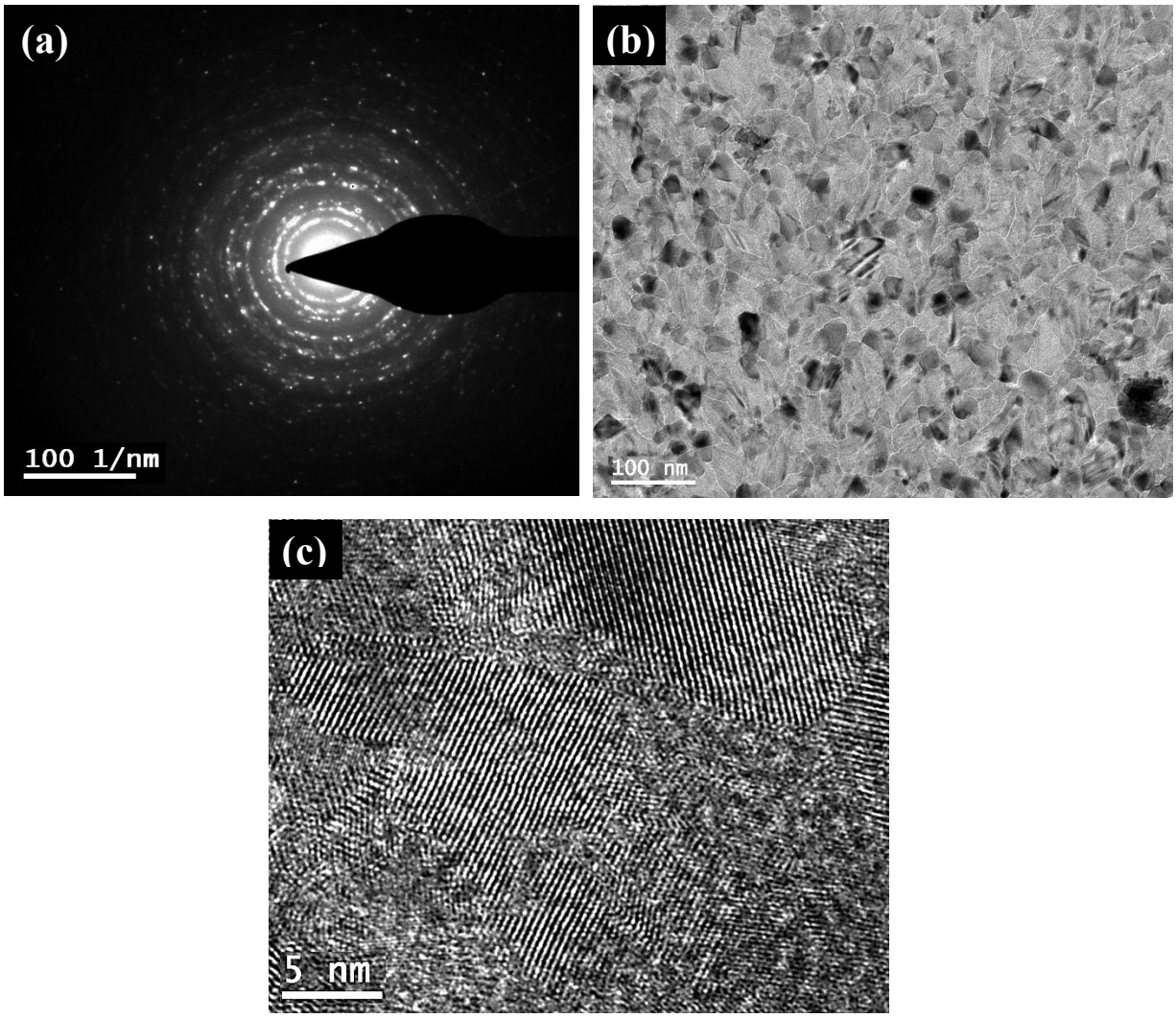

Figure 3-2: TEM images of $Sn_{80\%}$-$W_{20\%}$-oxide: (a) electron diffraction pattern; (b) polycrystalline structure; (c) lattice planes.

3.4.1.3. X-ray Photoelectron Spectroscopy (XPS)

To determine the chemical composition of the outer-most part of Sb-doped Sn-W-oxide coatings, XPS analysis was performed. As an example, results for $Sn_{20\%}$-$W_{80\%}$-oxide and $Sn_{80\%}$-$W_{20\%}$-oxide coatings are shown in **Figure 3-3**. To identify all elements in the coating material, general survey scans were first performed. Then, high-resolution binding energy spectra were recorded

in the C 1s, O 1s, W 4f, Sn 3d and Sb 3d regions. All the binding energy values were calibrated with respect to the peak of C 1s spectrum of adventitious carbon at 284.8 eV [54]. The typical doublet W 4f peaks were observed in the high-resolution core level spectra of all samples except pure Sn-oxide, as expected. As shown in **Figure 3-3**a, the W $4f_{7/2}$ and W $4f_{5/2}$ photoelectron peaks are, respectively, visible at around 35.6 and 37.7 eV for the $Sn_{20\%}$-$W_{80\%}$-oxide surface, and at 35.4 and 37.4 eV for the $Sn_{80\%}$-$W_{20\%}$-oxide surface, which is in agreement with the literature [47, 55-57]. The high-resolution XPS spectra in the W $4f_{7/2}$ region can be deconvoluted into two peaks at 34.5 and 35.6 eV for the $Sn_{20\%}$-$W_{80\%}$-oxide and into two peaks at 33.8 and 35.3 eV for the $Sn_{80\%}$-$W_{20\%}$-oxide coating, confirming the existence of W^{4+} and W^{6+}, respectively [47, 55-57]. According to the XPS results, the atomic ratio of W^{4+}/ W^{6+} on the most-outer part of the oxide surface is 1:29 for $Sn_{20\%}$-$W_{80\%}$-oxide and 1:5 for $Sn_{80\%}$-$W_{20\%}$-oxide, indicating that WO_3 is the predominant chemical state of W at the outermost part of the oxide coating surface (similar results were obtained for other coating compositions).

The XPS spectra in the Sn 3d region show binding energies of Sn $3d_{5/2}$ and Sn $3d_{3/2}$ peaks at 486.8 and 495.3 eV for $Sn_{20\%}$-$W_{80\%}$-oxide, and at 486.5 and 494.9 eV for $Sn_{80\%}$-$W_{20\%}$-oxide, respectively (**Figure 3-3**b). It is known that the Sn $3d_{5/2}$ photoelectron peak is expected to appear at 485 eV for pure Sn and within the range of 486.5–486.9 eV for Sn^{4+} oxide [47, 54, 55]. The Sn 3d core level peaks in **Figure 3-3**b show that in our thermally-prepared samples, tin exists as Sn^{4+} (e.g. SnO_2) in the outermost part region of the coating. XPS analyses of all the coating in this work suggest that the chemical oxidation states of W and Sn at the coating surface are not significantly affected by the change in the coating composition.

The main O 1s photoelectron peaks for $Sn_{20\%}$-$W_{80\%}$-oxide and $Sn_{80\%}$-$W_{20\%}$-oxide coatings were observed at 530.6 and 530.4 eV, respectively (**Figure 3-3**c). [55]. The O 1s peak for $Sn_{80\%}$-

$W_{20\%}$-oxide is shown in **Figure 3-3**c and can be deconvoluted into three components, the deconvoluted peak at 530.5 ± 0.1 (Peak A) is assigned to the oxygen in crystal lattice (O^{2-}), while the peaks at 531.9 ± 0.2 (Peak B) and 533.5 ± 0.2 (Peak C) can be assigned to the oxygen in hydroxyl groups (O-H) and surface adsorbed oxygen (O^{-}), respectively [56-58]. The result in **Figure 3-3**c demonstrates that oxygen is present in the metal-oxide coatings mostly as oxygen in the crystal lattice. The smaller peak observed at 540 ± 0.2 eV (Peak D) in **Figure 3-3**c corresponds to the Sb 3d3/2 transition [34, 47, 55], which can be attributed to Sb^{3+} (540.2 eV) as the main oxidation state of antimony in the coatings [55].

Table 3-1 shows the chemical composition of the produced metal oxide coatings. Unlike EDX, XPS penetrates only up to 10 nm below the surface. Thus, the data in the table show the relative enrichment of the outer-most part of the oxide film with Sn. This is, most likely, due to the higher affinity of Sn towards oxygen than that of W [53].

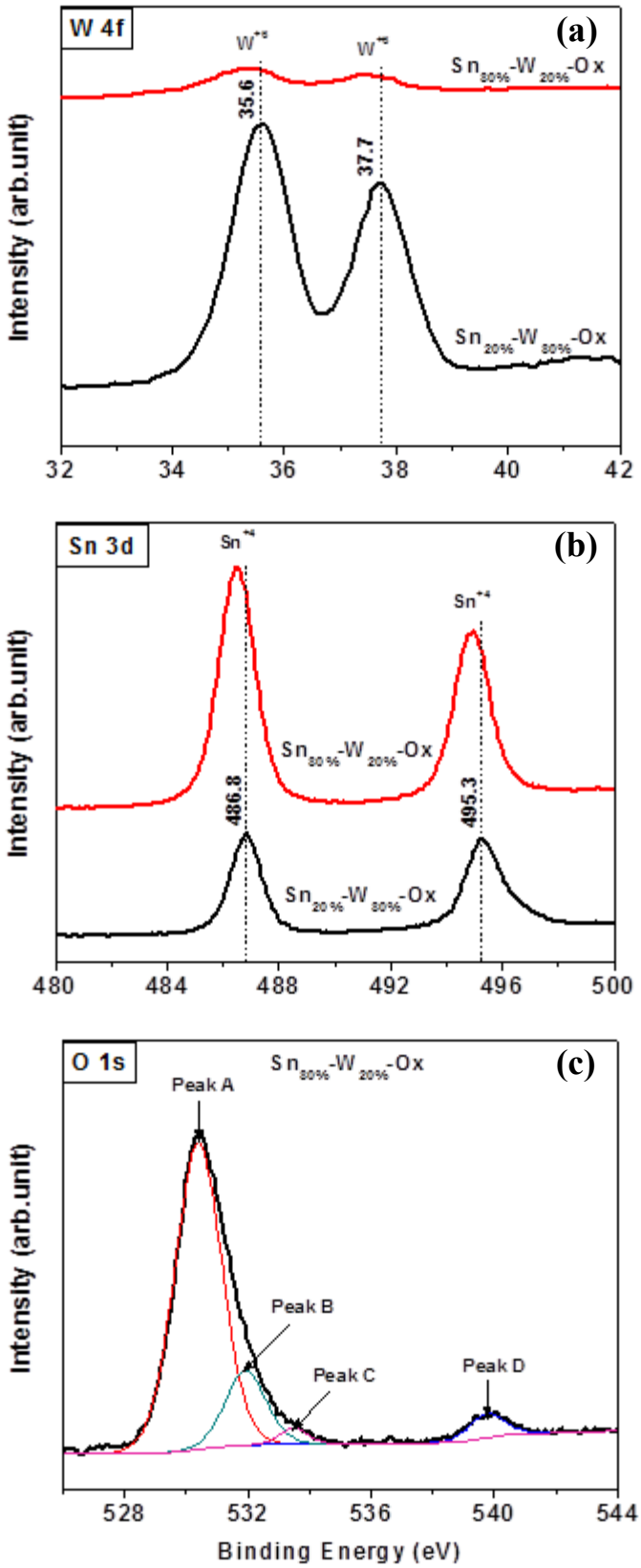

Figure 3-3: XPS spectra of Sb-doped Sn-W-oxide coatings: (a) W 4f, (b) Sn 3d, and (c) O 1s.

3.4.1.4. X-ray Diffraction (XRD)

The crystallinity and phase behaviour of the prepared electrode coatings were studied by means of XRD. The corresponding patterns of the electrode coatings with different composition are shown in **Figure 3-4** and the main diffraction peaks are labeled. The peaks at 26.6°, 33.9°, 38.0°, 51.9°, and 54.7° are attributed to the tetragonal cassiterite tin (IV) oxide (JCPDS no. 41-1445, lattice constant a = b = 4.7382 Å, c = 3.1871 Å). The small difference between the position of some observed peaks and the characteristic peaks of pure SnO_2 is due to the presence of antimony in the crystal of tin oxide. However, no diffraction peaks of antimony oxide (at 45.7°, 47.0° and 50.5°) are visible in XRD patterns except for the $W_{100\%}$-oxide coating, which can be due to the low doping level or the incorporation of doping ions into the SnO_2 crystal (i.e. solid solution) [59, 60]. As seen in **Figure 3-4**, the intensity of SnO_2 peaks decreases with a decrease in the Sn-oxide content in the coatings, while the intensity of Ti peaks increases, with some peaks appearing only when W-oxide > 20% (e.g. reflections 002 and 102 of Ti at 38.2° and 52.9°, respectively). The clearly visible metallic Ti peaks, as observed at 35.1°, 40.1°, 62.9°, 76.1° and 77.3°, come from the titanium substrate, because of small thickness of the coatings. The main diffraction peaks related to tungsten oxide are attributed to hexagonal WO_3. A TiO_2 peak at 41.7° was also identified. The peaks at 24.3°, 28.2°, and 70.7° correspond to hexagonal WO_3 (JCPDS no. 33-1387).

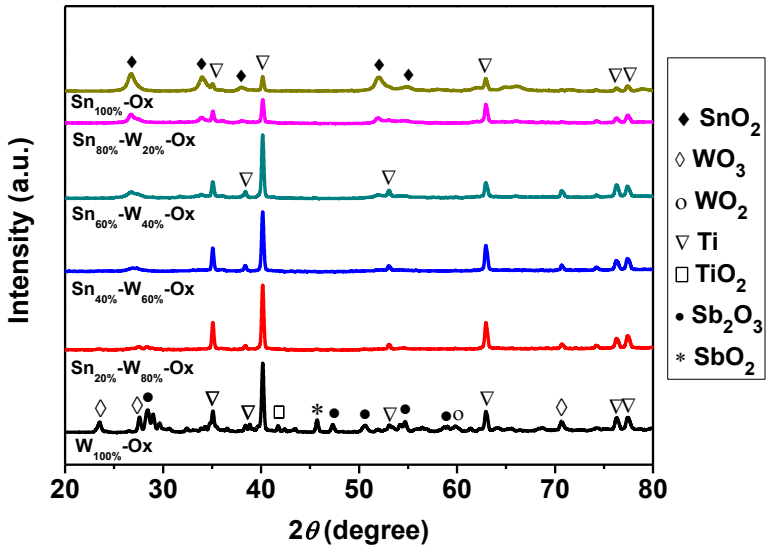

Figure 3-4: XRD patterns for the electrode coatings prepared with different Sn-W compositions.

.

3.4.1.5. True Surface Area and Surface Roughness

SEM images in **Figure 3-1** show that the topography of oxide coatings is rough. This indicates that the true electrochemically-active area of the metal-oxide coating is larger than its geometric (projected) area, i.e. the surface roughness factor is larger than one. Considering that (photo)electrochemical reactions are of heterogeneous nature, it is important to estimate the surface roughness of the coatings and relatively compare their true surface areas in order to determine the intrinsic activity of each coating composition. For the latter, the active surface area of each (working) electrode was measured electrochemically, by cyclic voltammetry, using ferricyanide/ferrocyanide redox couple in a three-electrode electrochemical cell, employing a well-established method [34]. **Table 3-2** shows the corresponding values, normalized with respect to the pure Sn-oxide coating roughness (for convenience of relative comparison). With an increase in the content of W in the coating composition, the relative true surface area of the coating

decreases, but then it increases again for the pure W-oxide coating, which seems to be in agreement with the visual inspection of the surface topography visible in SEM images in **Figure 3-1**.

Next, high definition confocal microscopy was used to determine the surface roughness of the coatings. **Figure 3-5** shows two representative results; $Sn_{80\%}$-$W_{20\%}$-oxide (**Figure 3-5**a) and $Sn_{20\%}$-$W_{80\%}$-oxide (**Figure 3-5**b). The images demonstrate that the surface with a lower W content is rougher at the micro scale than that one with a higher W content. In order to quantify this, the corresponding surface roughness of the coatings was determined and the values are outlined in **Table 3-2**. The results show that the surface roughness of the samples decreased with increasing the W content in the coating, but increased again for the pure W-oxide sample, which is in full agreement with the trend obtained by electrochemical measurements of the relative true surface area (**Table 3-2**). The data shows that with an increase in W content, the surface roughness decreases, and then increases sharply for the pure W-oxide coating. The behaviour is very similar to that one obtained from electrochemical measurements, and the agreement is more visible by comparing the two normalized sets of data (**Table 3-2**).

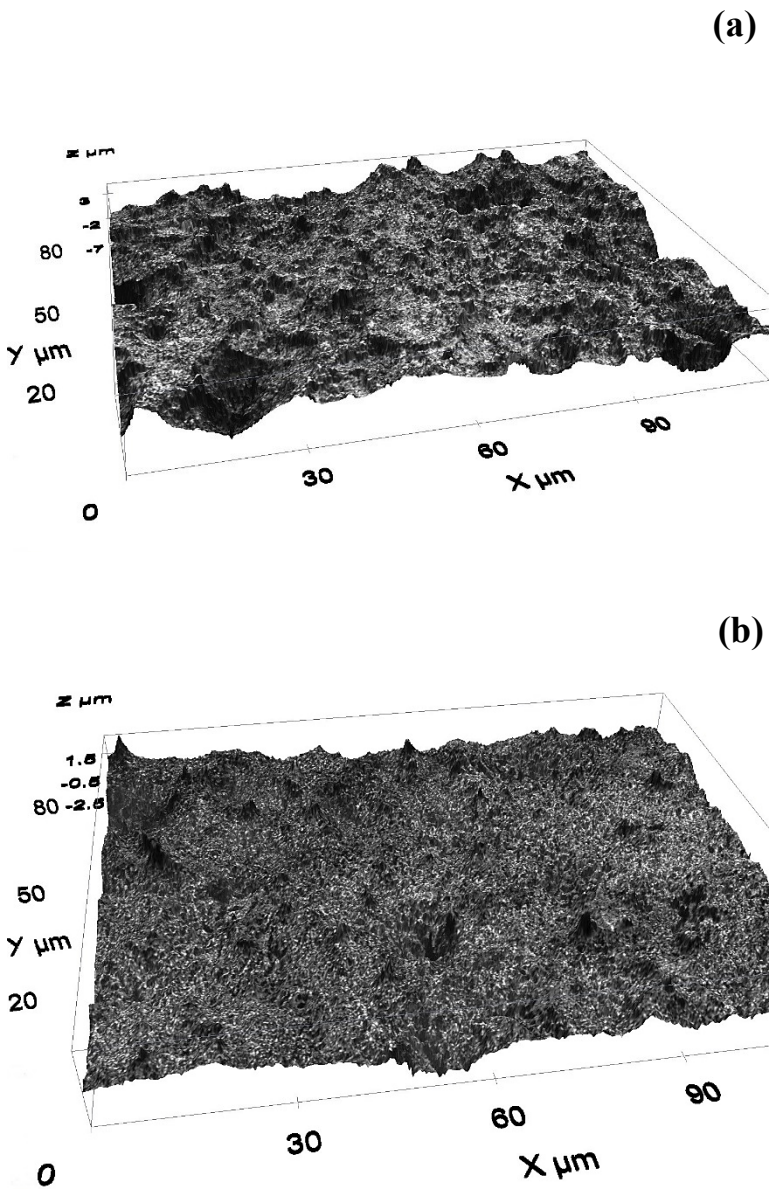

Figure 3-5: 3D images of (a) $Sn_{80\%}$-$W_{20\%}$-oxide (Ra = 1.45 µm) and (b) $Sn_{20\%}$-$W_{80\%}$-oxide (Ra = 0.42 µm) coatings, obtained by high definition confocal microscopy, showing surface roughness.

Table 3-2

Surface properties of Sn_x-$W_{(100-x)\%}$-oxide coatings. Values of active surface area have been normalized with respect to the maximum surface area which was obtained for the pure Sn-oxide coating.

Nominal Composition (mol%)	Normalized electrochemically-active surface area	Surface Roughness (μm)	Normalized surface roughness
$Sn_{100\%}$-$W_{0\%}$-Ox	1.00	2.73	1.00
$Sn_{80\%}$-$W_{20\%}$-Ox	0.79	1.45	0.53
$Sn_{60\%}$-$W_{40\%}$-Ox	0.69	1.13	0.41
$Sn_{40\%}$-$W_{60\%}$-Ox	0.38	0.89	0.33
$Sn_{20\%}$-$W_{80\%}$-Ox	0.23	0.42	0.15
$Sn_{0\%}$-$W_{100\%}$-Ox	0.60	1.63	0.60

3.4.1.6. Band Gap Determination

Since all the coating compositions produced are considered to be photoactive materials, the corresponding band gap values were measured by two methods: photoluminescence (PL) spectrometry with a 266-nm laser and UV-Vis spectroscopy. For each coating composition, two samples were tested and each measurement was performed at least twice to ensure reproducibility. The corresponding values are presented in **Table 3-3**.

The values obtained by PL evidence that the incorporation of W into the Sn-oxide coating up to 40% does not produce any statistical difference in the bandgap energy. The values are slightly lower than the values reported for pure Sb-doped SnO_2 films (3.85 ± 0.2 eV) [36, 61] and could be explained by the existence of doping states within the SnO_2 forbidden gap. However, when W is present in the coating at the 60% and larger quantity, the band gap energy decreased significantly (**Table 3-3**), indicating that the $Sn_{40\%}$-$W_{60\%}$-oxide's optical properties are governed predominantly

by the WO_3 properties. The values for the W-rich oxides in Table 3 are close to those reported in the literature for pure WO_3 (2.65 ± 1.5 eV) [50, 62].

Generally, the optical properties of semiconductors such as their band gaps (E_g) have been widely investigated by UV-Vis spectroscopy [63]. From the diffusive reflectance (R) data obtained over the UV-Vis wavelength range of 190 to 1100 nm, the absorption coefficient (α) for each oxide composition investigated in this work was calculated using the Kubelka-Munk function [63, 64]:

$$\alpha = \frac{(1-R)^2}{2R} \quad (1)$$

Then, the band gap energy of the films was determined using the Tauc relation [65], which expresses the dependence of the absorption coefficient, α (cm^{-1}), on the photon energy (hv):

$$\alpha hv = A(hv - E_g)^n \quad (2)$$

where hv is incident photon energy (eV), A is a constant depending on the material and n is an exponent which assumes values of 1/2, 2, 3/2 or 3, depending on the nature of the electronic transition, corresponding to allowed direct, allowed indirect, forbidden direct and forbidden indirect transitions, respectively [66]. Therefore, E_g corresponds to the intercept on the hv axis of a plot of $(\alpha hv)^{1/n}$ versus hv (**Figure 3-6**). Based on the literature, the value of n was selected to be 1/2 (allowed direct transition) for the Sn-oxide-rich coating compositions, and n = 2 (allowed indirect transition) for the W-oxide-rich coating compositions [61, 62, 67]. The calculated band gap values are presented in **Table 3-3**, and they are in agreement with the values already measured by PL spectroscopy.

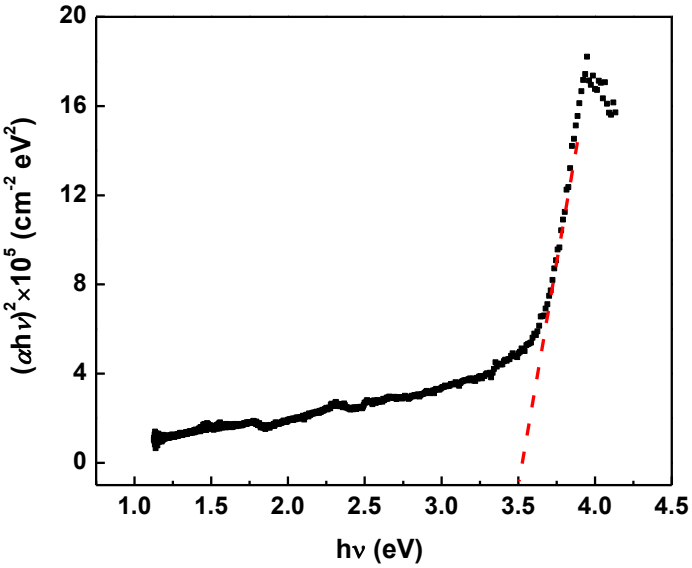

Figure 3-6: Tauc plots of $(\alpha h\nu)^2$ vs. hν for $Sn_{80\%}$-$W_{20\%}$-oxide coating.

Table 3-3

Values of optical band gap energy measured for the thermally prepared Sb-doped Sn_x-$W_{(100-x)\%}$-oxide coatings determined by photoluminescence (PL) spectroscopy and UV-Vis spectroscopy. Data presented as mean ± standard deviation.

Composition, mol% (nominal)	Band gap energy (eV)	
	Photoluminesence (PL)	UV-Vis spectroscopy
$Sn_{100\%}$-$W_{0\%}$-Ox	3.53 ± 0.06	3.53 ± 0.03
$Sn_{80\%}$-$W_{20\%}$-Ox	3.57 ± 0.07	3.58 ± 0.25
$Sn_{60\%}$-$W_{40\%}$-Ox	3.20 ± 0.03	3.42 ± 0.13
$Sn_{40\%}$-$W_{60\%}$-Ox	2.54 ± 0.02	2.32 ± 0.10
$Sn_{20\%}$-$W_{80\%}$-Ox	2.55 ± 0.03	2.43 ± 0.18
$Sn_{0\%}$-$W_{100\%}$-Ox	2.50 ± 0.02	2.66 ± 0.11

3.4.2. Photoelectrochemical Characterization

Photoelectrochemical characterization of Sb-doped Sn-W-oxide coatings was performed in a standard three-electrode cell containing 0.1 M KH_2PO_4 buffer electrolyte (pH 7) under UV light irradiation. The photocurrent is an indirect indication of water oxidation activity of a photoanode [39]. **Figure 3-7** shows representative linear polarization curves for the $Sn_{80\%}$-$W_{20\%}$-oxide coating (a similar behaviour was obtained for other coating compositions). The current response in the presence of light is higher in the potential region positive of -0.15 V, which evidences that the $Sn_{80\%}$-$W_{20\%}$-oxide is photoactive. The difference between the current measured when the light was turned on and that one when the light was turned off, represents the *photocurrent*. As **Figure 3-7** shows, with an increase in anodic potential, the corresponding photocurrent increases, confirming that the $Sn_{80\%}$-$W_{20\%}$-oxide is an *n*-type semiconductor.

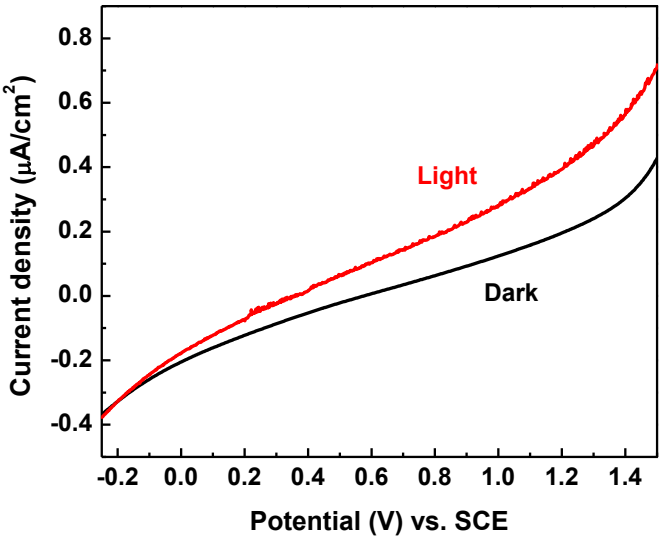

Figure 3-7: A typical experimental linear polarization curve for the $Sn_{80\%}$-$W_{20\%}$-oxide electrode recorded at a scan rate of 25 mV/s in 0.1 M KH_2PO_4 electrolyte at pH 7.

To investigate the photoelectrochemical behaviour of the metal-oxide coatings more closely, photocurrent measurements were made under potentiostatic conditions. **Figure 3-8** shows representative results for the $Sn_{0\%}$-$W_{100\%}$-oxide, $Sn_{80\%}$-$W_{20\%}$-oxide and $Sn_{100\%}$-$W_{0\%}$-oxide coatings. Upon switching the light on, the current instantly increases from the base value (dark), and then gradually keeps increasing until the light is switched off; at this point, the current instantly drops to the base (dark) value. **Figure 3-8** shows that this behaviour is reproducible. Analysis of the results performed under potentiostatic conditions confirmed that for all the coatings the measured photocurrent increases with anodic potential, which is in accordance with the potentiodynamic behaviour presented in **Figure 3-7**. Given that the metal-oxide coating is an *n*-type semiconductor, this behaviour indicates that the increase in anodic potential also (i) increases the driving force for the injection of the electrons from the donor level into the conducting band of the semiconducting oxide and (ii) decreases the electron-hole recombination, thus ultimately yielding a higher photocurrent.

Figure 3-9 shows the dependence of photocurrent on the coating composition. In order to eliminate the influence of surface area on photocurrent, the raw photocurrent values were normalized with respect to the coating true electrochemically-active surface area. The highest photocurrent was measured for the $W_{100\%}$-oxide coating. This is to expect as the bandgap for this oxide is the smallest among the coatings investigated in this work (**Table 3-3**). With an increase in Sn content in the coating, the photocurrent drops down and reaches a minimum for the $Sn_{40\%}$-$W_{60\%}$-oxide coating, followed by an increase in photocurrent. However, comparing the trend in **Figure 3-9** to the bandgap energy values (**Table 3-3**), it is obvious that the latter is not the sole factor that influences the photocurrent, but other physico-chemical properties of the metal-oxide

coating, the coating/electrolyte and coating/substrate interface, should also be considered (e.g. mobility of charge carriers, resistance of the coating/Ti_substrate interface for electron transfer, oxide coating pore-size/shape and pore-size distribution).

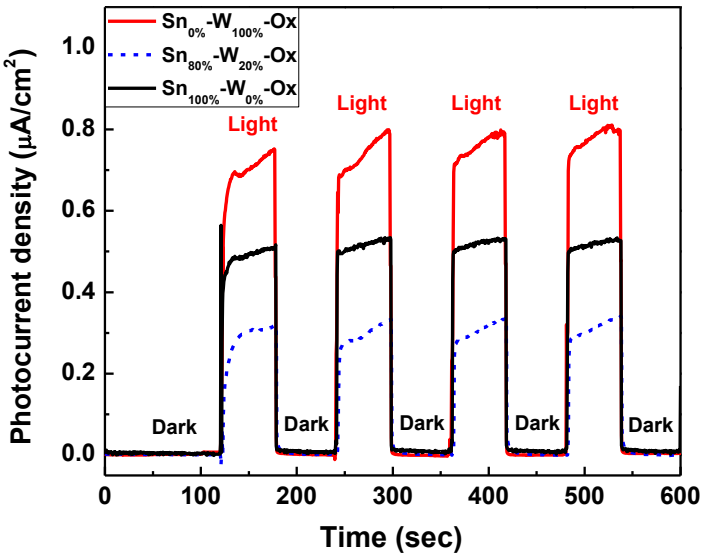

Figure 3-8: Chronoamperometry response of Sb-doped $Sn_{0\%}$-$W_{100\%}$-oxide (red), $Sn_{80\%}$-$W_{20\%}$-oxide (blue) and $Sn_{100\%}$-$W_{0\%}$-oxide (black) electrodes recorded in 0.1 M potassium phosphate buffer (pH 7) in dark and under UV light irradiation and at 1.2 V. The current measured in dark has been set as the background current, rendering the response in the figure as photocurrent.

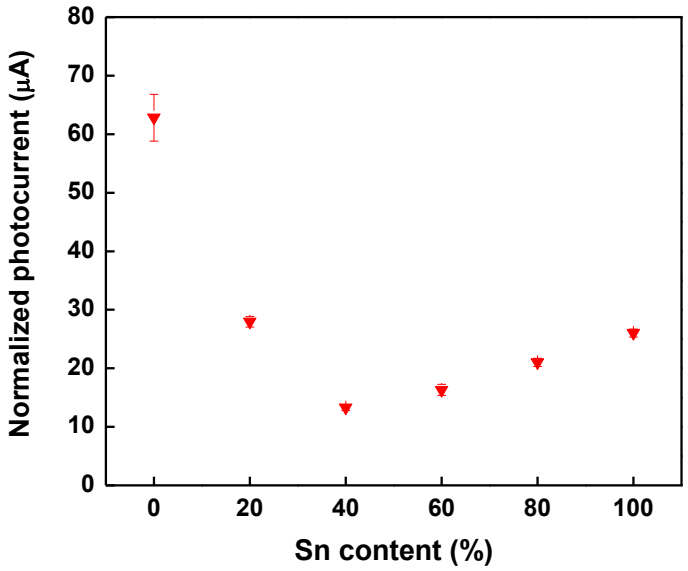

Figure 3-9: Photocurrent as a function of Sn-W-oxide composition. The photocurrent was normalized with respect to the coating true electrochemically-active surface area. Electrolyte: 0.1 M potassium phosphate buffer (pH 7). E = 1.2 V. Error bars represent standard deviations.

3.4.3. Photoelectrocatalytic Characterization

The photoelectrocatalytic activity of the Sb-doped Sn-W-oxide coatings was evaluated by the photoelectrochemical oxidation of a model organic compound, 0.1 mM phenol red (PR) dye aqueous solution under UV light irradiation The mechanism of (photo)electrochemical oxidation has already been established in the literature [68-70], and will thus not be discussed here. **Figure 3-10** shows that for all the metal-oxide coating compositions, oxidation (degradation) of PR occurs as evidenced by the concentration decrease with time; however, the kinetics of the oxidation process depends largely on the coating composition. As can be seen, the degradation degree obtained using $Sn_{100\%}$-$W_{0\%}$-oxide and $Sn_{80\%}$-$W_{20\%}$-oxide anodes was the highest among the anodes investigated. However, given that the $Sn_{80\%}$-$W_{20\%}$-oxide electrochemically-active area is 80% of

the area of $Sn_{100\%}$-$W_{0\%}$-oxide coating (**Table 3-2**), it appears that the former coating is intrinsically the most active photoelectrocatalyst for PR oxidation.

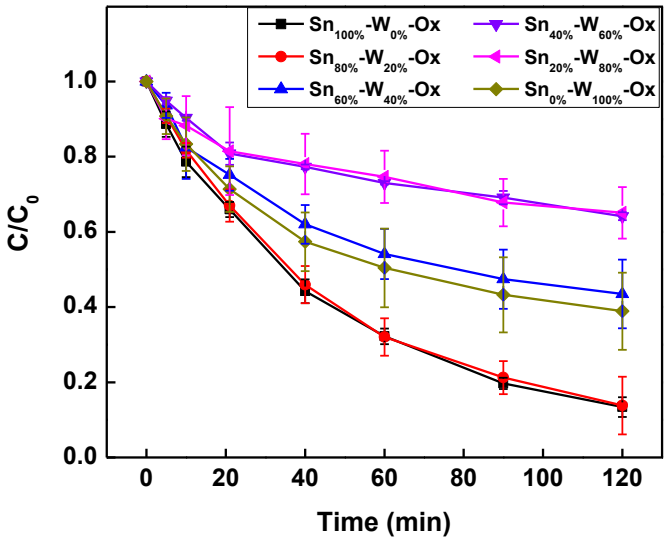

Figure 3-10: Photoelectrocatalytic degradation of phenol red dye by Sb-doped Sn-W oxide coatings. Current density: 20 mA/cm^2.

The results for the photoelectrocatalytic (PEC) degradation of PR dye were compared with those obtained from the electrochemical (EC) (in dark) and photocatalytic (PC) processes (**Figure 3-11**); it should be noted that the metal-oxide electrode in PC measurements was immersed in the PR solution, but no external current was applied. As it can be seen in **Figure 3-11**, the PC degradation of PR was negligible for all catalyst compositions used in this work (green bars). On the other hand, the PEC degradation of PR resulted in a significant decrease in PR concentration, at all metal-oxide anode compositions. The highest degradation degree was obtained for $Sn_{80\%}$-$W_{20\%}$-oxide and $Sn_{100\%}$-$W_{0\%}$-oxide coatings. Another interesting observation is that the degree of PR oxidation with PEC was higher than the sum of the two PC and EC degradation degrees, demonstrating the presence of a synergy effect. However, when normalized for the anode true

electrochemically-active surface area (**Table 3-2**), the highest degree of PR oxidation was obtained for the $Sn_{80\%}$-$W_{20\%}$-oxide composition. If we look at the surface-area-normalized photocurrent values in **Figure 3-7**, we can see that the highest photocurrent was obtained for pure W-oxide coating. However, the next-highest photocurrent value was recorded for the $Sn_{20\%}$-$W_{80\%}$-oxide and $Sn_{100\%}$-$W_{0\%}$-oxide coatings. Given that Sn-oxide is an excellent electrochemically-active material for anodic oxidation of organics (good electrocatalytic activity) and that W-oxide has the highest photoactivity, it could be expected that, under the conditions applied, neither pure Sn-oxide nor pure W-oxide would give the highest intrinsic photoelectrochemical activity in PR oxidation, but it would be a mixed metal-oxide. As it appears, the $Sn_{80\%}$-$W_{20\%}$-oxide appears to offer the highest intrinsic photoelectrochemical activity in PR oxidation, at least under the experimental conditions employed here.

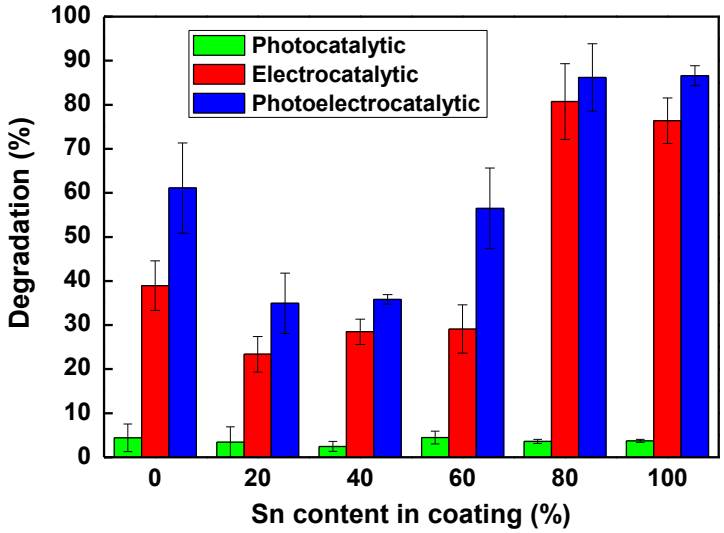

Figure 3-11: Comparison of the photocatalytic (PC), electrocatalytic (EC), and photoelectrocatalytic (PEC) activities of different Sb-doped Sn-W-oxide coatings for the degradation of phenol red dye. Degradation time: 120 min. Error bars are indicators of standard deviations. Current density: 20 mA/cm^2.

3.5. Conclusions

Sb-doped Sn_x-$W_{(100-x)\%}$-oxide coatings (x = 0, 20, 40, 60, 80 and 100) were fabricated on flat titanium substrates by thermal decomposition of metal salts. The electrochemically active surface area and the surface roughness of the coatings were found to be the coating-composition dependant. The XPS results confirmed the existence of Sn^{2+} (e.g. SnO_2) and W^{6+} (e.g. WO_3) as the main oxidation states of the elements in the coatings, while antimony was found to be present as Sb^{4+} and Sb^{3+}. The optical band gap decreased from 3.53 ± 0.05 eV for pure Sn-oxide to 2.56 ± 0.10 eV for pure W-oxide; however, this decrease occurred only when the content of W in the oxide was greater or equal to 60%. All the coatings were found to be photoactive under the anodic bias, indicating their *n*-type semiconductivity character. However, the corresponding photocurrent was found not to follow the band-gap trend, indicating that other physico-chemical properties of the metal-oxide coatings also influence the magnitude of photocurrent. $Sn_{100\%}$-$W_{0\%}$-oxide and $Sn_{80\%}$-$W_{20\%}$-oxide coated electrodes exhibited good apparent photoelectrocatalytic activity for the degradation of phenol red dye under UV light irradiation (~ 90% after 2 hours), but the latter coating was found to yield a higher intrinsic photoelectrocatalytic activity.

Acknowledgements

The present work was supported by the Natural Sciences and Engineering Research Council of Canada (NSERC) and McGill Engineering Doctoral Award (MEDA).

3.6. References

[1] D.W. Kolpin, E.T. Furlong, M.T. Meyer, E.M. Thurman, S.D. Zaugg, L.B. Barber, H.T. Buxton, Pharmaceuticals, hormones, and other organic wastewater contaminants in U.S. streams, 1999-2000: a national reconnaissance, Environmental science & technology, 36 (2002) 1202-1211.

[2] R.R. Giri, H. Ozaki, S. Ota, R. Takanami, S. Taniguchi, Degradation of common pharmaceuticals and personal care products in mixed solutions by advanced oxidation techniques, International Journal of Environmental Science & Technology, 7 (2010) 251-260.

[3] X. Qu, M. Tian, B. Liao, A. Chen, Enhanced electrochemical treatment of phenolic pollutants by an effective adsorption and release process, Electrochimica Acta, 55 (2010) 5367-5374.

[4] M. Tian, S.S. Thind, M. Simko, F. Gao, A. Chen, Quantitative structure-reactivity study of electrochemical oxidation of phenolic compounds at the SnO_2-based electrode, J Phys Chem A, 116 (2012) 2927-2934.

[5] M. Panizza, G. Cerisola, Direct and mediated anodic oxidation of organic pollutants, Chemical reviews, 109 (2009) 6541-6569.

[6] I.-S. Cho, C.H. Kwak, D.W. Kim, S. Lee, K.S. Hong, Photophysical, Photoelectrochemical, and Photocatalytic Properties of Novel $SnWO_4$ Oxide Semiconductors with Narrow Band Gaps, J. Phys. Chem. C, 113 (2009) 10647–10653.

[7] M. Capocelli, E. Joyce, A. Lancia, T.J. Mason, D. Musmarra, M. Prisciandaro, Sonochemical degradation of estradiols: Incidence of ultrasonic frequency, Chemical Engineering Journal, 210 (2012) 9-17.

[8] K. Ikehata, N. Jodeiri Naghashkar, M. Gamal El-Din, Degradation of Aqueous Pharmaceuticals by Ozonation and Advanced Oxidation Processes: A Review, Ozone: Science & Engineering, 28 (2006) 353-414.

[9] O.K. Dalrymple, D.H. Yeh, M.A. Trotz, Removing pharmaceuticals and endocrine-disrupting compounds from wastewater by photocatalysis, Journal of Chemical Technology & Biotechnology, 82 (2007) 121-134.

[10] L. Feng, E.D. van Hullebusch, M.A. Rodrigo, G. Esposito, M.A. Oturan, Removal of residual anti-inflammatory and analgesic pharmaceuticals from aqueous systems by electrochemical advanced oxidation processes. A review, Chemical Engineering Journal, 228 (2013) 944-964.

[11] A. Socha, E. Chrzescijanska, E. Kusmierek, Electrochemical and photoelectrochemical treatment of 1-aminonaphthalene-3,6-disulphonic acid, Dyes and Pigments, 67 (2005) 71-75.
[12] A. Socha, E. Sochocka, R. Podsiadły, J. Sokołowska, Electrochemical and photoelectrochemical treatment of C.I. Acid Violet 1, Dyes and Pigments, 73 (2007) 390-393.
[13] C.A. Martínez-Huitle, E. Brillas, Decontamination of wastewaters containing synthetic organic dyes by electrochemical methods: A general review, Applied Catalysis B: Environmental, 87 (2009) 105-145.
[14] X. Zhao, J. Qu, H. Liu, Z. Qiang, R. Liu, C. Hu, Photoelectrochemical degradation of anti-inflammatory pharmaceuticals at Bi_2MoO_6–boron-doped diamond hybrid electrode under visible light irradiation, Applied Catalysis B: Environmental, 91 (2009) 539-545.
[15] C.A. Martínez-Huitle, L.S. Andrade, Electrocatalysis in wastewater treatment: recent mechanism advances, Química Nova, 34 (2011) 850-858.
[16] J.R. Domínguez, T. González, P. Palo, J. Sánchez-Martín, Electrochemical Advanced Oxidation of Carbamazepine on Boron-Doped Diamond Anodes. Influence of Operating Variables, Industrial & Engineering Chemistry Research, 49 (2010) 8353-8359.
[17] M.M. Khan, S.F. Adil, A. Al-Mayouf, Metal oxides as photocatalysts, Journal of Saudi Chemical Society, 19 (2015) 462-464.
[18] A. Fujishima, K. Honda, Electrochemical Photolysis of Water at a Semiconductor Electrode, Nature, 238 (1972) 37-38.
[19] G. Palmisano, V. Augugliaro, M. Pagliaro, L. Palmisano, Photocatalysis: a promising route for 21st century organic chemistry, Chemical Communications, (2007) 3425-3437.
[20] H. Zhang, G. Chen, D.W. Bahnemann, Photoelectrocatalytic materials for environmental applications, Journal of Materials Chemistry, 19 (2009) 5089-5121.
[21] X. Chen, S.S. Mao, Titanium dioxide nanomaterials: synthesis, properties, modifications, and applications, Chemical reviews, 107 (2007) 2891-2959.
[22] N. Serpone, E.V. Emeline, Fundamentals in metal-oxide heterogeneous photocatalysis, in: M.D. Archer, A.J. Nozik (Eds.) Nanostructured and Photo-electrochemical Systems for Solar Photon Conversion, Imperial College Press, London, 2008, pp. 275–392.
[23] R. Asahi, T. Morikawa, T. Ohwaki, K. Aoki, Y. Taga, Visible-Light Photocatalysis in Nitrogen-Doped Titanium Oxides, Science, 293 (2001) 269-271.

[24] S. Sakthivel, H. Kisch, Daylight Photocatalysis by Carbon-Modified Titanium Dioxide, Angewandte Chemie International Edition, 42 (2003) 4908-4911.
[25] T. Umebayashi, T. Yamaki, H. Itoh, K. Asai, Band gap narrowing of titanium dioxide by sulfur doping, Applied Physics Letters, 81 (2002) 454-456.
[26] D. Wang, X. Li, J. Chen, X. Tao, Enhanced Visible-Light Photoelectrocatalytic Degradation of Organic Contaminants at Iodine-Doped Titanium Dioxide Film Electrode, Industrial & Engineering Chemistry Research, 51 (2012) 218-224.
[27] S. Song, Z. Sheng, Y. Liu, H. Wang, Z. Wu, Influences of pH value in deposition-precipitation synthesis process on Pt-doped TiO_2 catalysts for photocatalytic oxidation of NO, Journal of Environmental Sciences, 24 (2012) 1519-1524.
[28] V.S. Mohite, M.A. Mahadik, S.S. Kumbhar, Y.M. Hunge, J.H. Kim, A.V. Moholkar, K.Y. Rajpure, C.H. Bhosale, Photoelectrocatalytic degradation of benzoic acid using Au doped TiO_2 thin films, Journal of Photochemistry and Photobiology B: Biology, 142 (2015) 204-211.
[29] C. Sahoo, A.K. Gupta, I.M. Sasidharan Pillai, Photocatalytic degradation of methylene blue dye from aqueous solution using silver ion-doped TiO_2 and its application to the degradation of real textile wastewater, J Environ Sci Health A, 47 (2012) 1428–1438.
[30] D.W. Hwang, J. Kim, T.J. Park, J.S. Lee, Mg-Doped WO_3 as a Novel Photocatalyst for Visible Light-Induced Water Splitting, Catalysis Letters, 80 (2002) 53-57.
[31] R. Konta, T. Ishii, H. Kato, A. Kudo, Photocatalytic Activities of Noble Metal Ion Doped $SrTiO_3$ under Visible Light Irradiation, The Journal of Physical Chemistry B, 108 (2004) 8992-8995.
[32] T. Wu, G. Zhao, Y. Lei, P. Li, Distinctive Tin Dioxide Anode Fabricated by Pulse Electrodeposition: High Oxygen Evolution Potential and Efficient Electrochemical Degradation of Fluorobenzene, The Journal of Physical Chemistry C, 115 (2011) 3888-3898.
[33] L. Xu, M. Li, W. Xu, Preparation and characterization of Ti/SnO_2-Sb electrode with copper nanorods for AR 73 removal, Electrochimica Acta, 166 (2015) 64-72.
[34] F. Montilla, E. Morallón, A. De Battisti, S. Barison, S. Daolio, J.L. Vázquez, Preparation and Characterization of Antimony-Doped Tin Dioxide Electrodes. 3. XPS and SIMS Characterization, The Journal of Physical Chemistry B, 108 (2004) 15976-15981.

[35] R. Kötz, S. Stucki, B. Carcer, Electrochemical waste water treatment using high overvoltage anodes. Part I: Physical and electrochemical properties of SnO_2 anodes, Journal of Applied Electrochemistry, 21 (1991) 14-20.

[36] C.-F. Lin, C.-H. Wu, Z.-N. Onn, Degradation of 4-chlorophenol in TiO_2, WO_3, SnO_2, TiO_2/WO_3 and TiO_2/SnO_2 systems, Journal of Hazardous Materials, 154 (2008) 1033-1039.

[37] J. Wang, Y. Lv, L. Zhang, B. Liu, R. Jiang, G. Han, R. Xu, X. Zhang, Sonocatalytic degradation of organic dyes and comparison of catalytic activities of CeO_2/TiO_2, SnO_2/TiO_2 and ZrO_2/TiO_2 composites under ultrasonic irradiation, Ultrasonics Sonochemistry, 17 (2010) 642-648.

[38] M. Ilieva, A. Nakova, V. Tsakova, TiO_2/WO_3 hybrid structures produced through a sacrificial polymer layer technique for pollutant photo- and photoelectrooxidation under ultraviolet and visible light illumination, Journal of Applied Electrochemistry, 42 (2012) 121-129.

[39] Y. Li, P.-C. Hsu, S.-M. Chen, Multi-functionalized biosensor at WO_3–TiO_2 modified electrode for photoelectrocatalysis of norepinephrine and riboflavin, Sensors and Actuators B: Chemical, 174 (2012) 427-435.

[40] J. Luan, B. Pan, Y. Paz, Y. Li, X. Wu, Z. Zou, Structural, photophysical and photocatalytic properties of new Bi_2SbVO_7 under visible light irradiation, Physical chemistry chemical physics : PCCP, 11 (2009) 6289-6298.

[41] W. Yin, W. Wang, L. Zhou, S. Sun, L. Zhang, CTAB-assisted synthesis of monoclinic $BiVO_4$ photocatalyst and its highly efficient degradation of organic dye under visible-light irradiation, Journal of Hazardous Materials, 173 (2010) 194-199.

[42] J. Xu, W. Wang, M. Shang, S. Sun, J. Ren, L. Zhang, Efficient visible light induced degradation of organic contaminants by Bi_2WO_6 film on SiO_2 modified reticular substrate, Applied Catalysis B: Environmental, 93 (2010) 227-232.

[43] J. Luan, Y. Xu, Photophysical Property and Photocatalytic Activity of New Gd_2InSbO_7 and Gd_2FeSbO_7 Compounds under Visible Light Irradiation, International Journal of Molecular Sciences, 14 (2013) 999.

[44] J. Luan, M. Chen, W. Hu, Synthesis, Characterization and Photocatalytic Activity of New Photocatalyst $ZnBiSbO_4$ under Visible Light Irradiation, International Journal of Molecular Sciences, 15 (2014) 9459.

[45] J. Sheng, X. Li, Y. Xu, Generation of H_2O_2 and OH Radicals on Bi_2WO_6 for Phenol Degradation under Visible Light, ACS Catalysis, 4 (2014) 732-737.
[46] D. Zhang, Q. Wang, L. Wang, L. Zhang, Magnetically separable $CdFe_2O_4$/graphene catalyst and its enhanced photocatalytic properties, Journal of Materials Chemistry A, 3 (2015) 3576-3585.
[47] G. Zhu, W. Que, J. Zhang, P. Zhong, Photocatalytic activity of $SnWO_4$ and SnW_3O_9 nanostructures prepared by a surfactant-assisted hydrothermal process, Materials Science and Engineering: B, 176 (2011) 1448-1455.
[48] F. Vicent, E. Morallo´n, C. Quijada, J.L. Va´zquez, A. Aldaz, F. Cases, Characterization and stability of doped SnO_2 anodes, Journal of Applied Electrochemistry, 28 (1998) 607-612.
[49] E. Shanthi, V. Dutta, A. Banerjee, K.L. Chopra, Electrical and optical properties of undoped and antimony-doped tin oxide films, Journal of Applied Physics, 51 (1980) 6243-6251.
[50] X. Liu, F. Wang, Q. Wang, Nanostructure-based WO_3 photoanodes for photoelectrochemical water splitting, Physical Chemistry Chemical Physics, 14 (2012) 7894-7911.
[51] E.O. Scott-Emuakpor, A. Kruth, M.J. Todd, A. Raab, G.I. Paton, D.E. Macphee, Remediation of 2,4-dichlorophenol contaminated water by visible light-enhanced WO_3 photoelectrocatalysis, Applied Catalysis B: Environmental, 123–124 (2012) 433-439.
[52] S. Habibzadeh, L. Li, S. Omanovic, D. Shum-Tim, E.C. Davis, Biocompatibility of Ir/Ti-oxide coatings: Interaction with platelets, endothelial and smooth muscle cells, Applied Surface Science, 301 (2014) 530-538.
[53] A.A. Marakushev, N.I. Bezmen, Chemical affinity of metals for oxygen and sulfur, International Geology Review, 13 (1971) 1781-1794.
[54] J.F. Moulder, W.F. Stickle, P.E. Sobol, K.D. Bomben, Handbook of X-ray photoelectron spectroscopy: a reference book of standard spectra for identification and interpretation of XPS data, Physical Electronics Eden Prairie, MN, 1995.
[55] C.D. Wagner, NIST X-Ray Photoelectron Spectroscopy Database, in, Retrieved from NIST Standard Reference Data Program. Website http://www.nist.gov/srd/. 1989.
[56] M.R. Bayati, F. Golestani-Fard, A.Z. Moshfegh, R. Molaei, A photocatalytic approach in micro arc oxidation of WO_3–TiO_2 nano porous semiconductors under pulse current, Materials Chemistry and Physics, 128 (2011) 427-432.

[57] H. Dong, Z. Li, Z. Ding, H. Pan, X. Wang, X. Fu, Nanoplates of α-$SnWO_4$ and SnW_3O_9 prepared via a facile hydrothermal method and their gas-sensing property, Sensors and Actuators B: Chemical, 140 (2009) 623-628.
[58] Q.N. Zhao, C.L. Li, X. He, X.J. Zhao, XPS Study of N-doped TiOx Thin Films Prepared By DC Reactive Magnetron Sputtering, Key Engineering Materials, 249 (2003) 457-462.
[59] Q. Zhang, Y. Liu, D. Zeng, J. Lin, W. Liu, The effect of Ce doped in Ti/SnO_2-Sb_2O_3/SnO_2-Sb_2O_3-CeO_2 electrode and its electro-catalytic performance in caprolactam wastewater, Water Science and Technology, 64 (2011) 2023-2028.
[60] Y.-H. Cui, Y.-J. Feng, Z.-Q. Liu, Influence of rare earths doping on the structure and electro-catalytic performance of Ti/Sb–SnO_2 electrodes, Electrochimica Acta, 54 (2009) 4903-4909.
[61] C. Terrier, J.P. Chatelon, J.A. Roger, Electrical and optical properties of Sb:SnO_2 thin films obtained by the sol-gel method, Thin Solid Films, 295 (1997) 95-100.
[62] R.S. Vemuri, M.H. Engelhard, C.V. Ramana, Correlation between Surface Chemistry, Density, and Band Gap in Nanocrystalline WO_3 Thin Films, ACS Applied Materials & Interfaces, 4 (2012) 1371-1377.
[63] A. Murphy, Band-gap determination from diffuse reflectance measurements of semiconductor films, and application to photoelectrochemical water-splitting, Solar energy materials and solar cells, 91 (2007) 1326-1337.
[64] N. Parsi Benehkohal, M.A. Gomez, R. Gauvin, G.P. Demopoulos, Enabling aqueous electrophoretic growth of adherent nanotitania mesoporous films via intrafilm cathodic deposition of hydrous zinc oxide, Electrochimica Acta, 87 (2013) 169-179.
[65] J.C. Tauc, in: F. Abeles (Ed.) Optical Properties of Solids, North-Holland Publishing, Amsterdam, 1972, pp. 279.
[66] J.I. Pankove, Optical Processes in Semiconductors, Dover Publication Inc., New York, 1971.
[67] S. Baco, A. Chik, F.M. Yassin, Study on Optical Properties of Tin Oxide Thin Film at Different Annealing Temperature, Journal of Science and Technology, 4 (2012) 61-72.
[68] A.Y. Ahmed, T.A. Kandiel, I. Ivanova, D. Bahnemann, Photocatalytic and photoelectrochemical oxidation mechanisms of methanol on TiO_2 in aqueous solution, Applied Surface Science, 319 (2014) 44-49.

[69] H. Liu, X.Z. Li, Y.J. Leng, W.Z. Li, An Alternative Approach to Ascertain the Rate-Determining Steps of TiO2 Photoelectrocatalytic Reaction by Electrochemical Impedance Spectroscopy, The Journal of Physical Chemistry B, 107 (2003) 8988-8996.
[70] X. Li, J. Zhu, H. Li, Comparative study on the mechanism in photocatalytic degradation of different-type organic dyes on SnS2 and CdS, Applied Catalysis B: Environmental, 123–124 (2012) 174-181.

CHAPTER 4

4. Electrochemical Disinfection of Water Using Antimony-Doped Tin-Tungsten-Oxide Electrodes

4.1. Preface

The most prevalent method of disinfection in wastewater treatment, chlorination, is associated with serious safety and ecotoxicological concerns, related to the storage and transportation of dangerous chlorine as well as the generation of potentially toxic by-products. Electrochemical disinfection is an environmentally-friendly process, easy to operate, and effective in inactivation of a wide variety of microorganisms from bacteria to viruses and algae under safe operating conditions. The overall performance and efficiency of an electrochemical process is strongly dependent of the electrode material. In this research, the Sb-doped $Sn_{80\%}$-$W_{20\%}$-oxide/Ti anode material which showed the highest intrinsic activity for degradation of phenol red dye in the study presented in Chapter 3, was tested for electrochemical inactivation of bacteria in aqueous solutions and the influence of solution chemistry and several operating factors on the efficacy of the process were investigated. A manuscript has been prepared based on the results of this research and submitted to Water Research journal for publication, as:

S. Ghasemian, B. Asadishad, S. Omanovic. N. Tufenkji. "Electrochemical disinfection of bacteria-laden water using antimony-doped tin-tungsten oxide electrodes".

Abstract

Electrochemical disinfection has been shown to be an efficient method with a short-required contact time for treatment of drinking water supplies, industrial raw water supplies, liquid foodstuffs, and wastewater effluents. In the present work, the electrochemical disinfection of saline water contaminated with bacteria was investigated in chloride-containing solutions using Sb-doped $Sn_{80\%}$-$W_{20\%}$-oxide anodes. The influence of current density, bacterial load, initial chloride concentration, solution pH, and the type of bacteria (*E. coli* D21, *E. coli* O157:H7, and *E. faecalis*) on disinfection efficacy was systematically examined. The impact of natural organic matter and a hydroxyl radical scavenger on the disinfection process was also examined. The electrochemical system was highly effective in bacterial inactivation for a 0.1 M NaCl solution contaminated with ~10^7 CFU/mL bacteria by applying a current density ≥ 1 mA/cm^2. 100% inactivation of *E. coli* D21 was achieved with a contact time of less than 60 s and power consumption of 48 Wh/m^3, by applying a current density of 6 mA/cm^2 in a 0.1 M NaCl solution. Reactive chlorine species as well as reactive oxygen species (*e.g.* hydroxyl radicals) generated *in situ* during the electrochemical process were determined to be responsible for inactivation of bacteria.

4.2. Introduction

The elimination of pathogenic microorganisms, suspended or as attached biofilms, is a primary step in the treatment of water from many different sources, such as raw water supply (Trussell 1998), ballast water (Nanayakkara 2010), drinking water reservoirs and water distribution systems (Flemming 2002), process wash water in food processing plants (López-Gálvez et al. 2012), brackish or industrial briny waters for use in food industry, swimming pools and drinking water

(Feng et al. 2004, Martínez-Huitle and Brillas 2008), amongst many others. This is usually carried out by adding chemicals such as chlorine, chlorine dioxide and ozone (Harper et al. 2001, Rahmawati et al. 2010). The most common method, chlorination, is associated with some problems such as transport and storage of chlorine (Kraft et al. 1999, Rajeshwar and Ibanez 1997), generation of hazardous by-products such as trihalomethanes (THMs), haloacetic acids (HAAs), and N-nitrosodimethylamine (NDMA) (A. Lawton and K. J. Robertson 1999, Gusmão et al. 2010, Mitch et al. 2003), and the resistance of some pathogens including the bacteria *Escherichia coli* (*E. coli*) and *Campylobacter jejuni*, enteric viruses such as rotavirus and calicivirus, and the parasites *Cryptosporidium* and *Giardia lamblia* (Gusmão et al. 2010, Szewzyk et al. 2000).

Electrochemical (EC) disinfection has gained attention as a potential alternative to conventional chlorination (Jeong et al. 2007, López-Gálvez et al. 2012) due to its environmental compatibility, easy installation and operation, and effectiveness for inactivation of a wide variety of microorganisms from bacteria to viruses and algae under mild pressures and temperature (Diao et al. 2004, Drees et al. 2003, Long et al. 2015, Mascia et al. 2013). It has been demonstrated that electrochemical technology can provide high disinfection efficiency for drinking water (Matsunaga et al. 1992), raw water supply (Patermarakis and Fountoukidis 1990), liquid foodstuff (Grahl and Märkl 1996), and industrial and domestic wastewater effluents (Anglada et al. 2009, Schmalz et al. 2009). The practice of cleaning water by passing an electric current had been reported as early as the nineteenth century; however, only recently has this technology has come into long-term practical use (Kraft 2008).

Electrochemical water treatment is a green and powerful technology with a two-stage mechanism of action: (1) direct oxidation at the electrode surface, which is characterized by the instantaneous killing of microbial cells (Jeong et al. 2007), and (2) indirect oxidation in the bulk

solution by disinfecting species produced from water oxidation, such as hydroxyl radical ($^{\bullet}OH$), atomic oxygen ($^{\bullet}O$), hydrogen peroxide (H_2O_2), and ozone (O_3) (Eqs. (1-5)) (Liang et al. 2005, Martínez-Huitle and Brillas 2008, Panizza and Cerisola 2005) classified as reactive oxygen species (ROS), or by oxidants produced from the substances dissolved in the water, e. g., chloride is oxidized to free chlorine, according to Eq. (6) (Anglada et al. 2009, Kraft 2008). Dissolved chlorine is subsequently hydrolyzed to hypochlorous acid/hypochlorite ion and hydrochloric acid, in main side reactions of anodic production of chlorine, as given in Eqs. (7) and (8). In water treatment, the overall concentration of dissolved chlorine after the chlorination process is termed active chlorine, and is given by the summation of three species: free chlorine (Cl_2), hypochlorous acid (HClO) and hypochlorite ion (ClO^-). The mass distribution of these three main reactive chlorine species (RCS) depends on the pH of the medium (Bergmann and Koparal 2005).

$$H_2O \rightarrow HO^{\bullet} + H^+ + e^- \quad (4\text{-}1)$$

$$HO^{\bullet} \rightarrow O^{\bullet} + H^+ + e^- \quad (4\text{-}2)$$

$$2O^{\bullet} \rightarrow O_2 \quad (4\text{-}3)$$

$$2HO^{\bullet} \rightarrow H_2O_2 \quad (4\text{-}4)$$

$$O_2 + O^{\bullet} \rightarrow O_3 \quad (4\text{-}5)$$

$$2Cl^- \rightarrow Cl_2 + 2e^- \quad (4\text{-}6)$$

$$Cl_2 + H_2O \rightarrow Cl^- + HClO + H^+ \quad (4\text{-}7)$$

$$HClO \rightarrow ClO^- + H^+ \quad (4\text{-}8)$$

Other advantages of electrochemical disinfection are on-site generation of disinfectants with controllable dose (Jeong et al. 2007) and relatively low energy requirement that allows the use of green energy sources such as solar cells or fuel cells (Drogui et al. 2001, Ghernaout et al. 2008). Overall, the high efficacy of electrochemical disinfection is attributed to the synergistic effects of direct oxidation on the electrode surface (Grahl and Märkl 1996, Matsunaga et al. 2000), generation of the reactive intermediate species such as ROS or RCS with strong bactericidal activity (Diao et al. 2004, Feng et al. 2004, Liang et al. 2005), and/or the electric field effect (Butterfield et al. 1997, Grahl and Märkl 1996).

The selection of an appropriate anode material is a key factor in electrocatalytic processes, as it influences not only the efficiency of the process, but also the electrode selectivity (Feng et al. 2016). Common anode materials used in studies of electrochemical water disinfection are titanium with active coatings based on metal oxides, which are known as Dimensionally Stable Anodes (DSA®s) (Gusmão et al. 2010), platinum (Jeong et al. 2007) and boron-doped diamond (BDD) electrodes (Lacasa et al. 2013, Long et al. 2015). DSA® type electrode materials include IrO_2-RuO_2 (Bergmann and Koparal 2005), TiO_2-RuO_2 (Gusmão et al. 2010), SnO_2 (Watts et al. 2008), and IrO_2-Sb_2O_5-SnO_2 (Fang et al. 2006). These electrodes have shown higher efficiencies in the production of free chlorine compared to Pt and diamond electrodes, which is of primary importance in environmental applications of electrochemical technology in the presence of chloride salts (Bergmann et al. 2008, Kraft 2008). In addition, diamond electrodes may further oxidize hypochlorite to chlorate and perchlorate (Palmas et al. 2007) which are permissible in potable water only at very low concentrations (Kraft 2008). Therefore, DSA® type electrodes are more applicable for the electrochemical disinfection of water due to their higher efficiency in the production of oxidizing species.

The mechanism of electrochemical microbial inactivation is not completely understood. Fundamentally, the vital physiological functions of bacteria are based on the cell membrane, cytoplasm, and nucleic acids (DNA and RNA). Thus, damages to any of these subcellular constituents of bacteria could potentially lead to the inactivation of bacteria. Diao et al. (Diao et al. 2004) observed leakage of substantial intracellular materials from *E. coli* cells after electrochemical treatment by DSA®s under scanning electron microscope. In another study, Jeong et al. (Jeong et al. 2006) observed changes in the inner content and cell walls of *E. coli* as a result of BDD disinfection. The work of Tanaka et al. (Tanaka et al. 2013) revealed lipid peroxidation in the cell membranes of electrochemically disinfected bacteria in seawater using a Pt anode. Long et al. (Long et al. 2015) investigated the subcellular mechanisms of *E. coli* inactivation during BDD electrochemical disinfection in three electrolytes: in chloride solution, *E. coli* inactivation was attributed to damage to the intracellular enzymatic systems; in sulfate solution, the elimination of certain essential membrane proteins such as K^+ ion transport systems mainly induced cell inactivation; and in phosphate solution, mineralization of their organic intracellular components was responsible for cell inactivation.

To the best of our knowledge, the performance of mixed metal oxide (MMO) electrodes consisting of antimony-tin-tungsten-oxides in electrochemical inactivation of microorganisms has not been investigated. In this context, the main objective of the present work was to examine the potential of electrochemical disinfection of saline water employing antimony-doped tin-tungsten-oxide electrode coatings (Sb-doped $Sn_{80\%}$-$W_{20\%}$-oxide) formed on a titanium substrate *via* a thermal deposition method. This electrode was selected as it was found to have high intrinsic electrocatalytic activity for oxidation of phenol red in a previous study (Ghasemian and Omanovic 2017). A non-pathogenic strain of *E. coli* was selected as a model bacterium, while pathogenic *E.*

coli and *Enterococcus faecalis* (*E. faecalis*) were used to verify the inactivation efficiency of the process. To examine the disinfection potential of the system, the electrochemical production of free chlorine as well as process parameters such as current density, bacterial cell density, pH, and the presence of natural organic matter (NOM) and a radical scavenger were systematically investigated in chloride- and phosphate-containing solutions. Moreover, the energy requirement to reach a specific level of bacterial inactivation (3.5-log and 7.4-log reductions) at each current density was calculated.

4.3. Materials and Methods

4.3.1. Electrode Preparation

Sb-doped $Sn_{80\%}$-$W_{20\%}$-oxide anode coatings were prepared on 50 mm × 100 mm × 2 mm flat titanium substrates employing a thermal deposition method. The titanium sheets were pretreated (polished, degreased and etched) before the deposition of the coatings. The metal salts used to prepare the coating precursor solution were $SnCl_2.2H_2O$ (ACS reagent, ≥ 98.0%, Sigma Aldrich), $Na_2WO_4.2H_2O$ (Certified ACS, 100.0%, Fisher), and $SbCl_3$ (ACS reagent, ≥ 99.0%, Sigma Aldrich). All solutions were prepared using ultra-pure deionized water (resistivity: 18.2 MΩ cm). The metal-oxide coatings were formed by brushing the coating solution onto the pretreated side of Ti substrate (only one side of the Ti substrate was coated, while the other side was covered by an insulating tape), drying in oven at 100°C for 10 min to evaporate the solvent, and then baking in an air furnace at 500°C for 10 min. This process was repeated ten times and after the last coating application, the electrodes were annealed at 500°C for 2 hours to complete the formation of metal oxides in the coating.

4.3.2. Bacterial Strains and Growth Conditions

The mutant of the *E. coli* K12 strain, D21, used in this study was obtained from the *E. coli* Genetic Stock Center at Yale University (CGSC #5158). Results obtained with the model non-pathogenic organism *E. coli* D21 were compared with those obtained using two pathogenic strains; namely, *E. coli* O157:H7 ATCC 700927 (Gram-negative) and *Enterococcus faecalis* (*E. faecalis*) ATCC 29212 (Gram-positive). Inoculums were taken from pure cultures maintained at -80°C in Luria Bertani (LB) Broth (Fisher, BP1427), spread onto LB agar plates, and incubated at 37°C overnight. For each experiment, a single colony from a fresh plate was used to inoculate 30 mL of sterile LB broth. Cultures were grown at 37°C for 18 h in a shaking incubator set at 180 rpm. After 18 h of incubation, corresponding to the stationary phase, cells were harvested by centrifugation at 5000*g* for 10 min (Multifuge X3R, Thermo Heraeus) at 20°C. The growth medium was decanted and the bacterial pellet was resuspended in 0.1 M potassium phosphate buffer solution (pH 7.1 ± 0.05) prepared from KH_2PO_4 salt (ACS Certified, Fisher) with 0.1 M NaCl (ACS Certified, Fisher), which was used as the background electrolyte in this work, unless otherwise stated. Centrifugation and resuspension were repeated one more time. The concentration of the cell suspension was determined by measuring its optical density at 600 nm using a UV-Vis spectrophotometer (Agilent 8453). To study the impact of initial bacterial load on disinfection, bacterial suspensions were prepared at 10^5 and 10^7 colony forming units (CFU)/mL.

4.3.3. Electrochemical Reactor

The electrochemical reactor consisted of a 900-mL beaker (Pyrex glass) with a Teflon lid and was placed in a water bath to keep the temperature constant at 25°C during the experiments. A schematic diagram of the three-electrode batch electrochemical reactor is shown in Appendix as

Figure A- 1. The working electrode was the prepared Sb-doped $Sn_{80\%}$-$W_{20\%}$-oxide film. An 80 mm × 100 mm × 2 mm curved stainless steel plate (316L) served as the counter electrode. Both electrodes were placed vertically in the cell with 5.5 cm distance between them. Saturated calomel electrode (SCE) was used as the reference. The electrodes were connected to a power source providing constant current during experiments. The reactor medium was prepared using the bacterial inoculum diluted in the electrolyte (0.1 M potassium phosphate buffer with 0.1 M NaCl), yielding a 550-mL bacterial suspension with initial concentration of ~10^7 CFU/mL. The electrolyte and all the solutions used in this work were sterilized using 0.45 μm pore filters (Corning 430625). The temperature of the electrolyte was monitored using a thermometer. Filtered air was bubbled into the solution during the experiments to provide mixing.

4.3.4. Disinfection Experiments

The coated electrode was sonicated in deionized water for 20 min before experiments to remove residual contamination from the surface of the electrode. The reactor was operated in a three-electrode mode and potentials were noted relative to SCE. The disinfection of bacterial suspension was carried out at constant current densities of 0.2, 1, 2, 4, 6 and 10 mA/cm^2 with 10^7 CFU/mL initial bacterial concentration. The voltage and temperature at each sampling time were recorded. Before starting each electrochemical experiment, a 100 μL sample was taken from the reactor with a sterile pipette to determine the initial concentration of bacteria. Also, samples were collected during the runs at selected time intervals and were analyzed as described below.

4.3.5. Bacterial Sample Analysis

The drop plate method was used to estimate the concentration of viable bacteria in the samples by enumerating the CFU grown on a LB agar plate (Herigstad et al. 2001). The samples taken from

the bacterial suspension in the reactor were serially diluted down to 10^{-5} (with a factor of 10^{-1}) of its initial concentration using the background electrolyte. Each dilution was thoroughly mixed, from which the 10 μL drops were dispensed over the one-sixth of the surface of an agar plate which was then incubated at 37°C for 14 h. After this time, CFU were counted and the average of the total count of CFU over 3 drops at the countable dilution was determined to calculate the initial concentration of bacteria. The viable cell density was initially 10^7 CFU/mL in disinfection tests.

4.3.6. Modes of Disinfection Action

4.3.6.1. Adhesion of Microbial Cells onto Electrodes

Bacterial adhesion to the electrode surfaces and the culturability of the adhered cells was tested by performing control experiments with electrodes in place but without applying the current through the system. Furthermore, the viability of bacteria attached to the electrode surfaces was evaluated using BacLight Live/Dead assay (Live/Dead BacLight, Molecular Probes) which includes two DNA-binding stains: the green fluorescent stain, SYTO-9, and the red fluorescent stain, propidium iodide (PI). In this method, bacterial inactivation is measured based on the loss in membrane integrity of the cells (Boulos et al. 1999). Green fluorescing SYTO-9 is able to enter all cells, so is an indication of live cells, whereas red fluorescing PI enters only cells with damaged cytoplasmic membranes and is therefore an indication of non-viable cells (Asadishad et al. 2011, Boulos et al. 1999). After disinfecting *E. coli* D21 suspension for 30 min (at a mild current density of 2 mA/cm^2), the working electrode was removed from the reactor and rinsed with the background electrolyte to remove unattached cells. Then, the surface of the electrode was stained with Live/Dead BacLight (Invitrogen) and imaged by fluorescence microscopy (IX-71, Olympus). The same procedure was repeated for *E. coli* O157:H7 and *E. faecalis*.

4.3.6.2. Influence of Solution Chemistry

The role of electrochemically-produced hydroxyl radicals in inactivation of *E. coli* was investigated by adding methanol (0.1 M), a well-known hydroxyl radical scavenger into the reactor medium (El-Morsi et al. 2000, Page et al. 2011). The influence of NOM, ubiquitously present in all freshwater systems (Cantwell et al. 2008), on electrochemical disinfection efficacy was also investigated using Suwannee River NOM (SR-NOM, 2R101N, IHSS) at concentrations of 2 mg/L and 10 mg/L. To prepare the experimental suspension, SR-NOM was added to the electrolyte, well-mixed using a magnetic stir bar, and then the solution was filtered through a 0.45-μm pore filter before adding bacteria. The influence of chloride concentration on electrochemical disinfection performance was investigated at a fixed current density of 2 mA/cm^2 by adding NaCl to the solution at different concentrations of 0, 0.01, 0.05, and 0.1 M. The disinfecting ability of our electrochemical system through generation of oxidants other than chlorine was tested by conducting preliminary electrochemical experiments in chloride-free phosphate buffer solution. Moreover, the effect of pH on inactivation rate was studied. All experiments were run at least three times and after each experiment all the glassware and the reactor were cleaned with 10% bleach, washed twice with tap water and detergent, and then autoclaved at 121°C for 20 min.

4.3.6.3. Determination of Active Chlorine Production

To evaluate the disinfecting role of oxidants produced in the presence of chloride in the solution during the electrochemical process, the amount of dissolved chlorine in the solution was determined as mg/L Cl_2 by DPD (N,N-diethyl-p-phenylendiamine) colorimetric method (Clesceri et al. 1989) from the magenta color produced as a result of the instantaneous reaction between active chlorine species and DPD indicator. Aliquots of 2 mL of the treated solution were collected

in a cuvette containing 100 µL of the phosphate buffer reagent for chlorine determination (RICCA, 5805-16) and 100 µL DPD indicator (RICCA, 2655-16), and analyzed immediately by recording the absorption spectra in the range of 400-800 nm using a UV-Vis spectrophotometer. The concentration of free chlorine in samples was then calculated from the absorbance measured at 512 nm by using a calibration curve prepared previously with potassium permanganate solution as recommended (Clesceri et al. 1989), to a minimum detectable chlorine concentration of 50 µg/L.

4.4. Results and Discussion

4.4.1. Role of Bacterial Adhesion onto Electrodes

Control experiments performed with the electrodes in place but at zero current showed no observable decrease in *E. coli* D21 concentration in the reactor medium over a 60-min period (for an initial loading of 10^7 CFU/mL). This indicates that any observed decrease in bacterial load when the current is applied can be attributed to the electrochemical process. Microscope imaging (at 20X magnification) of the electrodes after 30 min of electrolysis at 2 mA/cm^2 showed no attached bacteria for *E. coli* O157:H7. For *E. coli* D21, most of the attached cells on the electrode were dead at the end of the test (as determined using the Live/Dead Baclight assay), whereas for *E. faecalis*, the number of attached bacteria was less than for *E. coli* D21 but most of the attached cells were live. The results show that the amount of cell adhesion to the electrodes and the extent of their inactivation were dependent on the type of bacteria with the Gram-positive *E. faecalis* being the most resistant and *E. coli* D21 the most susceptible to electrochemical disinfection.

4.4.2. Influence of Current Density on Bacterial Inactivation

Figure 4-1 presents the influence of current density on changes in bacterial concentration during the electrochemical treatment of *E. coli*-contaminated solutions containing 0.1 M NaCl (pH 7.1 ± 0.05). An increase in the current density from 0.2 to 1 mA/cm^2 resulted in more than 50% decrease in log_{10}-bacterial concentration after 20 min. Further increase in the current density led to a complete inactivation of 10^7 CFU/mL *E. coli* D21 within 5 min for 2 mA/cm^2, 2 min for 4 mA/cm^2, 1 min for 6 mA/cm^2, and 1 min for 10 mA/cm^2 current density. The higher inactivation rates were achieved by increasing the applied current density, which is consistent with previous reports (Gómez-López et al. 2013, Schmalz et al. 2009). At a higher current density, more oxidizing species are generated at the anode surface to attack and kill microorganisms. However, increase in the current density from 6 mA/cm^2 to 10 mA/cm^2 did not raise the inactivation rate appreciably. This implication supports the statement reported elsewhere (Särkkä et al. 2008) that after reaching a threshold value for current density, the energy will be mainly used to produce oxygen and not oxidizing species. Based on the results of the control experiment mentioned above, the decrease in the concentration of bacteria shown in **Figure 4-1** was due to the inactivation of *E. coli* cells, not due to the attachment of cells onto the electrode surface. Moreover, the fact that no notable decrease in bacterial concentration was observed at the current density of 0.2 mA/cm^2 implies that there is a threshold concentration for oxidants produced electrochemically, to cause bactericidal effects (Bensalah and Abdel-Wahab 2013a, b).

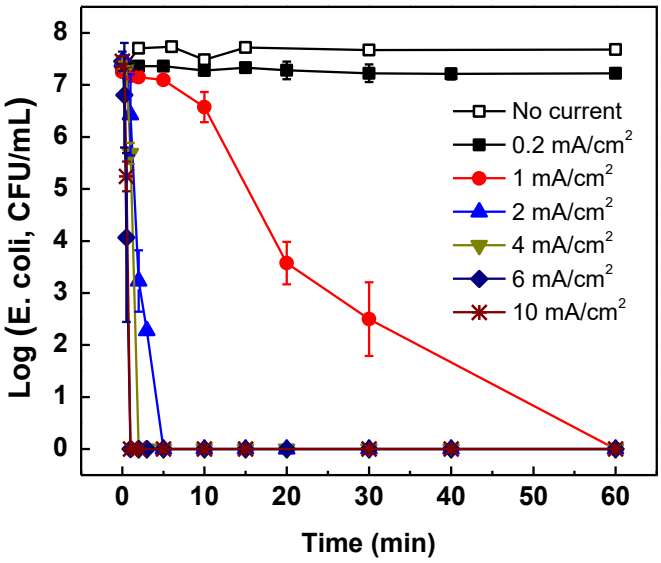

Figure 4-1: Influence of current density on bacterial inactivation during electrochemical treatment of solutions containing initial concentration of ~10^7 CFU/mL *E. coli* D21 in 0.1 M NaCl + 0.1 M potassium phosphate buffer (pH 7.1). Results represent mean value ± SD (n = 3).

4.4.3. Effect of Interfering Species

4.4.3.1. Inhibitory Effect of Radical Scavengers on Bacterial Inactivation

Practical application of disinfection systems is linked with their ability to maintain the disinfecting activity in the presence of radical scavengers such as bicarbonate, sulfate ions, halide ions, or alcohols (Billany et al. 1996, Grebel et al. 2010, Liao et al. 2001). Therefore, the possibility of their interference with disinfection activity must be considered for practical applications. We investigated the effect of methanol as a hydroxyl radical scavenger on the bacterial survival at two current densities of 2 and 4 mA/cm^2. Control experiments showed that addition of 0.1 M methanol had no effect on *E. coli* inactivation, when no current was applied (solid squares) under the conditions used in this work (**Figure 4-2**a). *E. coli* inactivation was significantly retarded by

addition of methanol when the current was flowing through the cell, leading to 80% and 19% bacterial survival after 30 min at current densities of 2 and 4 mA/cm^2, respectively (compare the solid with open symbols in **Figure 4-2**a). Since methanol is a known hydroxyl radical scavenger, thus reducing the potential formation of hydrogen peroxide, ozone and atomic oxygen (Eqs. (2-5)), this finding indicates that electrochemically-generated ROS play an essential role in the second stage inactivation of bacteria, assuming the first stage can be attributed to the direct oxidation at the electrode surface (Jeong et al. 2007).

4.4.3.2. Inhibitory Effect of Natural Organic Matter (NOM) on Bacterial Inactivation

Water supplies that require disinfection may contain varying loads of natural organic matter (NOM) that may impact treatment efficiency. Therefore, it is important to examine the effect of NOM on the efficacy of the electrochemical disinfection process. **Figure 4-2**b shows the removal of *E. coli* D21 in the absence and presence of 2 and 10 mg/L of SR-NOM as a function of time during the electrochemical treatment in 0.1 M NaCl + 0.1 M potassium phosphate buffer electrolyte. The contact time required to reach complete bacterial inactivation increased from 2 min in the absence of SR-NOM to 5 min and 15 min in the presence of 2 mg/L and 10 mg/L SR-NOM, respectively. Thus, SR-NOM reduced the inactivation efficiency of the electrochemical process. Overall, the strong inhibitory effect of organic matter on bacterial inactivation can be attributed to a combination of several effects such as radical scavenging, inhibition of the catalytic process by faster adsorption onto the catalyst sites and occupying them, and competition between the organic compounds and the microorganisms for hydroxyl radicals (Gomes et al. 2009, Rodrigues et al. 2007). It has also been found that humic substances offer protection against solar (Gomes et al. 2009, Rodrigues et al. 2007) and UV (Cantwell et al. 2008, Muela et al. 2002)

irradiation in photolytic or photocatalytic inactivation of bacteria (and also viruses (Templeton et al. 2006)) and lengthen the survival of microorganisms, mainly due to the formation of a thin coating on the surface of the cells presenting a blocking effect (Cantwell et al. 2008).

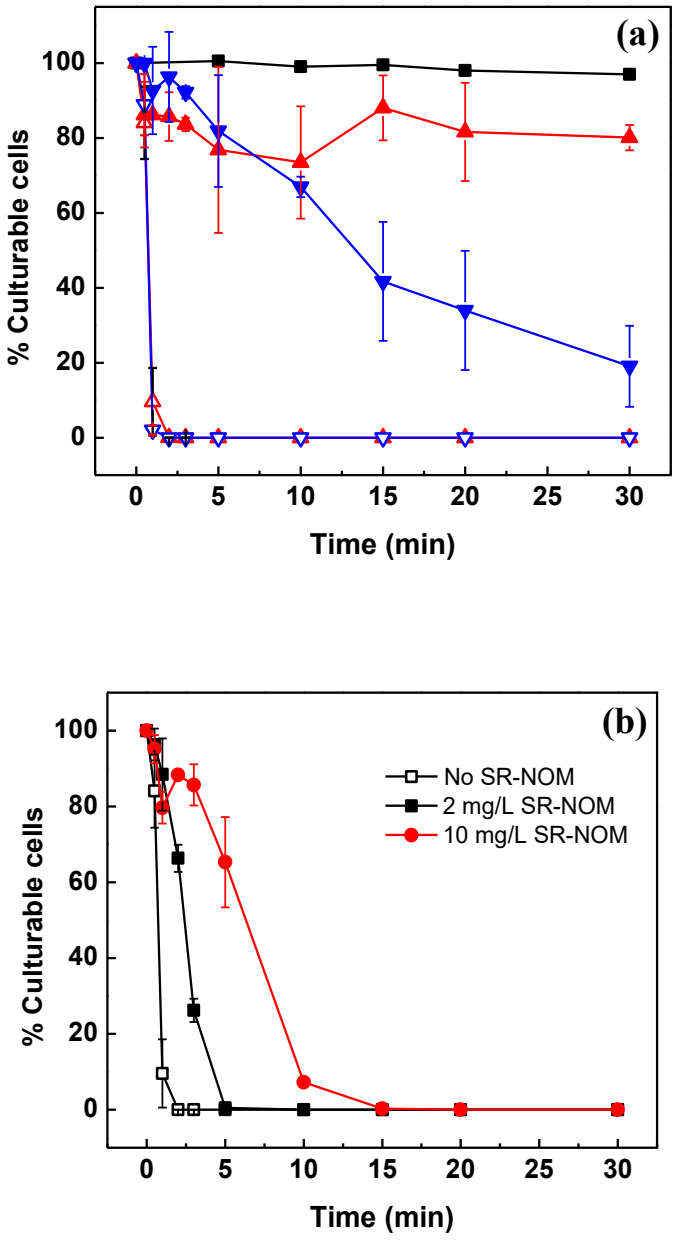

Figure 4-2: Inhibitory effects of (a) a radical scavenger at zero current (■), 2 mA/cm^2 current density without adding methanol (Δ), 2 mA/cm^2 current density with 0.1 M methanol (▲), 4 mA/cm^2 current density without adding methanol (∇), 4 mA/cm^2 current density with 0.1 M methanol (▼); and (b) SR-NOM at 2 mA/cm^2 current density, on changes in the number of *E. coli* D21 culturable cells in the reactor during the electrochemical treatment of 0.1 M NaCl + 0.1 M potassium phosphate buffer solution (pH 7.1). Results represent mean value ± SD (n = 3).

4.4.4. Role of Active Chlorine Oxidants

4.4.4.1. Influence of Current Density on Active Chlorine Production

The concentration of active chlorine species (dissolved Cl_2, HOCl and ClO^-) in the electrolyte samples was determined using the DPD colorimetric method. It should be noted that, in addition to chlorine, other possible oxidants (e.g. O_3, H_2O_2, ClO_2) generated in electrochemical disinfection process can also react with DPD and contribute to the magenta color, and therefore the DPD test results may in fact represent the total oxidizing potential of electrochemically produced oxidants (Harp 2002, Schmalz et al. 2009). **Figure 4-3**a shows the electrochemical generation of active chlorine at different constant current densities, obtained at fixed initial chloride concentration of 0.1 M and pH 7.1 ± 0.05 in the absence of bacteria. As shown in **Figure 4-3**a, no significant concentration of active chlorine was detected in experiments at the current density of 1 mA/cm^2. The chlorine production increased significantly from ~ 0.5 mg/L up to 3.3 mg/L after 20 min, as the current density was raised from 1 mA/cm^2 to 2 mA/cm^2, and it remained relatively constant with time. However, although further increase in current density to 4 and to 10 mA/cm^2 resulted in an increase in the maximum amount of chlorine produced (**Figure 4-3**a), the amount of chlorine decreased after 20 and 15 minutes, respectively. Having a relatively high concentration of ions, the system is not expected to be in a mass transport controlling regime, but increasing the applied current to higher values could shift the process to become limited by mass transport conditions and/or chlorate (ClO_3^-) production by possible side reactions occurring at the anode (Eq. (9)) or in the aqueous solution (Eq. (10)), as expressed below (Fraga et al. 2009):

$$6ClO^- + 3H_2O \rightarrow 2ClO_3^- + 6H^+ + 4Cl^- + 1.5O_2 + 6e^- \quad (4\text{-}9)$$

$$2HClO + ClO^- \rightarrow ClO_3^- + 2Cl^- + 2H^+ \quad (4\text{-}10)$$

However, due to the complexity of the method for determining the chlorate concentration, the measurements were not performed in this work.

4.4.4.2. Effect of Chloride Concentration on Active Chlorine Production

To determine the amount of active chlorine produced during the electrochemical treatment, the experiments were performed in the absence of bacteria. **Figure 4-3**b shows the effect of initial chloride concentration on the electrochemical generation of active chlorine at 2 mA/cm^2 current density. As expected, chlorine formation increased with the amount of NaCl added. This observation that the significant production of active chlorine started at 0.1 M NaCl, is in agreement with an earlier study regarding the requirement for a minimum chloride concentration for the formation of active chlorine leading to an effective inactivation of bacteria (Bergmann and Koparal 2005). However, the formation of free chlorine even at very low concentration of NaCl (0.01 M) was detected (**Figure 4-3**b).

4.4.4.3. Influence of pH on Active Chlorine Production

The influence of pH on active chlorine production was investigated by comparing the electrochemical disinfection results obtained for solutions containing 0.1 M NaCl at pH 5.0 and pH 9.0 conducted at 2 mA/cm^2 with results obtained at pH 7.1. The amount of active chlorine produced during 60 min of electrolysis was measured at different time intervals, as shown in **Figure 4-3**c. As can be seen, the free chlorine production decreased with increasing pH, and the decrease was sharper going from pH 7.1 to 9.0; the amount of active chlorine produced at pH 9 was significantly lower than those measured at both pH 5.0 and pH 7.1 (Student's t-test). However, the amount of generated chlorine measured at pH 5.0 and pH 7.1 were not significantly different, except at t = 45 min. The decrease in chlorine production at high pH values can be attributed to

the preferential adsorption of HO^- on the anode surface at basic conditions (Zanoni et al. 2004). Furthermore, at lower pH, more hypochlorous acid is produced (Eq. (7)), whereas at higher pH more hypochlorite ion is formed (Eq. (8)), which has lower oxidation potential than hypochlorous acid (Särkkä et al. 2008). Moreover, it is believed that increased acidity decreases the scavenging effect of potential radical scavengers (Lipczynska-Kochany et al. 1995). Thus, this system is expected to exhibit higher disinfection efficiency at neutral or acidic conditions.

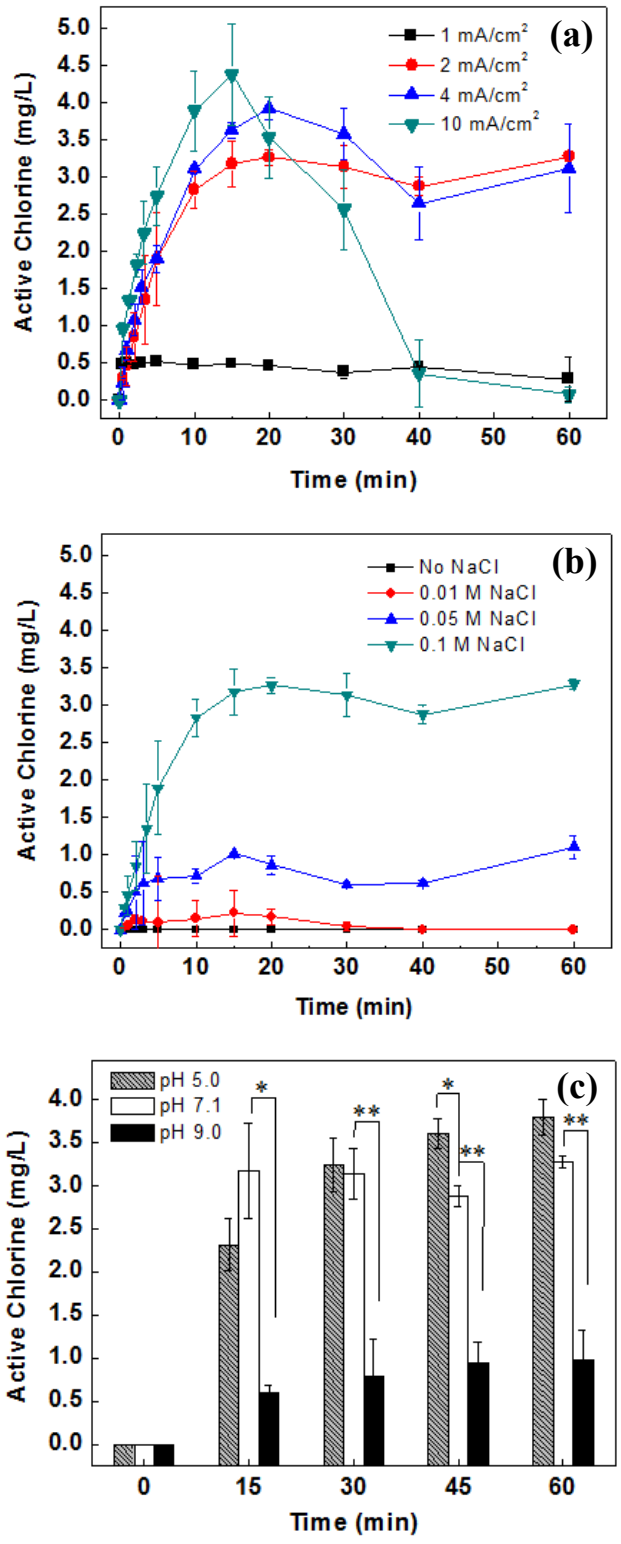

Figure 4-3: Effects of (a) current density in 0.1 M NaCl (pH 7.1), (b) chloride concentration at the current density of 2 mA/cm^2 (pH 7.1), and (c) solution pH at 0.1 M NaCl on active chlorine

production during electrochemical water treatment in 0.1 M potassium phosphate buffer. Results represent mean value ± SD (n = 3). * $p \leq 0.05$; ** $p \leq 0.01$.

4.4.5. Effect of Chloride Concentration on Bacterial Inactivation

Figure 4-4 presents the influence of initial chloride concentration on the electrochemical inactivation of 10^7 CFU/mL *E. coli* D21 at a fixed current density of 2 mA/cm^2. The bactericidal efficiency of the electrochemical process was improved by increasing the concentration of NaCl. For the experiment performed in the absence of NaCl, complete bacterial inactivation was achieved within 15 min of operation. Addition of 0.01 M and 0.05 M NaCl exhibited similar effects on the bacterial inactivation rate and shortened the contact time required for complete inactivation to 5 min. At the increased chloride concentration of 0.1 M, complete disinfection was achieved in 2 min. Increasing NaCl concentration results in an enhanced production of reactive oxidative species and, thus, faster bacterial inactivation.

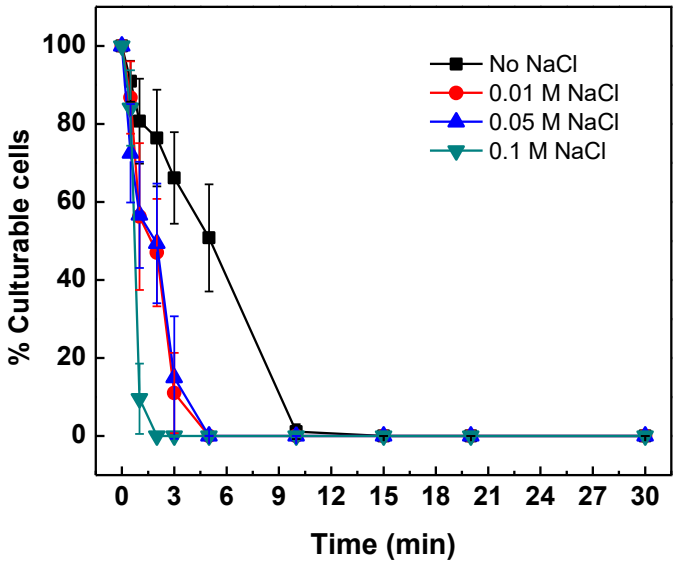

Figure 4-4: Influence of NaCl concentration on the number of culturable cells in the reactor during the electrochemical treatment of ~10^7 CFU/mL *E. coli* D21 at current density: 2 mA/cm^2 and in 0.1 M potassium phosphate buffer (pH 7.1). Results represent mean value ± SD (n = 3).

4.4.6. Effect of Initial Bacterial Load and Strain Type

The influence of initial bacterial cell density on the number of culturable cells in the reactor for *E. coli* D21 is shown in **Figure 4-5**. As can be seen, the required contact time for complete bacterial inactivation increased with bacterial load. At the current density of 0.2 mA/cm^2, the percentage of surviving cells of *E. coli* at an initial load of 10^5 and 10^7 CFU/mL was found to be 30% and 88%, respectively, within 5 min of electrolysis. A similar trend was observed at the applied current density of 1 mA/cm^2. This finding that the percentage of surviving cells increased with the initial bacterial density is in agreement with previous reports (Bekbölet 1997, Jeong et al. 2007). Besides the lower oxidants/bacteria ratio, higher coverage of the electrode surface by bacterial cells due to electrostatic attraction between positively charged anode surface and

negatively charged *E. coli* cells, in solutions with higher bacterial loads may cause a blocking effect at the electrode surface retarding the electron transfer to the ions and thus lower production of oxidative species.

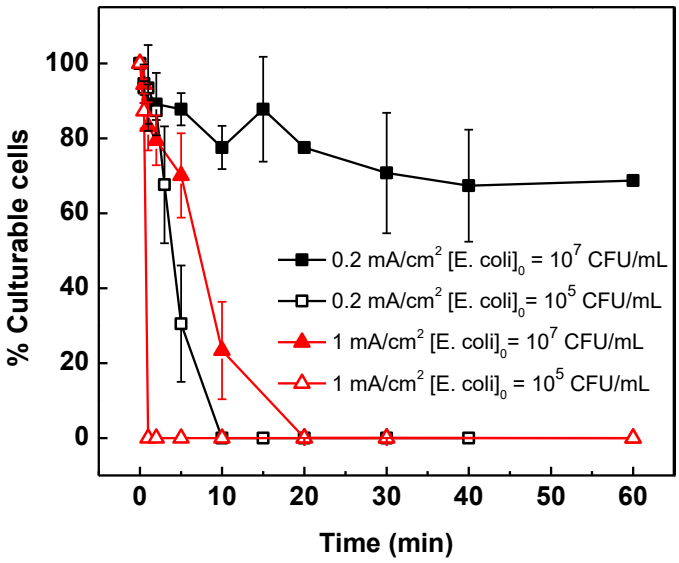

Figure 4-5: Effect of initial bacterial load on the percentage of culturable E. coli D21 cells during electrochemical treatment of 0.1 M NaCl + 0.1 M potassium phosphate buffer solution (pH 7.1). Results represent mean value ± SD (n = 3).

Figure 4-6 shows the decay of the number of culturable cells in the reactor with time during the electrochemical treatment of aqueous solutions containing 0.1 M NaCl contaminated with different model bacteria; namely, *E. coli* D21, *E. coli* O157:H7 and *E. faecalis*. As can be seen, total bacterial inactivation was achieved for all bacteria types. Although it appears that the inactivation of *E. coli* D21 and *E. coli* O157:H7 was slightly faster than that of *E. faecalis,* the differences are not statically significant, as determined by Student's t-test. These experiments

show that the electrochemical process is equally effective against the Gram+ and Gram- bacteria tested here.

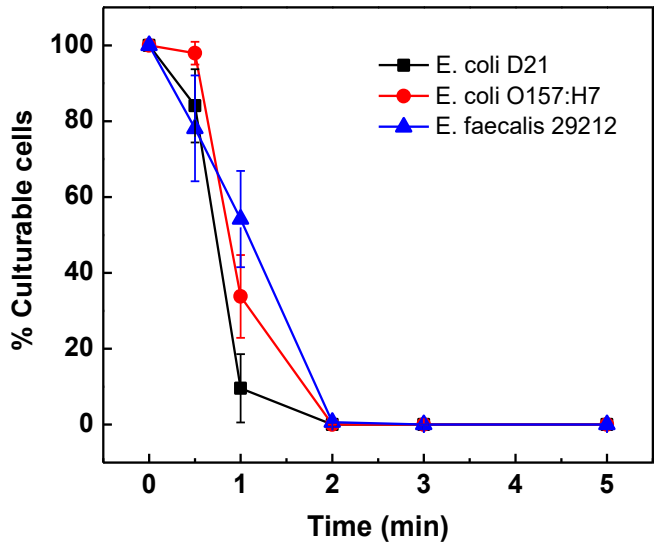

Figure 4-6: Changes in the number of culturable cells with time for different bacteria strains during the electrochemical treatment of 0.1 M NaCl + 0.1 M potassium phosphate buffer solution (pH 7.1). Results represent mean value ± SD (n = 4).

4.4.7. Energy Consumption During the Electrochemical Disinfection Process

Although higher current densities result in higher microbial inactivation, they are associated with greater energy consumption. To understand the cost effectiveness of the process, the performance of electrochemical disinfection was evaluated in terms of energy efficiency. The process intrinsic energy (considering only the electrical energy) required to achieve a 3.5-log reduction as well as complete inactivation (7.4-log reduction) of 10^7 CFU/mL *E. coli* D21 was calculated based on the required contact time, current density, and the resulting cell voltage (**Table**

4-1). The maximum increase in the temperature of the reactor medium was less than 1°C in all operations. By increasing the current density from 6 mA/cm^2 to 10 mA/cm^2, the treatment time required for complete removal of bacteria did not change, but the energy consumption increased by 100%. This result confirms the statement above that after a certain threshold value for current density, the additional energy input will mostly generate oxygen and not oxidative species. Thus, the current density of 6 mA/cm^2 was the most efficient in terms of energy consumption to achieve an equal *E. coli* inactivation, corresponding to an energy input of 48.18 Wh/m^3 for complete bacterial inactivation. This estimated value is considerably lower than that obtained by Lacasa et al. (Lacasa et al. 2013) (88 Wh/m^3) and Heim et al. (Heim et al. 2015) (250 Wh/m^3) required to completely inactivate 10^6-10^7 CFU/mL and 10^7-10^8 CFU/mL *E. coli* in water containing 30 g/L (~ 0.5 M) and 20 g/L (~ 0.35 M) NaCl using BDD anodes, respectively. Also, these values are on the same order of magnitude as values reported in the literature for inactivation of 10^7 CFU/mL *E. coli* in Na_2SO_4 electrolyte using BDD anode (Li et al. 2010). The calculated values for energy consumption listed in **Table 4-1** represent promising results when compared to the 7 kJ/L (~ 1944 Wh/m^3) UV energy used to reach a final concentration of 10 CFU/mL from an initial *E. coli* load of 4.25×10^5 CFU/mL by photolysis, as reported by Gomes et al. (Gomes et al. 2009), and 4.2 kJ/L (~ 1167 Wh/m^3) UV energy required to reduce the initial *E. coli* concentration of 10^7 to 90 CFU/mL by solar photocatalysis using TiO_2, as shown by Sichel et al. (Sichel et al. 2007).

Table 4-1

Calculated process intrinsic electrical energy consumption for 3.5-log removal and complete inactivation (7.4-log reduction) of *E. coli* D21 with the initial concentration of 10^7 CFU/mL during the electrochemical treatment of 0.1 M NaCl + 0.1 M potassium phosphate buffer solution (pH 7.1). Data represent mean value ± SD (n = 3).

Current density	3.5-log reduction			7.4-log reduction (complete inactivation)		
($mA/cm^{2)}$	Voltage (V)	Time (min)	$E_{3.5\text{-log}}$ (Wh/m^3)	Voltage (V)	Time (min)	$E_{7.4\text{-log}}$ (Wh/m^3)
0.2	1.1	> 60		1.1	> 60	
1	3.8	20	115.76 ± 5.81	3.9	60	355.45 ± 21.60
2	4.1	2	24.85 ± 1.25	4.2	5	63.64 ± 4.33
4	4.4	2	53.33 ± 2.15	4.4	2	53.33 ± 2.15
6	5.3	1	48.18 ± 3.22	5.3	1	48.18 ± 3.21
10	6.6	1	99.24 ± 2.57	6.6	1	99.24 ± 2.57

4.5. Conclusions

This study demonstrates the strong bactericidal activity of Sb-doped $Sn_{80\%}$-$W_{20\%}$-oxide anodes, which increased with increasing current density and NaCl concentration. This can be explained by the advancing role of mediated oxidation processes carried out by the electrogenerated oxidants including ROS and RCS in the inactivation of bacteria. It was found that the electrochemically-generated ROS (*e.g.* hydroxyl radicals, hydrogen peroxide, ozone) and RCS (*e.g.* Cl_2, HOCl, ClO^-) were mainly responsible for inactivation of bacteria at high and low current densities, respectively. It was also found that the presence of NOM and radical scavengers such as methanol adversely affect *E. coli* inactivation by electrochemical treatment. Increasing the pH of the solution also resulted in a lower bacterial inactivation rate. Moreover, the results showed that the treatment efficacy was comparable for three different bacterial strains. The highest efficiency for total electrochemical disinfection of *E. coli* D21 at an initial load of 10^7 CFU/mL was obtained

at 6 mA/cm^2 current density with 0.1 M NaCl at pH 7.1 with a power consumption of 0.048 kWh/m^3. The study concludes that Sb-doped $Sn_{80\%}$-$W_{20\%}$-oxide anodes are effective electrocatalysts for production of powerful oxidants in aqueous solutions towards the efficient disinfection of bacteria by electrochemical treatments. The potential production of disinfection by-products such as trihalomethanes and haloacetic acids was not monitored in this preliminary proof-of-concept work and should be considered for practical applications.

Acknowledgement

The authors acknowledge the Natural Sciences and Engineering Research Council of Canada (NSERC) for funding awarded to S.O. and N.T, the Canada Research Chairs Program and a McGill Engineering Doctoral Award to S.G.

4.6. References

[1] A. Lawton, L. and K. J. Robertson, P. (1999) Physico-chemical treatment methods for the removal of microcystins (cyanobacterial hepatotoxins) from potable waters. Chemical Society Reviews 28(4), 217-224.

[2] Anglada, Á., Urtiaga, A. and Ortiz, I. (2009) Contributions of electrochemical oxidation to waste-water treatment: fundamentals and review of applications. Journal of Chemical Technology & Biotechnology 84(12), 1747-1755.

[3] Asadishad, B., Ghoshal, S. and Tufenkji, N. (2011) Method for the Direct Observation and Quantification of Survival of Bacteria Attached to Negatively or Positively Charged Surfaces in an Aqueous Medium. Environmental Science & Technology 45(19), 8345-8351.

[4] Bekbölet, M. (1997) Photocatalytic bactericidal activity of TiO_2 in aqueous suspensions of *E. Coli*. Water Science and Technology 35(11–12), 95-100.

[5] Bensalah, N. and Abdel-Wahab, A. (2013a) Electrochemical Inactivation of *P. Aeruginosa*, *A. hydrophila*, *L. pneumophila* using Boron Doped Diamond Anodes, p. 9.

[6] Bensalah, N. and Abdel-Wahab, A. (2013b) Electrochemical Inactivation of P. Aeruginosa, A. hydrophila, L. pneumophila using Boron Doped Diamond Anodes. Journal of Advanced Oxidation Technologies 16(1), 9-15.

[7] Bergmann, H., Koparal, A.T., Koparal, A.S. and Ehrig, F. (2008) The influence of products and by-products obtained by drinking water electrolysis on microorganisms. Microchemical Journal 89(2), 98-107.

[8] Bergmann, M.E.H. and Koparal, A.S. (2005) Studies on electrochemical disinfectant production using anodes containing RuO_2. Journal of Applied Electrochemistry 35(12), 1321-1329.

[9] Billany, M.R., Khatib, K., Gordon, M. and Sugden, J.K. (1996) Alcohols and ethanolamines as hydroxyl radical scavengers. International Journal of Pharmaceutics 137(2), 143-147.

[10] Boulos, L., Prévost, M., Barbeau, B., Coallier, J. and Desjardins, R. (1999) LIVE/DEAD® BacLight™: application of a new rapid staining method for direct enumeration of viable and total bacteria in drinking water. Journal of Microbiological Methods 37(1), 77-86.

[11] Butterfield, I.M., Christensen, P.A., Curtis, T.P. and Gunlazuardi, J. (1997) Water disinfection using an immobilised titanium dioxide film in a photochemical reactor with electric field enhancement. Water Research 31(3), 675-677.
[12] Cantwell, R.E., Hofmann, R. and Templeton, M.R. (2008) Interactions between humic matter and bacteria when disinfecting water with UV light. Journal of Applied Microbiology 105(1), 25-35.
[13] Clesceri, L.S., Greenberg, A.E. and Trussell, R.R. (1989) Standard methods for the examination of water and wastewater, APHA-AWWA-WPCF, Washington, DC.
[14] Diao, H.F., Li, X.Y., Gu, J.D., Shi, H.C. and Xie, Z.M. (2004) Electron microscopic investigation of the bactericidal action of electrochemical disinfection in comparison with chlorination, ozonation and Fenton reaction. Process Biochemistry 39(11), 1421-1426.
[15] Drees, K.P., Abbaszadegan, M. and Maier, R.M. (2003) Comparative electrochemical inactivation of bacteria and bacteriophage. Water Research 37(10), 2291-2300.
[16] Drogui, P., Elmaleh, S., Rumeau, M., Bernard, C. and Rambaud, A. (2001) Oxidising and disinfecting by hydrogen peroxide produced in a two-electrode cell. Water Research 35(13), 3235-3241.
[17] El-Morsi, T.M., Budakowski, W.R., Abd-El-Aziz, A.S. and Friesen, K.J. (2000) Photocatalytic Degradation of 1,10-Dichlorodecane in Aqueous Suspensions of TiO_2: A Reaction of Adsorbed Chlorinated Alkane with Surface Hydroxyl Radicals. Environmental Science & Technology 34(6), 1018-1022.
[18] Fang, Q., Shang, C. and Chen, G. (2006) MS2 Inactivation by Chloride-Assisted Electrochemical Disinfection. Journal of Environmental Engineering 132(1), 13-22.
[19] Feng, C., Suzuki, K., Zhao, S., Sugiura, N., Shimada, S. and Maekawa, T. (2004) Water disinfection by electrochemical treatment. Bioresource Technology 94(1), 21-25.
[20] Feng, Y., Yang, L., Liu, J. and Logan, B.E. (2016) Electrochemical technologies for wastewater treatment and resource reclamation. Environmental Science: Water Research & Technology 2(5), 800-831.
[21] Flemming, H.-C. (2002) Biofouling in water systems – cases, causes and countermeasures. Applied Microbiology and Biotechnology 59(6), 629-640.
[22] Fraga, L.E., Anderson, M.A., Beatriz, M.L.P.M.A., Paschoal, F.M.M., Romão, L.P. and Zanoni, M.V.B. (2009) Evaluation of the photoelectrocatalytic method for oxidizing chloride and

simultaneous removal of microcystin toxins in surface waters. Electrochimica Acta 54(7), 2069-2076.

[23] Ghasemian, S. and Omanovic, S. (2017) Fabrication and characterization of photoelectrochemically-active Sb-doped Snx-W(100-x)%-oxide anodes: Towards the removal of organic pollutants from wastewater. Applied Surface Science 416, 318-328.

[24] Ghernaout, D., Badis, A., Kellil, A. and Ghernaout, B. (2008) Application of electrocoagulation in *Escherichia coli* culture and two surface waters. Desalination 219(1), 118-125.

[25] Gomes, A.I., Santos, J.C., Vilar, V.J.P. and Boaventura, R.A.R. (2009) Inactivation of Bacteria *E. coli* and photodegradation of humic acids using natural sunlight. Applied Catalysis B: Environmental 88(3–4), 283-291.

[26] Gómez-López, V.M., Gobet, J., Selma, M.V., Gil, M.I. and Allende, A. (2013) Operating conditions for the electrolytic disinfection of process wash water from the fresh-cut industry contaminated with *E. coli* O157:H7. Food Control 29(1), 42-48.

[27] Grahl, T. and Märkl, H. (1996) Killing of microorganisms by pulsed electric fields. Applied Microbiology and Biotechnology 45(1), 148-157.

[28] Grebel, J.E., Pignatello, J.J. and Mitch, W.A. (2010) Effect of Halide Ions and Carbonates on Organic Contaminant Degradation by Hydroxyl Radical-Based Advanced Oxidation Processes in Saline Waters. Environmental Science & Technology 44(17), 6822-6828.

[29] Gusmão, I.C.C.P., Moraes, P.B. and Bidoia, E.D. (2010) Studies on the electrochemical disinfection of water containing *Escherichia coli* using a Dimensionally Stable Anode. Brazilian Archives of Biology and Technology 53, 1235-1244.

[30] Harp, D.L. (2002) Current Technology of Chlorine Analysis for Water and Wastewater, HACH Company.

[31] Harper, J.C., Christensen, P.A., Egerton, T.A., Curtis, T.P. and Gunlazuardi, J. (2001) Effect of catalyst type on the kinetics of the photoelectrochemical disinfection of water inoculated with *E. coli*. Journal of Applied Electrochemistry 31(6), 623-628.

[32] Heim, C., Ureña de Vivanco, M., Rajab, M., Müller, E., Letzel, T. and Helmreich, B. (2015) Rapid inactivation of waterborne bacteria using boron-doped diamond electrodes. International Journal of Environmental Science and Technology 12(10), 3061-3070.

[33] Herigstad, B., Hamilton, M. and Heersink, J. (2001) How to optimize the drop plate method for enumerating bacteria. Journal of Microbiological Methods 44(2), 121-129.
[34] Jeong, J., Kim, J.Y., Cho, M., Choi, W. and Yoon, J. (2007) Inactivation of Escherichia coli in the electrochemical disinfection process using a Pt anode. Chemosphere 67(4), 652-659.
[35] Jeong, J., Kim, J.Y. and Yoon, J. (2006) The Role of Reactive Oxygen Species in the Electrochemical Inactivation of Microorganisms. Environmental Science & Technology 40(19), 6117-6122.
[36] Kraft, A. (2008) Electrochemical Water Disinfection: A Short Review. Platinum Metals Review 52(3), 177-185.
[37] Kraft, A., Stadelmann, M., Blaschke, M., Kreysig, D., Sandt, B., Schröder, F. and Rennau, J. (1999) Electrochemical water disinfection Part I: Hypochlorite production from very dilute chloride solutions. Journal of Applied Electrochemistry 29(7), 859-866.
[38] Lacasa, E., Tsolaki, E., Sbokou, Z., Rodrigo, M.A., Mantzavinos, D. and Diamadopoulos, E. (2013) Electrochemical disinfection of simulated ballast water on conductive diamond electrodes. Chemical Engineering Journal 223, 516-523.
[39] Li, H., Zhu, X. and Ni, J. (2010) Inactivation of Escherichia coli in Na2SO4 electrolyte using boron-doped diamond anode. Electrochimica Acta 56(1), 448-453.
[40] Liang, W., Qu, J., Chen, L., Liu, H. and Lei, P. (2005) Inactivation of Microcystis *aeruginosa* by Continuous Electrochemical Cycling Process in Tube Using Ti/RuO_2 Electrodes. Environmental Science & Technology 39(12), 4633-4639.
[41] Liao, C.-H., Kang, S.-F. and Wu, F.-A. (2001) Hydroxyl radical scavenging role of chloride and bicarbonate ions in the H_2O_2/UV process. Chemosphere 44(5), 1193-1200.
[42] Lipczynska-Kochany, E., Sprah, G. and Harms, S. (1995) Influence of some groundwater and surface waters constituents on the degradation of 4-chlorophenol by the Fenton reaction. Chemosphere 30(1), 9-20.
[43] Long, Y., Ni, J. and Wang, Z. (2015) Subcellular mechanism of *Escherichia coli* inactivation during electrochemical disinfection with boron-doped diamond anode: A comparative study of three electrolytes. Water Research 84, 198-206.
[44] López-Gálvez, F., Posada-Izquierdo, G.D., Selma, M.V., Pérez-Rodríguez, F., Gobet, J., Gil, M.I. and Allende, A. (2012) Electrochemical disinfection: An efficient treatment to inactivate

Escherichia coli O157:H7 in process wash water containing organic matter. Food Microbiology 30(1), 146-156.

[45] Martínez-Huitle, C.A. and Brillas, E. (2008) Electrochemical Alternatives for Drinking Water Disinfection. Angewandte Chemie International Edition 47(11), 1998-2005.

[46] Mascia, M., Vacca, A. and Palmas, S. (2013) Electrochemical treatment as a pre-oxidative step for algae removal using Chlorella vulgaris as a model organism and BDD anodes. Chemical Engineering Journal 219, 512-519.

[47] Matsunaga, T., Nakasono, S., Takamuku, T., Burgess, J.G., Nakamura, N. and Sode, K. (1992) Disinfection of drinking water by using a novel electrochemical reactor employing carbon-cloth electrodes. Applied and Environmental Microbiology 58(2), 686-689.

[48] Matsunaga, T., Okochi, M., Takahashi, M., Nakayama, T., Wake, H. and Nakamura, N. (2000) TiN electrode reactor for disinfection of drinking water. Water Research 34(12), 3117-3122.

[49] Mitch, W.A., Sharp, J.O., Trussell, R.R., Valentine, R.L., Alvarez-Cohen, L. and Sedlak, D.L. (2003) N-Nitrosodimethylamine (NDMA) as a Drinking Water Contaminant: A Review. Environmental Engineering Science 20(5), 389-404.

[50] Muela, A., García-Bringas, J.M., Seco, C., Arana, I. and Barcina, I. (2002) Participation of Oxygen and Role of Exogenous and Endogenous Sensitizers in the Photoinactivation of *Escherichia coli* by Photosynthetically Active Radiation, UV-A and UV-B. Microbial Ecology 44(4), 354-364.

[51] Nanayakkara, K.G.N. (2010) Ballast WaterTreatment Using Electrochemical Disinfection Technology. Ph.D. Thesis, National University of Singapore.

[52] Page, S.E., Arnold, W.A. and McNeill, K. (2011) Assessing the Contribution of Free Hydroxyl Radical in Organic Matter-Sensitized Photohydroxylation Reactions. Environmental Science & Technology 45(7), 2818-2825.

[53] Palmas, S., Polcaro, A.M., Vacca, A., Mascia, M. and Ferrara, F. (2007) Characterization of boron doped diamond during oxidation processes: Relationship between electronic structure and electrochemical activity. Journal of Applied Electrochemistry 37(1), 63-70.

[54] Panizza, M. and Cerisola, G. (2005) Application of diamond electrodes to electrochemical processes. Electrochimica Acta 51(2), 191-199.

[55] Patermarakis, G. and Fountoukidis, E. (1990) Disinfection of water by electrochemical treatment. Water Research 24(12), 1491-1496.
[56] Rahmawati, F., Kusumaningsih, T., Hapsari, A.M. and Hastuti, A. (2010) Ag and Cu loaded on TiO_2/graphite as a catalyst for *Escherichia coli*-contaminated water disinfection. Chemical Papers 64(5), 557-565.
[57] Rajeshwar, K. and Ibanez, J.G. (1997) Environmental electrochemistry : fundamentals and applications in pollution abatement, Academic Press, San Diego.
[58] Rodrigues, C.P., Ziolli, R.L. and Guimarães, J.R. (2007) Inactivation of *Escherichia coli* in water by TiO_2-assisted disinfection using solar light. Journal of the Brazilian Chemical Society 18, 126-134.
[59] Särkkä, H., Vepsäläinen, M., Pulliainen, M. and Sillanpää, M. (2008) Electrochemical inactivation of paper mill bacteria with mixed metal oxide electrode. Journal of Hazardous Materials 156(1–3), 208-213.
[60] Schmalz, V., Dittmar, T., Haaken, D. and Worch, E. (2009) Electrochemical disinfection of biologically treated wastewater from small treatment systems by using boron-doped diamond (BDD) electrodes--contribution for direct reuse of domestic wastewater. Water Research 43(20), 5260-5266.
[61] Sichel, C., Blanco, J., Malato, S. and Fernández-Ibáñez, P. (2007) Effects of experimental conditions on E. coli survival during solar photocatalytic water disinfection. Journal of Photochemistry and Photobiology A: Chemistry 189(2–3), 239-246.
[62] Szewzyk, U., Szewzyk, R., Manz, W. and Schleifer, K.-H. (2000) Microbiological Safety of Drinking Water. Annual Review of Microbiology 54(1), 81-127.
[63] Tanaka, T., Shimoda, M., Shionoiri, N., Hosokawa, M., Taguchi, T., Wake, H. and Matsunaga, T. (2013) Electrochemical disinfection of fish pathogens in seawater without the production of a lethal concentration of chlorine using a flow reactor. Journal of Bioscience and Bioengineering 116(4), 480-484.
[64] Templeton, M.R., Hofmann, R. and Andrews, R.C. (2006) UV inactivation of humic-coated bacteriophages MS2 and T4 in water. Journal of Environmental Engineering and Science 5(6), 537-543.
[65] Trussell, R.R. (1998) Overview of disinfectant residuals in drinking water distribution systems. Water Suply 16(3-4), 1-15.

[66] Watts, R.J., Finn, D.D., Wyeth, M.S. and Teel, A.L. (2008) Performance Comparison of Tin Oxide Anodes to Commercially Available Dimensionally Stable Anodes. Water Environment Research 80(6), 490-496.
[67] Zanoni, M.V.B., Sene, J.J., Selcuk, H. and Anderson, M.A. (2004) Photoelectrocatalytic Production of Active Chlorine on Nanocrystalline Titanium Dioxide Thin-Film Electrodes. Environmental Science & Technology 38(11), 3203-3208.

CHAPTER 5

5. Photoelectrochemical Degradation of Pharmaceutical Carbamazepine Using Sb-Doped $Sn_{80\%}$-$W_{20\%}$-Oxide Electrodes

5.1. Preface

The increased production and consumption of human and veterinary pharmaceuticals have led to the widespread occurrence of these compounds and their metabolites/transformation products in water resources. The emerging concerns over the potential negative impacts of these bioactive compounds on the ecosystem and human health has sparked research on wastewater treatment. In this study, the Sb-doped $Sn_{80\%}$-$W_{20\%}$-oxide/Ti anode material which had showed the highest intrinsic activity for degradation of phenol red dye in the study presented in Chapter 3 and also showed promising electrocatalytic activity for electrochemical inactivation of bacteria in the study presented in Chapter 3, was tested for photoelectrocatalytic degradation of persistent pharmaceutical, carbamazepine. A manuscript has been prepared based on the results of this research and submitted to the journal of Separation and Purification Technology for publication, as:

S. Ghasemian, D. Nasuhoglu, S. Omanovic, V. Yargeau. "Photoelectrochemical degradation of pharmaceutical carbamazepine using Sb-doped $Sn_{80\%}$-$W_{20\%}$-oxide Electrodes".

Abstract

The continuous release of pharmaceutical compounds in the environment is of concern due to their potential toxicological effects on living organisms, even at low concentrations. The insufficient removal of bioactive contaminants such as pharmaceuticals by conventional wastewater treatment processes has led scientists to investigate and develop efficient technologies such as advanced oxidation processes (AOPs) to address the issue. The objective of the present work was to study the applicability of thermally-prepared Sb-doped $Sn_{80\%}$-$W_{20\%}$-oxide thin film coated electrodes for the photoelectrocatalytic degradation of a recalcitrant pharmaceutical compound, carbamazepine (CBZ). The efficiency of photolytic and photocatalytic processes for removal of CBZ were also evaluated for comparison. The formation of transformation products was investigated and the results showed lower levels of transformation products in the water treated by the photoelectrocatalytic method compared to the photolytic and photocatalytic methods, by the end of 60-min treatment. This suggests a potentially lower overall toxicity of the final solution treated by the photoelectrocatalytic method. An estimation of the energy consumption to reach an order of magnitude reduction in the concentration of CBZ for each type of process indicated a lower energy requirement for the photoelectrocatalytic method, with the highest energy efficiency observed at the applied current density of 6 mA/cm^2.

5.2. Introduction

Over recent decades, increased awareness of impact of organic contaminants on the environment have stimulated research on wastewater treatment. The extensive production, consumption, and resulting discharge of organic products such as pharmaceuticals into the environment continuously deteriorate the quality of natural waters impacting the quality of

drinking water supplies. Most of the pharmaceutically-active compounds (PhACs) and/or their bioactive metabolites enter water bodies via direct or indirect sources such as the indiscriminate discharge of pharmaceutical industry and hospital effluents or the urban and agricultural runoff [1]. These compounds are not fully eliminated during wastewater treatment and are consequently discharged into receiving water bodies [2, 3]. Detection of pharmaceuticals in groundwater [4, 5] and surface waters [6, 7], has been reported worldwide, in concentrations ranging from ng/L to μg/L. The low concentration of pharmaceuticals in aquatic environment is due to dilution effects, bio- and photodegradation, or sorption to sediments. Studies have shown that certain pharmaceuticals may pose various risks for aquatic organisms at such low concentrations [8, 9]. Biological treatment is commonly used for the removal of organic contaminants but this approach is not always suitable for the treatment of industrial wastewaters containing recalcitrant and toxic compounds that are resistant to biodegradation or negatively impact biological treatments [10]. The major concerns related to presence of pharmaceutical compounds in the environment include aquatic toxicity, development of antibiotic resistance in pathogenic bacteria, genotoxicity, and endocrine disruption [11]. To prevent the potential harmful effects of these pollutants and protect our drinking water resources, research efforts are being conducted to develop effective treatment technologies for their elimination and the minimization of their residual biological activity.

In particular, carbamazepine (CBZ) is one of the most frequently detected pharmaceuticals in wastewater treatment plant (WWTP) effluents [12, 13], surface water [14, 15], groundwater [16], and even in drinking water [2]. Carbamazepine is a widely prescribed antiepileptic drug with an estimated global consumption of 1,014 tons per year in 2008 [17]. The frequent occurrence of CBZ in aquatic environment (often found at 1 to 2 μg/L [14]) is also linked to the high persistence of the drug (practically non-biodegradable [18]) and inadequacy of the treatment methods applied in

WWTPs, with removal efficiency usually below 10% [17]. In a classification scheme proposed by Joss et al. (2006) [19] for biological degradation of pharmaceuticals, CBZ was classified in the category “no removal”. Because of potential adverse effects of CBZ on aquatic life [12] and the higher toxicity of some of its transformation products such as acridine [20], numerous efforts have been made in recent years to prevent the release of CBZ and its transformation products in the aquatic environment [17, 21]; however, there is still a need for the development of efficient treatment technologies for the removal of CBZ and its potentially hazardous transformation products.

Advanced oxidation processes (AOPs) have shown to be promising methods to remove many toxic and bio-recalcitrant organic compounds from water [10, 22, 23]. AOPs are chemical oxidation processes based on the *in situ* generation of highly reactive and non-selective oxidizing species such as hydroxyl radicals ($^{\bullet}$OH) with half-life of approximately 10^{-9} s [24]. These reactive species react efficiently with refractory organic compounds such as CBZ [22], leading to the destruction of the organic molecule. AOPs for water and wastewater treatment include electrochemical oxidation, ozonation, photocatalysis, ultrasonic radiation, Fenton and photo-Fenton processes, among which ozone-based techniques are the most commonly investigated methods followed by ultraviolet (UV) radiation-based techniques [25]. Combined AOPs such as photoelectrocatalysis, which combines electrochemical oxidation and UV irradiation, provide higher efficiency for degradation of organic contaminants in aqueous solution [10, 26]. Photoelectrocatalysis offers several advantages such as modularity, portability, easy automation, low specific footprint, and the possibility of treating highly concentrated and bio-refractory wastes. Since the generation of oxidizing species such $^{\bullet}$OH radicals takes place at the anode surface, the

nature of electrode materials is a key element in the photoelectrocatalytic treatment, governing the efficiency, stability, cost, catalytic activity and selectivity of the system [27].

Semiconductors can be used as promising electrode materials due to their ability to efficiently produce charge carriers (electron/hole pairs) by absorbing light [28, 29]. However, the main limitation in the use of semiconductors in photocatalytic processes is the recombination of photogenerated charge carriers (i. e. electrons/holes). To address this issue, many efforts have been made to minimize the recombination of electron/holes by applying techniques such as coupling semiconductors with the possibility of tuning their electronic band structures, or incorporating noble metals into their matrix [29]. Previous studies have investigated the applications of TiO_2 [30], RuO_2-IrO_2 [31], ZnO [32], SnO_2-Sb_2O_3/PbO_2 [33], Ti/PbO_2 [34] , SnO_2 [35], WO_3 [36], TiO_2-SnO_2 and TiO_2-WO_3 [37], and boron-doped diamond (BDD) [23, 34] as anode materials for the removal of organic contaminants through catalytic advanced oxidation processes.

To our knowledge, antimony-doped tin-tungsten oxide anode material has not yet been investigated for the elimination of organic pollutants from wastewaters. The aim of the present study was to evaluate the effectiveness of Sb-doped $Sn_{80\%}$-$W_{20\%}$-oxide electrode coatings synthesized *via* a thermal deposition method, as a photoelectrocatalyst for the removal of aqueous CBZ. A range of Sn/W-oxide compositions had previously been produced and characterized by our laboratory and evaluated for their capability for degradation of a model organic dye. Our results showed that the Sb-doped $Sn_{80\%}$-$W_{20\%}$-oxide composition exhibited the highest intrinsic photoelectrocatalytic activity [38] and this composition was thus selected as the anode composition in the current study. For comparison purposes, the photolytic, photocatalytic and photoelectrocatalytic experiments were conducted to evaluate differences in the level of CBZ removal, apparent degradation kinetics and formation of transformation products (TPs). The effect

of current density on photoelectrocatalytic degradation efficiency was investigated, and the energy consumption of each treatment strategy was also estimated.

5.3. Experimental

5.3.1. Electrode Preparation

Sb-doped $Sn_{80\%}$-$W_{20\%}$-oxide anode coatings were fabricated on 50 mm × 100 mm × 2 mm flat titanium substrates *via* a thermal deposition method. The titanium substrates, which were used as the support for metal-oxide films, were pretreated before the deposition of the coatings in the following order: polishing using 600-grit SiC sandpaper, rinsing with acetone and sonicating in deionized water, and then etching in a boiling solution of HCl (37wt.%, Fisher) and water (1:1, v/v) for 45 min. For each coating, a coating precursor solution was prepared by adding metal salt solutions of $SnCl_2 \times 2H_2O$ (ACS reagent, ≥ 98.0%, Sigma Aldrich), $Na_2WO_4 \times 2H_2O$ (Certified ACS, 100.0%, Fisher), and $SbCl_3$ (ACS reagent, ≥ 99.0%, Sigma Aldrich) in proper amounts to yield a coating with a relative Sn/W molar composition of 80% Sn and 20% W. A small amount of Sb (~3 mol%) was always present in the coating solution, however this amount is not reflected in the coating abbreviation further in the text. All solutions in this work were prepared using Milli-Q water (resistivity: 18.2 MΩ.cm). To form a metal-oxide coating, the coating solution was painted onto the pretreated side of the Ti substrate, dried in an oven at 100°C for 10 min to evaporate the solvent, and then baked in an air furnace at 500°C for 10 min. This process was repeated ten times to form a proper thickness of the coating. After the last application, the electrodes were annealed at 500°C for 2 hours to complete the formation of metal oxides.

5.3.2. Photoelectrochemical Reactor

The photoelectrochemical reactor consisted of a 900-mL cylindrical beaker made of Pyrex glass with a Teflon lid to hold the cell components. The reactor was placed in a water bath to keep the temperature constant at 25°C during experiments. A schematic diagram of the three-electrode batch photoelectrochemical reactor is shown in Appendix as **Figure A- 2**. The Ti substrate coated with Sb-doped $Sn_{80\%}$-$W_{20\%}$-oxide thin film served as the working electrode (anode). Only one side of the anode was coated with the oxide, while the other side was covered by an electrochemically insulating tape. A 93 mm × 100 mm × 2 mm curved stainless steel plate (316L) served as the counter electrode (cathode). The electrodes were placed vertically in the cell facing each and 5.5 cm apart. Saturated calomel electrode (SCE) was used as the reference electrode. The electrodes were connected to a power source operated in the constant current mode during experiments. UV light irradiation was supplied by a 10W UV lamp (GPH212T5L, Atlantic Ultraviolet Corp.) with the maximum emission at 254 nm. The lamp was placed in the middle of the cell between the working and counter electrodes. 0.1 M potassium phosphate buffer solution at pH 7, prepared from KH_2PO_4 salt (ACS Certified, Fisher), was used as the supporting electrolyte. A thermometer was used to monitor the temperature of the solution in the reactor during experiments. Filtered air was blown into the reactor medium through a Pyrex gas dispersion tube (Fisher) to provide oxygen as an electron scavenger (to promote the redox reactions) as well as for mixing. The reactor was fully covered by aluminum foil to avoid exposure of the operator to UV light.

5.3.3. Degradation Experiments

A stock solution of 10 mg/L carbamazepine (Powder, Sigma Aldrich) in 0.1 M potassium phosphate buffer (pH 7) was prepared. The solution was stirred for 24 hours and stored at 4°C to

be used within 1-2 days. For each experiment, a certain volume of the stock solution was mixed with the supporting electrolyte to yield a 550-mL solution of 0.2 mg/L CBZ in 0.1 M potassium phosphate buffer. A freshly coated electrode was sonicated in deionized water for 20 min before each experiment to remove residual contamination from the surface of the electrode. Photolysis experiments were performed under UV irradiation. Photocatalysis experiments were performed under UV light irradiation while the electrodes were placed inside the cell without being connected to a power source. Furthermore, photoelectrocatalytic degradation experiments were performed under UV light irradiation and by applying different constant current densities of 1, 2, 4, 6 and 10 mA/cm^2. In each experiment, one sample was taken from the working solution before inserting the electrodes into the solution (namely, at $t < 0$) and one sample was taken after placing the electrodes inside the cell and before starting the experiment (at $t = 0$), to investigate the possible adsorption of dissolved organic molecules onto the electrode surfaces. Aliquots of 500 µL were taken from the solution at pre-determined intervals during the experiments over a 60-min period. The aliquots were then diluted with a water-methanol mixture (90:10, v/v) by a factor of 2 and then analyzed by Liquid Chromatography-High Resolution Mass Spectrometry (LC-HRMS) to determine the concentration of CBZ in the solution. Each experiment was performed in duplicates or triplicates.

5.3.4. Analysis of Carbamazepine and Transformation Products (TPs)

The analysis was performed on an Accela 600 LC System (Thermo Scientific, Waltham MA, USA) in tandem with an LTQ XL Orbitrap mass spectrometer. Both the LC and the MS systems were controlled by the ThermoXcalibur 2.0 software (Thermo Scientific, San Jose CA, USA). A 0.2 µm in-line filter unit followed by a guard column (5 mm × 2.1 mm ID; 1.8 µm) was used prior to the analytical column (50 mm × 2.1 mm ID; 1.8 µm C18 Zorbax Eclipse Plus) (Agilent Technologies, Santa Clara CA, USA). Separation of a 25 µL injection was conducted at 30°C with

a binary buffer system composed of 2 mM ammonium formate and 0.1% formic acid in Mili-Q water (Solvent A) and methanol 0.1% formic acid (Solvent B). A gradient elution at 0.25 mL/min of A:B was conducted as follows; initial 90:10 (0-1 min), 65:35 (1-2 min), ramp to 60:40 (2-5 min), 0:100 (5-9 min) and hold at 100% B (9-12 min).

Detection of carbamazepine and its transformation products was performed using an electrospray ionization source (ESI) in positive mode. Optimization of the instrument parameters for quantification of carbamazepine was performed by direct infusion of a standard solution at 10 µL/min, while source optimization conditions were determined using infusion flow analysis. Nitrogen was used as sheath, auxiliary and sweep gas, while helium was used as the collision gas. Analysis was done on full scan mode at 30000 resolution for the FT-MS Orbitrap detector (*m/z* 50-500) while the ion trap was used to generate the MS2 spectra for confirmation of carbamazepine. Post-acquisition data processing was carried out for the detection of carbamazepine transformation products (TP) previously reported in the literature [20, 39-42]. The mass accuracy windows was set at ±10 ppm monoisotopic mass tolerance for molecular ion exact mass (M)+ or (M+H)+. Due to the absence of internal standards to identify the TPs based on their retention time, isomeric compounds could not be discriminated using a post-acquisition analysis and these TPs were grouped together.

5.4. Results and Discussion

5.4.1. Photolytic vs. Photocatalytic Treatment: Degradation Efficiency and Reaction Kinetics

The photolysis experiments were performed under UV light irradiation in the absence of electrodes in the electrolyte, whereas the photocatalysis experiments were performed under UV

irradiation in the presence of electrodes in the cell. In both cases, there was no current applied to the cell. Comparison of the CBZ concentration in the electrolyte before and after inserting the electrode into the solution revealed that the change in CBZ concentration in the solution due to a possible adsorption of dissolved molecules onto the electrode surfaces was negligible (< 5%). **Figure 5-1** shows decay of carbamazepine concentration as a function of irradiation time. After 60 min of UV treatment, 75% and 83% of initial carbamazepine (0.2 mg/L) was removed by photolysis and photocatalysis, respectively. However, the difference between the removal percentage of the two processes was not statically significant (Student's t-test, $p > 0.05$). For both processes, the degradation was well-described by the pseudo-first-order reaction kinetics ($R^2 \geq 0.98$) over the whole 60-min treatment time. The corresponding apparent kinetic rate constants, k_{app}, were equal to 0.022 min^{-1} and 0.029 min^{-1} for photolytic and photocatalytic degradation, respectively (not significantly different, as per Student's t-test, $p > 0.05$).

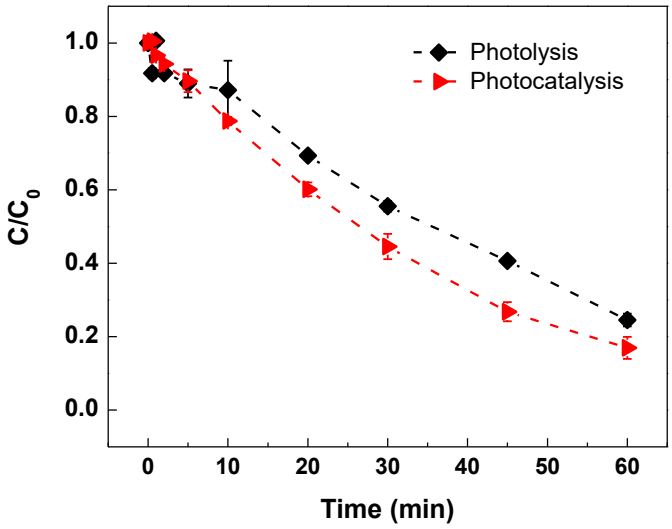

Figure 5-1: Carbamazepine concentration as a function of treatment time during photolytic and photocatalytic carbamazepine oxidation; $[CBZ]_0$ = 0.2 mg/L. Error bars represent the difference between the mean value and upper/lower values of the range (n = 2).

5.4.2. Photoelectrocatalytic Degradation

Photoelectrocatalytic degradation experiments were carried on a 0.2 mg/L carbamazepine solution in a three-electrode configuration at different current densities of 1, 2, 4, 6 and 10 mA/cm^2 and constant light intensity. The dependence of the CBZ removal kinetics on the applied current density is shown in **Figure 5-2**a. The kinetics of CBZ degradation increased with an increase in applied current density up to 6 mA/cm^2 and then the degradation rate levelled off in the range of 6 to 10 mA/cm^2. The initial increase in kinetics might be due to an increasing number of oxidative species (*e. g.* hydroxyl radicals) formed at the electrode-electrolyte interface. However, after a threshold value is reached, the extra energy provided by the increased current will unfavorably serve to produce oxygen rather than additional oxidizing species [43]. In addition, mass transport of CBZ to the electrode surface at high current densities might become a rate-determining-step,

leading to a constant CBZ oxidation rate. It also worth noting that the apparent kinetics of CBZ degradation depends not only on the current density, but also on the electrolyte volume to electrode surface area ratio, which is the case for heterogeneous catalytic reactions. Thus, the time needed to fully oxidize CBZ can conveniently be shortened by increasing the anode surface area.

The kinetic analysis revealed the pseudo-first-order kinetic ($R^2 \geq 0.98$) for the initial photoelectrocatalytic degradation of CBZ (within the first 5 min of degradation reaction) at different current densities. The apparent photoelectrocatalytic degradation initial rate constants, k_{app}, are summarized in **Table 5-1**. The positive effect of current density on k_{app} was pronounced, indicating the beneficial impact of the increased current density on the degradation kinetics. However, when the rate constant is normalized with respect to the current density, a decrease in normalized initial apparent rate constant is obtained (**Figure 5-2**b). This indicates that with an increase in current density, there is also an increased portion of current that is used for some parallel processes. Given that only the CBZ concentration was monitored in these experiments, it is possible that formation of CBZ transformation products were part of these parallel processes as well as oxygen evolution.

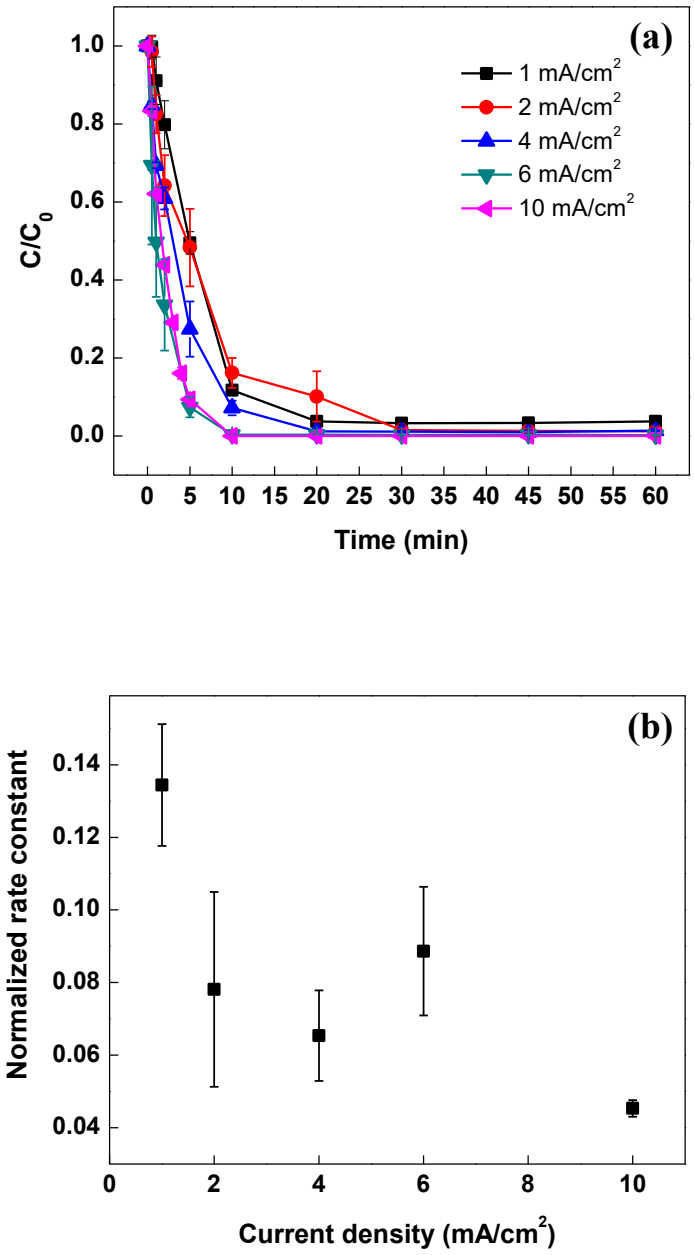

Figure 5-2: (a) Concentration decay over 60 min and (b) normalized apparent initial rate constant with respect to the current density, for the photoelectrocatalytic degradation of carbamazepine at different current densities using Sb-doped Sn80%-W20%-oxide coated anodes; [CBZ]0 = 0.2 mg/L. Error bars represent the difference between the mean value and upper/lower values of the range (n = 3).

Table 5-1

Apparent initial kinetic rate constants, k_{app}, for photoelectrocatalytic degradation of carbamazepine in potassium phosphate buffer (pH 7) at different current densities using Sb-doped $Sn_{80\%}$-$W_{20\%}$-oxide coated anodes; $[CBZ]_0$ = 0.2 mg/L. Data represent mean values ± the difference between the mean and upper/lower values of the range (n = 3).

Current density (mA/cm^2)	Apparent rate constant, k_{app} (min^{-1})
1	0.13 ± 0.02
2	0.16 ± 0.05
4	0.26 ± 0.05
6	0.53 ± 0.11
10	0.45 ± 0.02

5.4.3. Identification of Transformation By-Products (TBPs)

To evaluate the applicability of the photoelectrocatalytic treatment method for the removal of CBZ, the analysis of transformation products is necessary as they can be found at higher concentrations and/or exhibit ecotoxicological activity than the parent compound [44]. Several studies have demonstrated that some compounds produced from photodegradation of carbamazepine may pose important risks to human health and the environment [45, 46]. Samples collected for the different treatments investigated (photolysis, photocatalysis and photoelectrocatalysis) were analyzed for the detection of transformation products of CBZ. In the case of photoelectrocatalysis, only samples from experiments performed at the lowest and highest current densities (1 and 10 mA/cm^2) were analyzed. The CBZ transformation detected are summarized in **Table 5-2**. None of the TPs were detected in the stock solution or at time 0.

Table 5-2

List of carbamazepine transformation products detected.

Analyte	Formula	Ions	Exact mass	Reference(s)
10,11-dihydro-10,11-epoxycarbamazepine	$C_{15}H_{12}N_2O_2$	[M+H]+	253.0977	[39]
2-hydroxycarbamazepine	$C_{15}H_{12}N_2O_2$	[M+H]+		[39, 41]
3-hydroxycarbamazepine	$C_{15}H_{12}N_2O_2$	[M+H]+		[39, 41]
TP266	$C_{15}H_{10}N_2O_3$	[M+H]+	267.0770	[41]
1-(2-benzadehyde)-(1H,3H)-quinazoline-2,4-dione	$C_{15}H_{10}N_2O_3$	[M+H]+		[20, 40]
TP223	$C_{14}H_9NO_2$	[M+H]+	224.0712	[41]
acridone-N-carbaldehyde	$C_{14}H_9NO_2$	[M+H]+		[20]
9-carboxylic acid-acridine	$C_{14}H_9NO_2$	[M+H]+		[42]
9(10H)-acridone	$C_{13}H_9NO$	[M+H]+	196.0765	[20, 42]
9-hydroxy-acridine	$C_{13}H_9NO$	[M+H]+		[20]
acridine	$C_{13}H_9N$	[M+H]+	180.0814	[20]
acridine 9-carbaldehyde	$C_{14}H_9NO$	[M+H]+	208.0757	[20]
TP251	$C_{15}H_{11}N_2O_2$	[M]+	251.0821	[41]
TP268	$C_{15}H_{12}N_2O_3$	[M+H]+	269.0926	[41]

For the treatment of CBZ solution by UV radiation (photolysis only), the TPs *m/z* 251.1 and *m/z* 253.1 were detected in addition to carbamazepine (*m/z* 237.1) (**Figure 5-3**a). The detected TP *m/z* 251.1 was reported as 1-(2-benzaldehyde)-4-hydro-(1H,3H)-quinazoline-2-one (BQM) [40] and may be a mono-keto derivative of a hydroxylated compound [47]. The *m/z* 253.1 response corresponds to 10,11-dihydro-10,11-epoxycarbamazepine [48]. In **Figure 5-3**a, the fact that the TP *m/z* 253.1 remains unchanged after 30 min while carbamazepine (*m/z* 237.1) concentration continue to decrease and the TP *m/z* 251.1 has already been degraded suggests that carbamazepine is oxidized into other transformation products that were not investigated in this study.

Figure 5-3b shows the transformation products formed during photocatalysis. In addition to the products detected for photolysis, TPs *m/z* 196.1, *m/z* 180.1, *m/z* 224.1, and *m/z* 269.1 were detected. The molecular ion identified at *m/z* 224.1 was considered to be 4-aldehyde-9-acridone, according to Li et al. (2013) [49] and Hübner et al. (2014) [50]. This compound was characterized by two fragment ions of *m/z* 196.1 (loss of CO) and *m/z* 180.1 (loss of CO_2) [51], well-known as 9(10H)-acridone and acridine, respectively. Acridine, a stable azaarene compound, is a highly toxic compound with known mutagenic and carcinogenic activity [45]. Donner et al. (2013) [52] demonstrated that the carbamazepine transformation products acridine and acridone were shown to be significantly more toxic than the parent compound across three standardized ecotoxicity assays using bacteria *Vibrio fischeri*, algae *Pseudokirchneriella subcapitata*, and cladoceran *Daphnia magna*, with acridone reported to be less toxic than acridine across all three assays. The molecular weights of some transformation products being greater than CBZ imply the addition of oxygen into the molecular structure [47]. As can be seen in **Figure 5-3**b, the photocatalytic degradation of CBZ led to the formation of transformation products, including acridine and acridone which remain in solution even after 60 min of treatment. This observation indicates that the photocatalytically-treated solution is potentially more toxic than the initial solution as it contains compounds more toxic than CBZ. However, concentrations of these toxic TPs were not determined.

The analysis of aliquots from photoelectrocatalytic degradation of carbamazepine at a current density of 1 mA/cm^2 (**Figure 5-3**c), led to detection of the same TPs as those formed during photolysis (**Figure 5-3**a). However, both *m/z* 251.1 and *m/z* 253.1 compounds first increased and then decreased until disappearance after 20 min of photoelectrocatalysis. As shown in **Figure 5-3**d, relatively more transformation products were detected during photoelectrocatalytic process carried

out at a higher current density, 10 mA/cm^2. The TP *m/z* 267.1 was identified as 1-(2-benzaldehyde)-(1H,3H)-quinazoline-2,4-dione (BQD) [40] and formed as a result of oxidation of hydroxy-groups of di-hydroxylated compound (CBZ + 2OH, *m/z* 271.1) [36]. The TP *m/z* 208 was identified as acridine 9-carbaldehyde [20], which is considered to have higher cytotoxicity than carbamazepine. Furst et al. (1995) [53] demonstrated that this compound caused 40% death in lymphocytes while carbamazepine had no effect on the viability of cells. As can be seen in **Figure 5-3**d, the transformation products were detectable in samples taken from the solution within 30 s to 5 min of treatment, as carbamazepine concentration was constantly decreasing, confirming their formation as the combined effects of UV-irradiation and the electrical current. However, acridine and acridone as well as other products disappeared after 10 min of photoelectrocatalysis, implying that they had higher transformation rates than production rates afterwards. The results showed that the photoelectrocatalytic process at a current density of 10 mA/cm^2 led to an appreciable reduction in the amount of detectable transformation products concurrently with reduction in carbamazepine concentration when compared to photolytic and photocatalytic processes alone. It is therefore probable to expect a lower toxic response for this case; however, cell or whole organism based bioassays should be performed to verify this hypothesis.

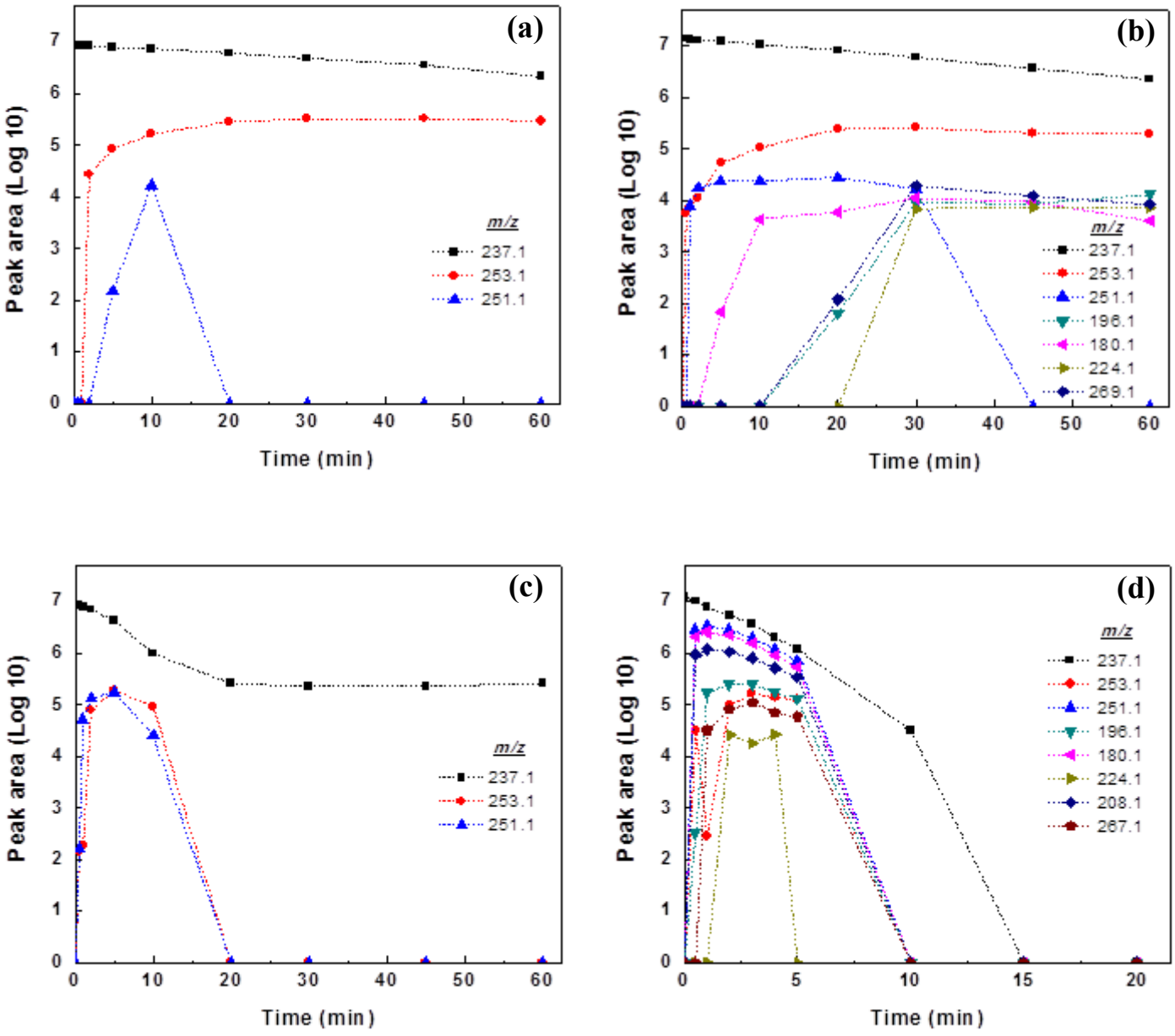

Figure 5-3: Carbamazepine transformation products for various treatment conditions (a) photolysis, (b) photocatalysis, (c) photoelectrocatalysis at 1 mA/cm^2, and (d) photoelectrocatalysis at 10 mA/cm^2. Anode: Sb-doped $Sn_{80\%}$-$W_{20\%}$-oxide coated electrodes; [CBZ]0 = 0.2 mg/L; pH 7.

5.4.4. Energy Consumption

To assess the cost-effectiveness and overall performance of an alternative treatment technology, evaluation of the energy requirement of the process is necessary. In general, the energy consumption of AOPs depends on experimental parameters including the nature and concentration of the target contaminant, configuration of the reactor, and the type of the light source (if any) [54]. In this work, the total energy consumption during a process was estimated as the sum of the electrical energy used and the input power of the UV lamp. An estimate of the electrical energy consumption per volume of treated solution (kWh/m^3) was calculated using the following equation [55]:

$$E_{Electrical} = \frac{Current\ (A) \times Time\ (h) \times Cell\ Voltage\ (V)}{1000 \times Treated\ Volume\ (m^3)} \quad (5\text{-}1)$$

Assuming the first-order CBZ degradation kinetics, the UV input energy (kWh/m^3) was calculated for all three processes using the following equation [54]:

$$E_{UV} = \frac{Lamp\ Power\ (W) \times Time\ (h)}{1000 \times Treated\ Volume\ (m^3)} \quad (5\text{-}2)$$

The $E_{Electrical}$ and E_{UV} have been defined as the energy required to reach 90% removal or, in other words, one order of magnitude reduction in the concentration of the pollutant. The treatment time required to reach the desired level of degradation was obtained from the plot of log C/C_0 versus time (for photolysis and photocatalysis, the values were estimated by extrapolation). **Figure 5-4** presents the total energy consumption for photolytic, photocatalytic, and photoelectrocatalytic degradation of 0.2 mg/L carbamazepine to reach 90% removal. Results revealed that photolytic and photocatalytic processes required much greater treatment time and energy input (32 and 24 kWh/m^3, respectively) than the photoelectrocatalytic process to reach a certain degree of CBZ removal. These results are similar to those obtained in another study to remove 90% of 0.01 mg/L

carbamazepine by photochemical treatment employing UV light (22.7 kWh/m^3) [56]. This observation implies that the electrochemical oxidation played a more important role in removal of the organic pollutant than the photochemical oxidation. The electrochemical oxidation is mainly controlled by the transfer of electrons and the consequent production of charge carriers at the electrode surface, whereas the photochemical oxidation is mainly controlled by the mass transport of generated oxidants to the bulk solution. Since at high current densities the degradation reactions become diffusion-limited, the contribution of photochemical energy (E_{UV}) to the oxidation of CBZ decreases relative to the electrochemical energy ($E_{Electrical}$) (**Figure 5-4**). In photoelectrocatalytic processes, the total energy consumption decreased with increasing applied current density up to 6 mA/cm^2 as the required treatment time decreased. In other words, the photoelectrocatalytic process with the current density of 6 mA/cm^2 had the lowest energy requirement and, thus, the highest degradation efficiency for the removal of carbamazepine under the conditions of this work. These results confirm the findings of the above-mentioned degradation kinetic analysis, and are comparable with the energy requirement of UV/H_2O_2 processes for 90% removal of 0.01 mg/L carbamazepine as reported in the literature [56, 57].

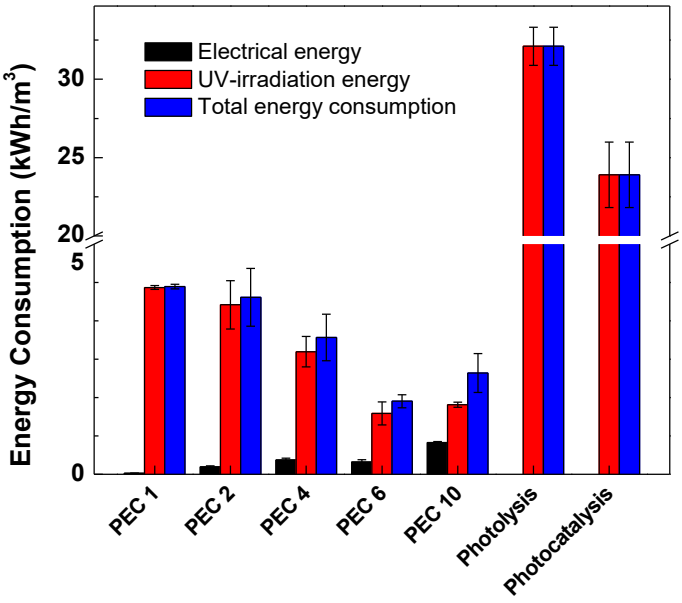

Figure 5-4: Estimation of the energy consumption to reach 90% removal of carbamazepine by different treatment processes; $[CBZ]_0$ = 0.2 mg/L. PEC 1 to 10 refer to photoelectrocatalytic processes at current density of 1 to 10 mA/cm^2. Error bars represent the difference between the mean value and upper/lower values of the range (n = 3).

5.5. Conclusions

The Sb-doped $Sn_{80\%}$-$W_{20\%}$-oxide coated anode was found to be a good candidate for the photoelectrocatalytic oxidation (removal) of carbamazepine (CBZ) present in an aqueous electrolyte. The CBZ degradation rate increased with increasing applied current density, but then levelled off after reaching a threshold value. Acridine and acridone, two transformation products of CBZ with known ecotoxicological effects, were identified as TPs in water subjected to photocatalytic and photoelectrocatalytic (at 10 mA/cm^2) treatments but these compounds were further oxidized (removed) in the photoelectrocatalytic process at longer treatment times, before complete removal of CBZ was achieved, and within the 60-min treatment time. The UV-based treatment processes in the absence of applied current, exhibited much lower efficiency for the

removal of CBZ compared to the simultaneous use of UV irradiation and electrical current (the photoelectrocatalytic process). During photoelectrocatalysis, the contribution of the electrochemical oxidation to the removal of CBZ was found to be more significant than that of the photochemical oxidation. Results demonstrated that the Sb-doped $Sn_{80\%}$-$W_{20\%}$-oxide anode is a promising photoelectrocatalyst for effective and energy-efficient degradation of CBZ in neutral aqueous environment. The findings of this study also further demonstrate the importance of a careful consideration of the formation of transformation products and residual toxicity while assessing the potential of new treatment technologies for the removal of recalcitrant contaminants.

Acknowledgements

The authors would like to thank Mr. Marco Aurelio Pineda Castro and Mrs. Marie-line Peyot for their great work for the analysis of carbamazepine samples and transformation products. The authors would also like to thank Natural Science and Engineering Council for funding the research.

5.6. References

[1] N. Bolong, A.F. Ismail, M.R. Salim, T. Matsuura, A review of the effects of emerging contaminants in wastewater and options for their removal, Desalination, 239 (2009) 229-246.

[2] T. Heberer, K. Reddersen, A. Mechlinski, From municipal sewage to drinking water: Fate and removal of pharmaceutical residues in the aquatic environment in urban areas, in: Water Science and Technology, 2002, pp. 81-88.

[3] R. Reif, A. Santos, S.J. Judd, J.M. Lema, F. Omil, Occurrence and fate of pharmaceutical and personal care products in a sewage treatment works, Journal of Environmental Monitoring, 13 (2011) 137-144.

[4] J.E. Drewes, T. Heberer, K. Reddersen, Fate of pharmaceuticals during indirect potable reuse, Water Science and Technology, 46 (2002) 73-80.

[5] K. Ikehata, N. Jodeiri Naghashkar, M. Gamal El-Din, Degradation of Aqueous Pharmaceuticals by Ozonation and Advanced Oxidation Processes: A Review, Ozone: Science & Engineering, 28 (2006) 353-414.
[6] D.W. Kolpin, E.T. Furlong, M.T. Meyer, E.M. Thurman, S.D. Zaugg, L.B. Barber, H.T. Buxton, Pharmaceuticals, Hormones, and Other Organic Wastewater Contaminants in U.S. Streams, 1999−2000: A National Reconnaissance, Environmental Science & Technology, 36 (2002) 1202-1211.
[7] B.D. Blair, J.P. Crago, C.J. Hedman, R.D. Klaper, Pharmaceuticals and personal care products found in the Great Lakes above concentrations of environmental concern, Chemosphere, 93 (2013) 2116-2123.
[8] K. Fent, A.A. Weston, D. Caminada, Ecotoxicology of human pharmaceuticals, Aquatic Toxicology, 76 (2006) 122-159.
[9] A.M. Christensen, B. Markussen, A. Baun, B. Halling-Sørensen, Probabilistic environmental risk characterization of pharmaceuticals in sewage treatment plant discharges, Chemosphere, 77 (2009) 351-358.
[10] J.O. Tijani, O.O. Fatoba, G. Madzivire, L.F. Petrik, A Review of Combined Advanced Oxidation Technologies for the Removal of Organic Pollutants from Water, Water, Air, & Soil Pollution, 225 (2014) 2102.
[11] B. Halling-Sørensen, S. Nors Nielsen, P.F. Lanzky, F. Ingerslev, H.C. Holten Lützhøft, S.E. Jørgensen, Occurrence, fate and effects of pharmaceutical substances in the environment- A review, Chemosphere, 36 (1998) 357-393.
[12] B.t. Ferrari, N. Paxéus, R.L. Giudice, A. Pollio, J. Garric, Ecotoxicological impact of pharmaceuticals found in treated wastewaters: study of carbamazepine, clofibric acid, and diclofenac, Ecotoxicology and Environmental Safety, 55 (2003) 359-370.
[13] C.D. Metcalfe, B.G. Koenig, D.T. Bennie, M. Servos, T.A. Ternes, R. Hirsch, Occurrence of neutral and acidic drugs in the effluents of Canadian sewage treatment plants, Environmental Toxicology and Chemistry, 22 (2003) 2872-2880.
[14] T.A. Ternes, Occurrence of drugs in German sewage treatment plants and rivers1, Water Research, 32 (1998) 3245-3260.

[15] A. Bahlmann, M.G. Weller, U. Panne, R.J. Schneider, Monitoring carbamazepine in surface and wastewaters by an immunoassay based on a monoclonal antibody, Analytical and Bioanalytical Chemistry, 395 (2009) 1809.
[16] D.J. Lapworth, N. Baran, M.E. Stuart, R.S. Ward, Emerging organic contaminants in groundwater: A review of sources, fate and occurrence, Environmental Pollution, 163 (2012) 287-303.
[17] Y. Zhang, S.-U. Geißen, C. Gal, Carbamazepine and diclofenac: Removal in wastewater treatment plants and occurrence in water bodies, Chemosphere, 73 (2008) 1151-1161.
[18] T.A. Larsen, J. Lienert, A. Joss, H. Siegrist, How to avoid pharmaceuticals in the aquatic environment, Journal of Biotechnology, 113 (2004) 295-304.
[19] A. Joss, S. Zabczynski, A. Göbel, B. Hoffmann, D. Löffler, C.S. McArdell, T.A. Ternes, A. Thomsen, H. Siegrist, Biological degradation of pharmaceuticals in municipal wastewater treatment: Proposing a classification scheme, Water Research, 40 (2006) 1686-1696.
[20] T. Kosjek, H.R. Andersen, B. Kompare, A. Ledin, E. Heath, Fate of Carbamazepine during Water Treatment, Environmental Science & Technology, 43 (2009) 6256-6261.
[21] P. Palo, J.R. Dominguez, J. Sánchez-Martín, T. González, Electrochemical Degradation of Carbamazepine in Aqueous Solutions – Optimization of Kinetic Aspects by Design of Experiments, CLEAN – Soil, Air, Water, 42 (2014) 1534-1540.
[22] L. Feng, E.D. van Hullebusch, M.A. Rodrigo, G. Esposito, M.A. Oturan, Removal of residual anti-inflammatory and analgesic pharmaceuticals from aqueous systems by electrochemical advanced oxidation processes. A review, Chemical Engineering Journal, 228 (2013) 944-964.
[23] J.R. Domínguez, T. González, P. Palo, J. Sánchez-Martín, Electrochemical Advanced Oxidation of Carbamazepine on Boron-Doped Diamond Anodes. Influence of Operating Variables, Industrial & Engineering Chemistry Research, 49 (2010) 8353-8359.
[24] K.-i. Ishibashi, A. Fujishima, T. Watanabe, K. Hashimoto, Quantum yields of active oxidative species formed on TiO_2 photocatalyst, Journal of Photochemistry and Photobiology A: Chemistry, 134 (2000) 139-142.
[25] R.R. Giri, H. Ozaki, S. Ota, R. Takanami, S. Taniguchi, Degradation of common pharmaceuticals and personal care products in mixed solutions by advanced oxidation techniques, International Journal of Environmental Science & Technology, 7 (2010) 251-260.

[26] X. Zhao, J. Qu, H. Liu, Z. Qiang, R. Liu, C. Hu, Photoelectrochemical degradation of anti-inflammatory pharmaceuticals at Bi_2MoO_6–boron-doped diamond hybrid electrode under visible light irradiation, Applied Catalysis B: Environmental, 91 (2009) 539-545.
[27] C. Comninellis, G. Chen, Electrochemistry for the Environment, Springer New York, 2010.
[28] M.X. Tan, P.E. Laibinis, S.T. Nguyen, J.M. Kesselman, C.E. Stanton, N.S. Lewis, Principles and Applications of Semiconductor Photoelectrochemistry, in: Progress in Inorganic Chemistry, John Wiley & Sons, Inc., 2007, pp. 21-144.
[29] H. Zhang, G. Chen, D.W. Bahnemann, Photoelectrocatalytic materials for environmental applications, Journal of Materials Chemistry, 19 (2009) 5089-5121.
[30] R. Liang, A. Hu, W. Li, Y.N. Zhou, Enhanced degradation of persistent pharmaceuticals found in wastewater treatment effluents using TiO_2 nanobelt photocatalysts, Journal of Nanoparticle Research, 15 (2013) 1990.
[31] J. Radjenovic, A. Bagastyo, R.A. Rozendal, Y. Mu, J. Keller, K. Rabaey, Electrochemical oxidation of trace organic contaminants in reverse osmosis concentrate using RuO_2/IrO_2-coated titanium anodes, Water Research, 45 (2011) 1579-1586.
[32] L. Haroune, M. Salaun, A. Ménard, C.Y. Legault, J.-P. Bellenger, Photocatalytic degradation of carbamazepine and three derivatives using TiO_2 and ZnO: Effect of pH, ionic strength, and natural organic matter, Science of The Total Environment, 475 (2014) 16-22.
[33] W. Zhao, J. Xing, D. Chen, D. Jin, J. Shen, Electrochemical degradation of Musk ketone in aqueous solutions using a novel porous Ti/SnO_2-Sb_2O_3/PbO_2 electrodes, Journal of Electroanalytical Chemistry, 775 (2016) 179-188.
[34] C. García-Gómez, P. Drogui, F. Zaviska, B. Seyhi, P. Gortáres-Moroyoqui, G. Buelna, C. Neira-Sáenz, M. Estrada-alvarado, R.G. Ulloa-Mercado, Experimental design methodology applied to electrochemical oxidation of carbamazepine using Ti/PbO_2 and Ti/BDD electrodes, Journal of Electroanalytical Chemistry, 732 (2014) 1-10.
[35] M. Tian, S.S. Thind, M. Simko, F. Gao, A. Chen, Quantitative Structure–Reactivity Study of Electrochemical Oxidation of Phenolic Compounds at the SnO_2–Based Electrode, The Journal of Physical Chemistry A, 116 (2012) 2927-2934.
[36] G. Longobucco, L. Pasti, A. Molinari, N. Marchetti, S. Caramori, V. Cristino, R. Boaretto, C.A. Bignozzi, Photoelectrochemical mineralization of emerging contaminants at porous WO_3 interfaces, Applied Catalysis B: Environmental, 204 (2017) 273-282.

[37] C.-F. Lin, C.-H. Wu, Z.-N. Onn, Degradation of 4-chlorophenol in TiO_2, WO_3, SnO_2, TiO_2/WO_3 and TiO_2/SnO_2 systems, Journal of Hazardous Materials, 154 (2008) 1033-1039.
[38] S. Ghasemian, S. Omanovic, Fabrication and characterization of photoelectrochemically-active Sb-doped Sn_x-$W_{(100-x)\%}$-oxide anodes:

Towards the removal of organic pollutants from wastewater, Submitted, (2017).
[39] X.-S. Miao, C.D. Metcalfe, Determination of Carbamazepine and Its Metabolites in Aqueous Samples Using Liquid Chromatography−Electrospray Tandem Mass Spectrometry, Analytical Chemistry, 75 (2003) 3731-3738.
[40] D.C. McDowell, M.M. Huber, M. Wagner, U. von Gunten, T.A. Ternes, Ozonation of Carbamazepine in Drinking Water: Identification and Kinetic Study of Major Oxidation Products, Environmental Science & Technology, 39 (2005) 8014-8022.
[41] A. Jelic, I. Michael, A. Achilleos, E. Hapeshi, D. Lambropoulou, S. Perez, M. Petrovic, D. Fatta-Kassinos, D. Barcelo, Transformation products and reaction pathways of carbamazepine during photocatalytic and sonophotocatalytic treatment, Journal of Hazardous Materials, 263, Part 1 (2013) 177-186.
[42] E. Kaiser, C. Prasse, M. Wagner, K. Bröder, T.A. Ternes, Transformation of Oxcarbazepine and Human Metabolites of Carbamazepine and Oxcarbazepine in Wastewater Treatment and Sand Filters, Environmental Science & Technology, 48 (2014) 10208-10216.
[43] H. Särkkä, M. Vepsäläinen, M. Pulliainen, M. Sillanpää, Electrochemical inactivation of paper mill bacteria with mixed metal oxide electrode, Journal of Hazardous Materials, 156 (2008) 208-213.
[44] B. Kasprzyk-Hordern, R.M. Dinsdale, A.J. Guwy, The occurrence of pharmaceuticals, personal care products, endocrine disruptors and illicit drugs in surface water in South Wales, UK, Water Research, 42 (2008) 3498-3518.
[45] T.E. Doll, F.H. Frimmel, Removal of selected persistent organic pollutants by heterogeneous photocatalysis in water, Catalysis Today, 101 (2005) 195-202.
[46] S. Chiron, C. Minero, D. Vione, Photodegradation Processes of the Antiepileptic Drug Carbamazepine, Relevant To Estuarine Waters, Environmental Science & Technology, 40 (2006) 5977-5983.

[47] L. Hu, H.M. Martin, O. Arce-Bulted, M.N. Sugihara, K.A. Keating, T.J. Strathmann, Oxidation of Carbamazepine by Mn(VII) and Fe(VI): Reaction Kinetics and Mechanism, Environmental Science & Technology, 43 (2009) 509-515.
[48] Q. Zhang, J. Chen, C. Dai, Y. Zhang, X. Zhou, Degradation of carbamazepine and toxicity evaluation using the UV/persulfate process in aqueous solution, Journal of Chemical Technology & Biotechnology, 90 (2015) 701-708.
[49] J. Li, L. Dodgen, Q. Ye, J. Gan, Degradation Kinetics and Metabolites of Carbamazepine in Soil, Environmental Science & Technology, 47 (2013) 3678-3684.
[50] U. Hübner, B. Seiwert, T. Reemtsma, M. Jekel, Ozonation products of carbamazepine and their removal from secondary effluents by soil aquifer treatment – Indications from column experiments, Water Research, 49 (2014) 34-43.
[51] B. Yang, R.S. Kookana, M. Williams, J. Du, H. Doan, A. Kumar, Removal of carbamazepine in aqueous solutions through solar photolysis of free available chlorine, Water Research, 100 (2016) 413-420.
[52] E. Donner, T. Kosjek, S. Qualmann, K.O. Kusk, E. Heath, D.M. Revitt, A. Ledin, H.R. Andersen, Ecotoxicity of carbamazepine and its UV photolysis transformation products, Science of The Total Environment, 443 (2013) 870-876.
[53] S.M. Furst, J.P. Uetrecht, The effect of carbamazepine and its reactive metabolite, 9-acridine carboxaldehyde, on immune cell function in vitro, International Journal of Immunopharmacology, 17 (1995) 445-452.
[54] M. Muruganandham, K. Selvam, M. Swaminathan, A comparative study of quantum yield and electrical energy per order (E_{Eo}) for advanced oxidative decolourisation of reactive azo dyes by UV light, Journal of Hazardous Materials, 144 (2007) 316-322.
[55] O. Rodríguez-Nava, H. Ramírez-Saad, O. Loera, I. González, Evaluation of the simultaneous removal of recalcitrant drugs (bezafibrate, gemfibrozil, indomethacin and sulfamethoxazole) and biodegradable organic matter from synthetic wastewater by electro-oxidation coupled with a biological system, Environmental Technology, 37 (2016) 2964-2974.
[56] H.R. Andersen, K.M.S. Hansen, T. Kosjek, E. Heath, P. Kaas, A. Ledin, Photochemical treatment of pharmaceuticals, in: 6th IWA World Water Congress and Exhibition, Vienna, Austria, 2008.

[57] J.M. Barazesh, T. Hennebel, J.T. Jasper, D.L. Sedlak, Modular Advanced Oxidation Process Enabled by Cathodic Hydrogen Peroxide Production, Environmental Science & Technology, 49 (2015) 7391-7399.

CHAPTER 6

6. Summary and Conclusions

6.1. Summary

In this thesis, mixed metal oxide electrode coatings composed of antimony, tin and tungsten oxides with different relative molar ratios of tin and tungsten as base elements (Sn_x-$W_{(100-x)mol\%}$-oxide; x = 0, 20, 40, 60, 80 and 100) were formed on a titanium substrate *via* a thermal deposition method, in order to find the bi-component composition of tin and tungsten oxides exhibiting the highest photoelectrochemcial activity towards environmental water-treatment applications. The reason that Sn and W were chosen was that SnO_2 is known to be an electroactive material but also photoactive, while WO_3 is known to be photoactive and offer a lower band-gap energy that SnO_2. Doping with a small amount of antimony (~ 3 mol%) is done to increase the electrical conductivity of SnO_2. The electrochemical, optical, and surface characterization of as-prepared coatings were performed using several experimental techniques such as SEM, EDX, XPS, XRD, TEM, Confocal Laser Scanning Microscopy (CLSM), Photoluminescence (PL) spectroscopy, and cyclic voltammetry (CV); the corresponding surface roughness, surface microstructure and elemental composition, crystallinity, and photocurrent production under UV light irradiation were determined. Then, all prepared coatings with six different compositions were screened by performing photochemical, electrochemical, and photoelectrochemical experiments for the degradation of phenol red dye, as a model organic molecule. Based on the obtained results, the coating composition with the greatest photoelectrochemical activity (Sb-doped $Sn_{80\%}$-$W_{20\%}$-oxide) was selected to be used in further experiments.

In the next step of the project, the selected coating composition (Sb-doped $Sn_{80\%}$-$W_{20\%}$-oxide) was tested as an anode for electrochemical disinfection of water contaminated with bacteria. The investigation of the effects of various experimental parameters such as current density, initial population of bacteria, initial chloride concentration, pH, type of bacterial strain, the presence of natural organic matter (NOM) and radical scavengers on the disinfecting ability of the electrochemical system was undertaken. By calculating the estimated energy consumption under different applied current densities, the optimum experimental conditions associated with the highest energy efficiency were determined.

In the third part of the project, the selected Sb-doped $Sn_{80\%}$-$W_{20\%}$-oxide anode was tested as a photoelectrocatalyst for the degradation of a pharmaceutical, carbamazepine. To evaluate the performance of the photoelectrochemical system, photolytic experiments utilizing UV light as the energy source (no electricity) and photocatalytic degradation experiments utilizing UV light with the photocatalysts present in the reactor (no electricity) were also carried out for comparison purposes. The kinetics of the degradation reactions were analyzed and the apparent rate constants, k_{app}, were determined. The formation of transformation products during carbamazepine degradation by different processes was investigated. The evaluation of the overall performance of the three processes for carbamazepine degradation in terms of degradation rate and energy consumption was performed.

6.2. Conclusions

- The electrochemically active surface area and the surface roughness of the coatings were found to be dependant on the coating composition.
- Sn^{4+} (e.g. SnO_2), W^{6+} (e.g. WO_3) and Sb^{3+} (e.g. Sb_2O_3) were found to be the main oxidation states of the elements in the coatings.
- The optical band gap decreased from 3.53 ± 0.05 eV for pure Sn-oxide to 2.56 ± 0.10 eV for pure W-oxide; however, this decrease occurred only when the content of W in the oxide was greater or equal to 60%.
- All the coatings showed an anodic photocurrent response under UV light irradiation, indicating their *n*-type semiconductor behavior.
- $Sn_{100\%}$-$W_{0\%}$-oxide and $Sn_{80\%}$-$W_{20\%}$-oxide coated electrodes exhibited good apparent photoelectrocatalytic activity for the degradation of phenol red dye under UV light irradiation (~ 90% after 2 hours), however, considering the measured electrochemically-active surface area of the electrodes, the Sb-doped $Sn_{80\%}$-$W_{20\%}$-oxide coating was selected as the best anode material possessing the highest intrinsic photoelectrocatalytic activity.
- Sb-doped $Sn_{80\%}$-$W_{20\%}$-oxide anodes were demonstrated to be effective electrocatalysts for inactivation of bacteria. The bacterial inactivation rate increased with increasing the applied current density and NaCl concentration in the solution.
- The electrochemically-generated ROS (*e.g.* hydroxyl radicals, hydrogen peroxide, ozone) and RCS (*e.g.* Cl_2, HOCl, ClO^-) were mainly responsible for inactivation of bacteria at high and low current densities, respectively.

- The presence of natural organic matter (NOM) and methanol as a radical scavenger hindered the *E. coli* D21 inactivation by electrochemical treatment. Increasing the pH of the solution also showed an adverse effect on the bacterial inactivation.
- The highest efficiency for complete electrochemical disinfection of *E. coli* D21 with initial concentration of 10^7 CFU/mL was obtained at the current density of 6 mA/cm^2 and at 0.1 M NaCl concentration in potassium phosphate buffer (pH 7.1) within 60 seconds with a power consumption of approximately 48 Wh/m^3.
- The Sb-doped $Sn_{80\%}$-$W_{20\%}$-oxide coated anodes were found to be promising photoelectrocatalysts for the effective and energy-efficient degradation of carbamazepine at 0.2 mg/L initial concentration in a natural solution.
- The carbamazepine degradation rate increased with increasing the applied current density, but then levelled off after a threshold value was reached (6 mA/cm^2 in our case).
- Some highly toxic transformation products of carbamazepine, such as acridine and acridone, were identified under photocatalytic and photoelectrocatalytic conditions. However, during the photoelectrocatalysis, they disappeared by the time that the complete removal of carbamazepine was reached.
- Photolysis and photocatalysis processes utilizing UV light irradiation in the absence of applied current, exhibited much lower efficiency for the removal of carbamazepine compared to the photoelectrocatalysis process, which employs both UV irradiation and electrical current at the same time.
- In the photoelectrochemical treatment using the Sb-doped $Sn_{80\%}$-$W_{20\%}$-oxide anode, the contribution of the electrochemical oxidation to the carbamazepine degradation was found to be more significant than that of the photochemical oxidation.

6.3. Original Contributions to Knowledge

The work presented in this thesis is considered to have several original contributions to knowledge, as listed below:

- The development and characterization of antimony-doped tin-tungsten oxide (Sb-Sn-W-oxide) thin films on titanium substrates as anode materials used for the degradation of organic pollutants in wastewaters and water disinfection.
- Promising disinfection results obtained from the electrochemical treatment of bacteria-contaminated water using the antimony-doped tin-tungsten oxide anodes can furnish new insights into the germicidal ability and energy-saving characteristics of electrochemical processes for the inactivation of pathogenic microorganisms without the utilization of UV light and without addition of chemical compounds in electrochemical water purification technology.
- Conducting a comparative study on the degradation of a persistent pharmaceutical, demonstrating the advantages of photoelectrocatalytic treatment using a mixed metal oxide anode over photolytic and photocatalytic methods in terms of potential toxicity of the final solution as well as degradation and energy efficiency.

6.4. Recommendations for Future Works

- Sb-doped Sn-W-oxide electrode coatings can be developed in the form of nanostructured 3D materials to investigate the influence of nano-sized structure on their photoelectrochemical activity.
- The effect of drying and annealing temperatures on the electrochemical, optical, and surface characteristics of the coatings and consequently on their photo- and electrochemical activity towards destruction of organics can be investigated.
- The possible mechanisms of microbial inactivation during electrochemical disinfection tests using Sb-doped Sn-W-oxide coated anodes can be studied.
- The disinfecting ability of Sb-doped Sn-W-oxide anodes towards inactivation of viruses and other pathogenic microorganisms can be evaluated.
- The effect of several factors such as initial concentration of the organic compound, pH, temperature, and the presence of interfering substances on the photochemical, electrochemical, or photoelectrochemical degradation of organic pollutants using Sb-doped Sn-W-oxide anodes can be investigated.
- Complete identification and analysis of the intermediate and products of carbamazepine transformation and assessment of the toxicity of the solution being treated at different intervals during the treatment can be carried out.
- The performance of the developed electrode materials in simultaneous degradation of organic compounds and inactivation of microorganisms can be examined.

Appendix

A.

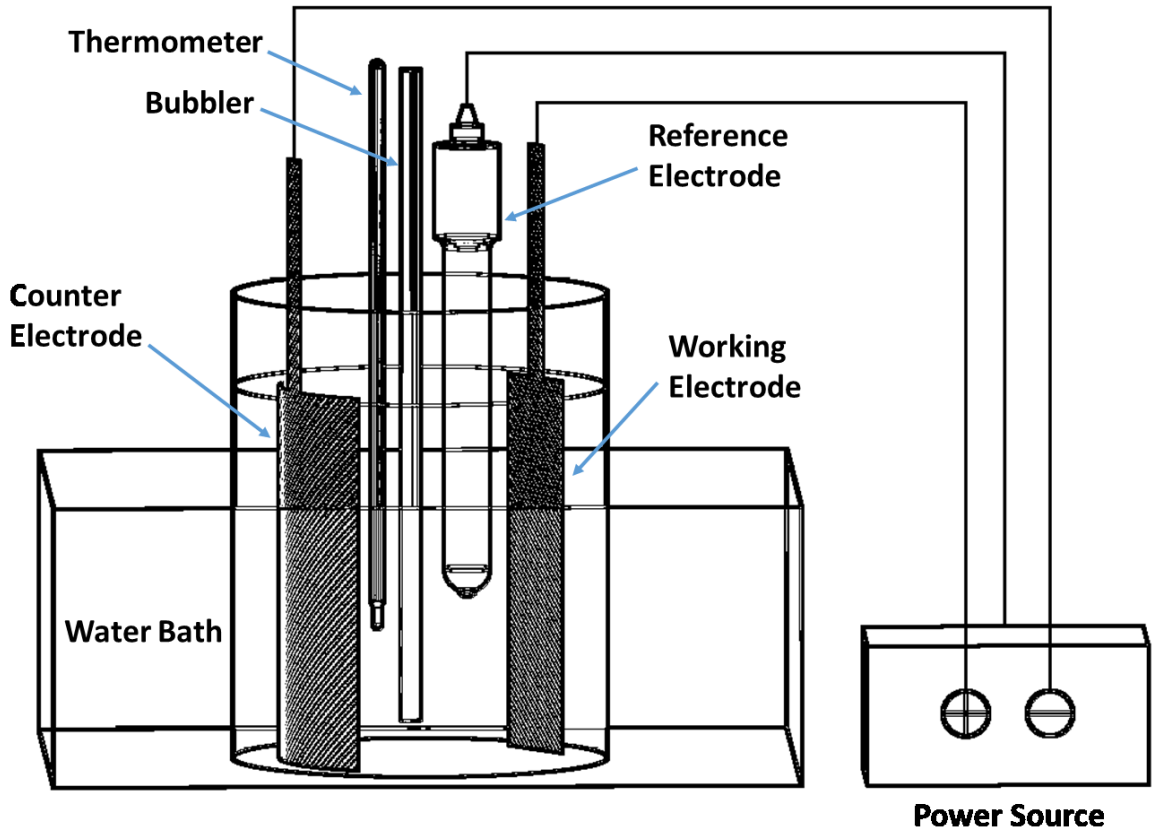

Figure A- 1: Schematic diagram of the electrochemical reactor for disinfection experiments.

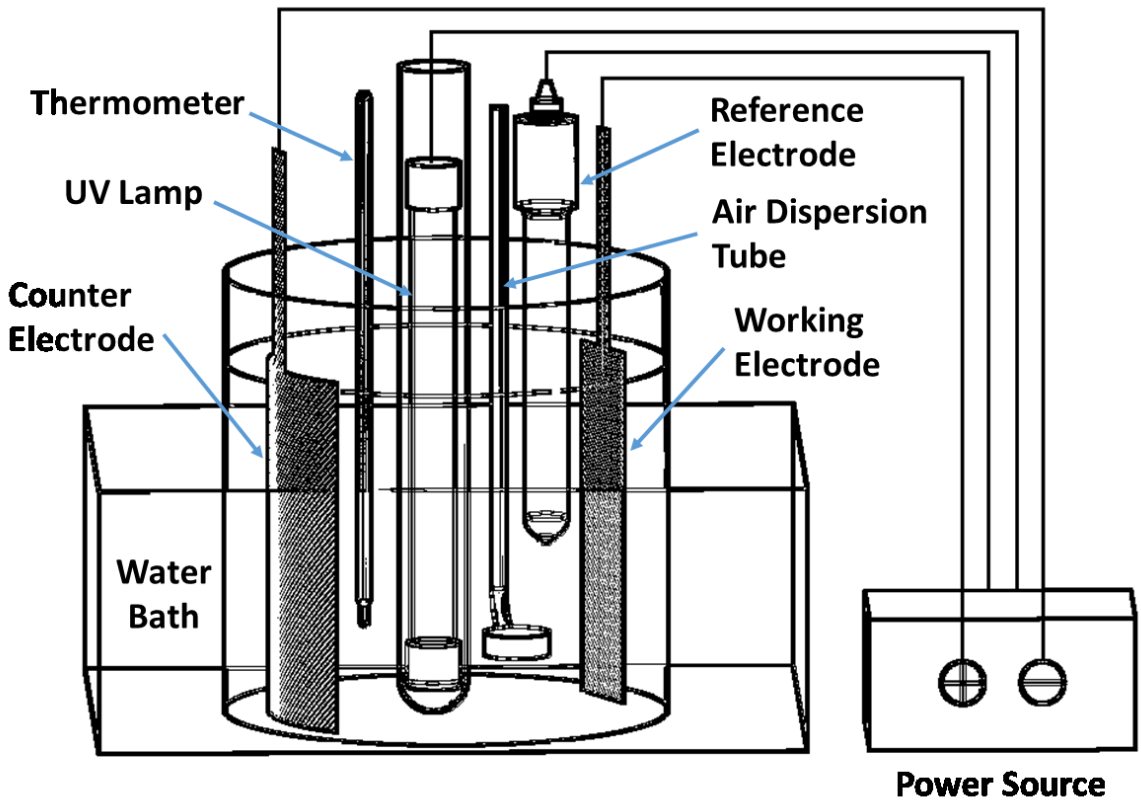

Figure A- 2: Schematic diagram of the photoelectrochemical reactor for CBZ degradation experiments.